



universität
wien

*Dissertation zur Erlangung des Akademischen Grades
Doktor der Naturwissenschaften (Dr. rer. nat.)*

NMR Relaxation under Spin-Locking Conditions

Mag. Renate Auer

Wien, Juni 2010

Dissertationsgebiet: Chemie (A091 419)

Betreuer: Prof. Robert Konrat

The most exciting phrase to hear in science,
the one that heralds new discoveries,
is not 'Eureka!' (I found it!) but
'That's funny ...'

- ISAAC ASIMOV

Silent gratitude isn't much use to anyone.
G.B. STERN

This work would not have been possible without the help and support of many people. Them I would like to thank.

My supervisor in Vienna **Prof. Robert Konrat**, who inspired this work and was a never failing source of answers. All the members of the NMR group at the Department of Structural and Computational Biology, especially **Dr. Karin Kloiber**, **Dr. Martin Tollinger**, **Dr. Georg Kontaxis** and **Mag. Andrea Vavrinska**, who were most involved in the projects I was working on and helped with the solution of many problems. **Karin, Bettina, Martina, Rose** and **Gönül** for making downstairs a true think-tank with brainstorming, networking and socializing. **Prof. L.E. Kay** at the University of Toronto for providing me with a most fitting research project and teaching me many things about NMR. The members of the NMR group at the Department of Molecular Genetics, especially **Dr. Philipp Neudecker**, **Dr. D. Fleming Hansen** and **Dr. D. Ranjith Muhandiram**, for the warm welcome in their group and their competent help in all matters. **Dr. Ilya Kuprov** for inspiring insight in matlab programming and spin dynamics. My **parents** and my close **friends** for always being there for me.

The **Austrian Academy of Science** for funding in the form of a three-year DOC-fFORTE fellowship.

C U R R I C U L U M V I T A E

Mag. Renate Auer

Campus Vienna Biocenter 5 A-1030 Wien

renate.auer@univie.ac.at

Tel: +43 1 4277 52293

P E R S O N A L D A T A

- Born on 5th November 1982 in Bruneck, Italy
- Nationality: Italian

E D U C A T I O N

April-October 2009	Research stay at the Department of Molecular Genetics, University of Toronto, Canada. Supervisor: Prof. L. E. Kay
since January 2007	Doctoral Thesis in NMR at the Department of Structural and Computational Biology, MFPL, University of Vienna, Austria. Supervisor: Prof. R. Konrat
6 th December 2006	Diploma degree (with honours)
March-December 2006	Diploma thesis at the Department of Organic Chemistry, University of Vienna, Austria. Supervisors: Prof. W. Schmid and Prof. R. Konrat. "NMR Filter and Relaxation Experiments of the C-Terminal SH2 Domain of PLC γ 1 with Backbone- ¹³ C-Labelled Isoleucines and Valines."
April-June 2005	Erasmus term at the Department of Inorganic Chemistry, University of Warwick, UK. Supervisor: Prof. M. Hannon
20 th October 2004	Intermediate degree (with honours)
2001-06	Studies of chemistry, University of Vienna (Austria)
1996-2001	High school orientated to modern languages Humanistisches Gymnasium "Nikolaus Cusanus", Bruneck, Italy, passed with 100/100 points
1988-96	Primary and secondary school, Bruneck (Italy)

A W A R D S and G R A N T S

January 2008	Three-year DOC-fFORTE fellowship by the Austrian Academy of Science.
September 2007	Prize for the diploma thesis (Förderpreis) of the Austrian chemical society (GÖCH)
October 2001	Appointment to "Alfiere del Lavoro" due to scholastic success, awarded by the Italian president Carlo Azaglio Ciampi.

P R O F E S S I O N A L E X P E R I E N C E

- Tutor during inorganic and organic chemistry practical courses at the University of Vienna, Austria, 2005 and 2006
- Practical work in the metallurgic laboratory at GKN Birfield Bruneck, Italy, summer 2002

S K I L L S

- Languages: German (mother tongue), English (fluent), Italian (fluent), Spanish (intermediate), Russian (intermediate). Language courses in Britain (1999), Spain (2003) and Russia (2007, 2008).
- Computational skills: Windows (ECDL), Linux, L^AT_EX, matlab

C O N F E R E N C E C O N T R I B U T I O N S

- ENC 2009 (Asilomar, USA) poster: Adiabatic Fast Passage Probing of Milli-to-Microsecond Time-Scale Motions in Proteins (R. Auer, K. Kloiber, M. Tollinger, R. Konrat)
- Gordon Research Conference, Computational Aspects - Biomolecular NMR 2008 (Il Ciocco, Italy) poster: Adiabatic Fast Passage Probing of Milli-to-Microsecond Time-Scale Motions in Proteins (R. Auer, M. Tollinger, R. Konrat, K. Kloiber)
- EUROMAR 2007 (Tarragona, Spain) poster: Selective ¹³C Protein - Backbone Labeling and NMR Relaxation Experiments involving Adiabatic Fast Passage (R. Auer, K. Ledolter, M. Tollinger, K. Kloiber, R. Lichtenecker, W. Schmid, R. Konrat)

P A P E R S

- **R. Auer**, K. Kloiber, A. Vavrinska, L. Geist, N. Coudeville, R. Konrat, *J. Am. Chem. Soc.*, 2010, 132(5):1480-1481
Pharmacophore Mapping via Cross-Relaxation during Adiabatic Fast Passage
- **R. Auer**, D. F. Hansen, P. Neudecker, D. M. Korzhnev, D. R. Muhandiram, R. Konrat, L. E. Kay, *J. Biomol. NMR*, 2010, 46:205-216
Measurement of signs of chemical shift differences between ground and excited protein states: a comparison between H(S/M)QC and $R_{1\rho}$ methods
- **R. Auer**, P. Neudecker, D. R. Muhandiram, P. Lundstrom, D. F. Hansen, R. Konrat, L. E. Kay, *J. Am. Chem. Soc.*, 2009, 131(31):10832-10833
Measuring the Signs of $^1H^\alpha$ Chemical Shift Differences Between Ground and Excited Protein States by Off-Resonance Spin-Lock $R_{1\rho}$ NMR Spectroscopy
- A. Schedlbauer, N. Coudeville, **R. Auer**, K. Kloiber, M. Tollinger, R. Konrat, *J. Am. Chem. Soc.*, 2009, 131(17):6038-6039
Autocorrelation Analysis of NOESY Data Provides Residue Compactness for Folded and Unfolded Proteins
- A. Schedlbauer, **R. Auer**, K. Ledolter, M. Tollinger, K. Kloiber, R. Lichtenecker, S. Ruedisser, U. Hommel, W. Schmid, R. Konrat, G. Kontaxis, *J. Biomol. NMR*, 2008, 42(2):111-127
Direct methods and residue type specific isotope labeling in NMR structure determination and model-driven sequential assignment

Contents

Quotes	i
Acknowledgements	iii
Curriculum Vitae	v
Preface	xi
1 Exchange in NMR	1
2 Adiabatic Fast Passage Pulses	5
2.1 General Features	5
2.2 Numerical Treatment of AFP Pulses	8
2.3 Analytical Treatment of AFP Pulses	11
3 NOE and ROE Effects	21
3.1 Introduction	21
3.2 AFP in NOESY	25
3.2.1 AFP-NOESY Experiments	26
3.2.2 The Effect of Internal Mobility	28
3.2.3 The Effect of Spin Diffusion	29
3.2.4 The Effect of J-coupling	31
4 Measurement of the Sign of $\Delta\omega$	35
5 Summary - Zusammenfassung	39
5.1 Paper I: NOESY-AFP	39
5.2 Papers II and III: Sign of $\Delta\omega$	40
A Product Operator Formalism	43
B Relaxation in the Rotating Frame	47

Bibliography	53
Paper I	55
Paper II	69
Paper III	83

Preface

Over the last decades, nuclear magnetic resonance (NMR) has become an increasingly powerful tool for structure determination and investigation of properties of large biomolecules, particularly proteins [1]. These advances have been made possible by improvements in hard- and software (e.g development of sophisticated pulse sequences, availability of higher magnetic fields, etc.) in combination with the possibility to introduce amino acids selectively labelled with NMR-active isotopes [2, 3, 4, 5, 6]. Structural features of stable systems (protein, protein-ligand complexes etc.) can be routinely assessed by X-ray crystallography and electron microscopy. Structure determination is a key feature also of NMR, albeit being restricted mostly to smaller systems (usually $<30\text{kDa}$). In recent years this weight limit has been pushed further and further to allow quantitative, site-specific investigations even of large protein complexes [7, 8, 9].

A key advantage of NMR methods is the possibility to probe dynamic features of macromolecules at atomic resolution. One main focus of this thesis is concerned with systems undergoing chemical exchange in solution (see **Chapter 1**) i.e. they can be found in a number of different, interconverting states. Frequently just one of these conformational substates is populated to an extent that permits characterization by conventional methods. On the other hand, the low populated, so called *excited* or *invisible* states, which are in many cases the biologically relevant ones, are accessible to NMR spectroscopic techniques. Dynamic processes have been observed that range from protein-ligand interaction over allosteric regulation and catalysis to protein unfolding [6, 7, 10]. A special interest is given to the structure of the invisible state. The structure determination of the ground state using NMR methodology is straightforward by first assigning all the signals in a number of NMR spectra to the respective atom positions in the protein and subsequently performing a structure calculation on the basis of assigned distance restraints [11, 12]. On the other hand, information about the excited state can be obtained by Carr-Purcell-Meiboom-Gill (CPMG) [13, 14, 15] experiments. In particular, population (p_E), the rate with which the two states

interconvert (k_{ex}) and the position of the excited state's resonance signals with respect to the ground state ($|\Delta\omega|$) are obtained. The latter parameter is of vital importance for the structure determination of the invisible state, but since no information on the sign of $\Delta\omega$ is provided by CPMG experiments, a structure calculation cannot be performed at this point. A series of experiments have been developed in order to gain sign information for various protein positions [16, 17, 18]. In the context of this work a method based on spin-lock relaxation $R_{1\rho}$ was developed to extract the sign of $\Delta\omega$ for the $^1\text{H}^\alpha$ position [19]. The methodology was extended to $^1\text{H}^\text{N}$ and $^{13}\text{C}^\alpha$ and compared (in the cases where it was possible) to the conventionally used H(S/M)QC method [16, 19]. An outline of the theory behind this work is given in **Chapter 4** and the results are given in **Papers II and III**.

As mentioned above, NMR can be used to investigate protein-ligand interactions. In the first part of this doctoral thesis a method shall be presented that measures a mixture of longitudinal (NOE) and transverse (ROE) cross-relaxation by introducing an adiabatic fast passage (AFP) pulse in a conventional NOESY mixing time. For a free small ligand NOE and ROE enhancements are essentially the same, thus no dependence on the relative contribution of NOE and ROE can be observed. For a ligand in solution which reversibly binds to a protein NOE and ROE enhancements differ significantly and even display opposite signs. A clear dependence on the relative weights of NOE and ROE can be seen in this case. By probing various ligand positions it is possible to obtain information about the binding epitope, an information useful e.g. for pharmacophore mapping. **Chapter 2 and 3.1** give the theoretical background for AFP pulses and cross-relaxation, respectively. A thorough investigation of the phenomena observed was performed with numerical simulations (**Chapter 3.2**). Experimental details and results are given in **Paper I**.

Chapter 1

Exchange in NMR

NMR spectroscopy offers a powerful tool for the investigation of molecules that are affected by dynamic events on different time scales. Various NMR experiments have been designed to probe them (see figure 1.1). Several biologically relevant processes on the μs -ms timescale such as catalysis, ligand binding or allosteric effects. [6, 7, 10] are described as exchange between two (or more) different conformations. As the interconversion between two states affects the magnetic environment, these processes are accessible to NMR relaxation methods.

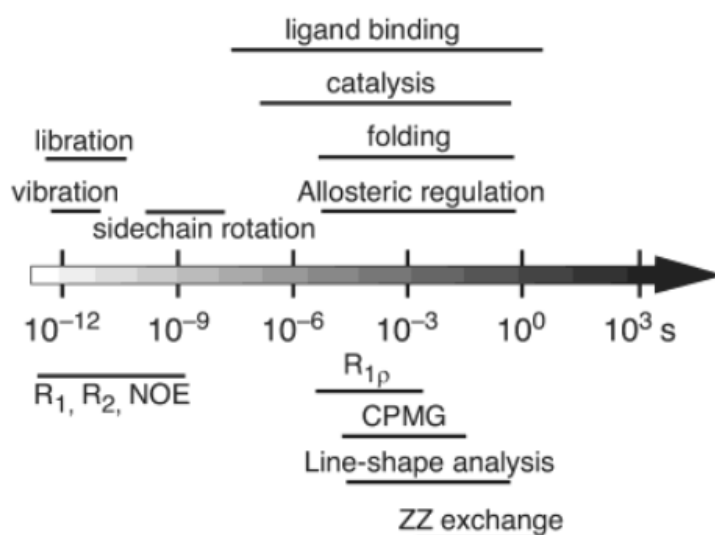


Figure 1.1: " Time scales for protein dynamics and NMR techniques. Protein motions and NMR spin relaxation techniques for studying them span more than 12 orders of magnitude in time scale" [10].

Conformational exchange between a (usually highly populated) ground state G at a resonance frequency Ω_G and a (usually low populated) excited state E at Ω_E is described by three parameters: the exchange rate k_{ex} , the population of the two exchanging sites p_G and p_E , and the chemical shift difference between the two sites $\Delta\omega = \Omega_E - \Omega_G$ [20]. If the two species in solution do not exchange or exchange slowly, the spectrum consists of two sets of signals given both species are sufficiently populated. If the exchange rate k_{ex} increases the corresponding signals of the two subsets approach each other and the lines broaden. When $k_{ex} \approx \Delta\omega$ the lines coalesce and often cannot be observed. As the exchange rate increases further, only one narrow line is visible at the population weighted average of the two individual resonance frequencies $\omega = p_G\Omega_G + p_E\Omega_E$. A classification into slow, intermediate, and fast exchange can be made by determining the coefficient α defined for highly skewed populations ($p_G \gg p_E$) by:

$$\alpha = \frac{2(k_{ex}/\Delta\omega)^2}{1 + (k_{ex}/\Delta\omega)^2}. \quad (1.1)$$

$0 \leq \alpha < 1$	$k_{ex} < \Delta\omega$	Slow exchange
$\alpha \approx 1$	$k_{ex} \approx \Delta\omega$	Intermediate exchange
$1 < \alpha \leq 2$	$k_{ex} > \Delta\omega$	Fast exchange

It is important to notice that changing the spectrometer frequency might result in a different exchange time scale.

Relaxation rate in the absence of a spin-lock field

For highly skewed populations ($p_G \gg p_E$) the relaxation rate of the higher populated species G is given for all time-scales by the Swift-Connick relationship [21]:

$$R_{2G} = p_G R_{2G}^0 + p_G p_E k_{ex} \frac{R_{2E}^0 (R_{2E}^0 + p_G k_{ex}) + \Delta\omega^2}{(R_{2E}^0 + p_G k_{ex})^2 + \Delta\omega^2} \quad (1.2)$$

where R_2^0 is the intrinsic transverse relaxation rate.

Slow exchange regime. In the slow exchange regime, the relaxation of the two separate signals in the absence of an r.f. field is given by

$$R_{2G} = R_{2G}^0 + p_E k_{ex} \quad (1.3)$$

$$R_{2E} = R_{2E}^0 + p_G k_{ex}. \quad (1.4)$$

If the populations of the two states are approximately equal, two signals can be observed. If they are, however, highly skewed, the low populated one may be undetectable since it has less intense signals which are additionally broadened.

Fast exchange regime. In the fast exchange regime, the relaxation rate of the averaged signal observed in the absence of an r.f. field is given by

$$R_2 = p_G R_{2G}^0 + p_E R_{2E}^0 + \frac{p_G p_E \Delta \omega^2}{k_{ex}}. \quad (1.5)$$

Relaxation in the presence of a spin-lock field

Palmer and co-workers have calculated the rotating frame relaxation rate of the major species of an exchanging two-state system for all time regimes to be [22, 23]

$$R_{1\rho} = R_1 \cos^2 \theta + \frac{1}{\gamma} R_2 \sin^2 \theta + \frac{1}{\gamma} \frac{p_G p_E \Delta \omega^2 k_{ex} \sin^2 \theta}{\omega_{G,eff}^2 \omega_{E,eff}^2 \omega_{eff}^2 + k_{ex}^2 - 2 p_G p_E \Delta \omega^2 \sin^2 \theta + (1 - \gamma) \omega_1^2} \quad (1.6)$$

with

$$\begin{aligned} \gamma &= 1 + \mu c \\ \mu &= \frac{p_G p_E \Delta \omega^2}{k_{ex}^2 (\sigma^2 + k_{ex}^2 + \omega_1^2)^2} \\ \sigma &= p_E \delta_G + p_G \delta_E \\ c &= k_{ex}^2 (\sigma^2 - k_{ex}^2 + \omega_1^2)^2 \\ \omega_{eff}^2 &= \Delta \Omega^2 + \gamma \omega_1^2 \\ \omega_{G,eff}^2 &= \delta_G^2 + \gamma \omega_1^2 \\ \omega_{E,eff}^2 &= \delta_E^2 + \gamma \omega_1^2 \\ \theta &= \arctan(\sqrt{\gamma} \omega_1 / \Delta \omega) \\ \delta_G &= \Omega_G - \omega_{RF} \\ \delta_E &= \Omega_E - \omega_{RF} \\ \Delta \omega &= \delta_E - \delta_G = \Omega_E - \Omega_G \\ \Delta \Omega &= p_G \Omega_G + p_E \Omega_E - \omega_{RF} \end{aligned} \quad (1.7)$$

Ω_G and Ω_E are the resonance frequencies of species G and E, respectively. ω_{RF} is the frequency of the applied spin-lock field and ω_1 is its field strength.

γ is a small correction factor. Frequently $\gamma \rightarrow 1$, and $R_{1\rho}$ can be simplified to

$$R_{1\rho} = R_1 \cos^2 \theta + R_2 \sin^2 \theta + \frac{p_G p_E \Delta \omega^2 k_{ex} \sin^2 \theta}{\omega_{G,eff}^2 \omega_{E,eff}^2 \omega_{eff}^2 + k_{ex}^2 - 2p_G p_E \Delta \omega^2 \sin^2 \theta}. \quad (1.8)$$

A previous result by Trott *et al.* [22] neglects the last term of the denominator. In addition, for the fast-exchange limit the following approximation can be made:

$$R_{1\rho} = R_1 \cos^2 \theta + R_2 \sin^2 \theta + \frac{p_G p_E \Delta \omega^2 k_{ex} \sin^2 \theta}{\omega_{eff}^2 + k_{ex}^2} \quad (1.9)$$

Chapter 2

Adiabatic Fast Passage Pulses

2.1 General Features

An adiabatic fast passage (AFP) pulse is a relatively long (on the order of hundreds of ms) pulse with a frequency sweep (e.g. linear) over a defined spectral region. The pulse does neither start nor end abruptly but reaches its high power through (for example) a sine-shaped ramp. At the end of the pulse a cosine-shaped ramp decreases its power to zero. The net effect of such a pulse is the full inversion of the spectral range covered (with the exception of the ramps) given the field strength is large enough to effectively spin-lock the magnetization and the sweep rate fulfills the adiabatic condition $|d\theta/dt| < \omega_{eff}$ [24]. The outstanding inversion profile, which is nearly independent of offset and exact radiofrequency power used, makes AFP pulses interesting for broadband inversion and decoupling [25, 26, 24].

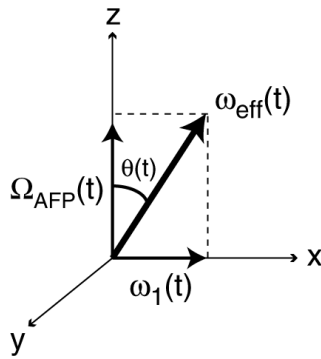


Figure 2.1: Adiabatic spin-lock frame with offset $\Omega_{AFP}(t)$, r.f. field $\omega_1(t)$, effective field $\omega_{eff}(t)$, and the angle $\theta(t)$ between offset and effective field.

The effect of an AFP pulse on a spin I at resonance frequency Ω_I can be understood intuitively by defining a co-ordinate system (see figure 2.1) where the x -axis is represented by the pulse power $\omega_1(t)$ and the z -axis stands for the pulse offset at every time step during the pulse $\Omega_{AFP}(t) = \omega_{RF}(t) - \Omega_I$. At every time step the vector sum of these two vectors corresponds to the effective magnetic field affecting spin I. $\Omega_{AFP}(t)$ starts at $+z$, crosses zero (i.e. the spin is on-resonance) and ends in $-z$. The magnetization rotates around the effective magnetic field with a very small angle. Thus it is spin-locked and will be inverted efficiently. The effect of an AFP pulse on a spin can be seen in figure 2.2.

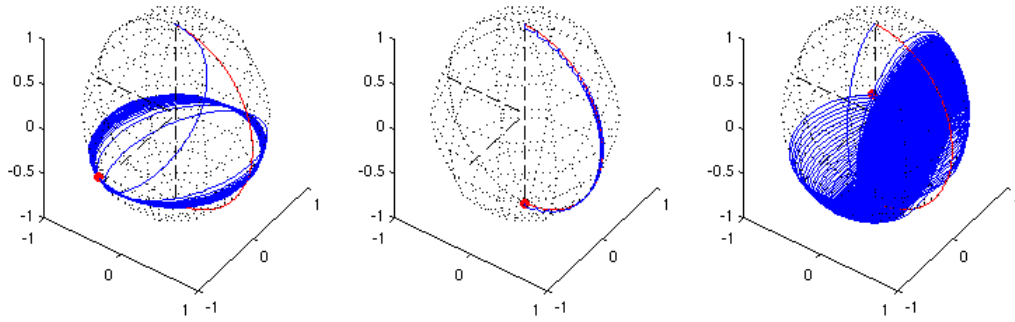


Figure 2.2: Magnetization trajectory during an AFP pulse. In the first two plots the pulse is on-resonance during maximum power. In the last plot the resonance frequency is hit by the AFP pulse during the ramped part. The corresponding maximum ω_1 values are 50, 2000, and 2000 Hz on ^{15}N . Apparently, a spin-lock field of 50 Hz does not effectively spin-lock the magnetization, which, as a consequence, is dephased. Also the magnetization of spins that are on-resonance during the ramped part of the pulse is not perfectly inverted. For this simulation scalar coupling, relaxation, and exchange were neglected.

The relaxation during an AFP pulse can be described by the following equation (the derivation is given in appendix B):

$$R_{1\rho} = R_1 \cos^2 \theta_{eff} + R_2 \sin^2 \theta_{eff} = R_1 + (R_2 - R_1) \sin^2 \theta_{eff}. \quad (2.1)$$

In this equation $\sin^2 \theta_{eff}$ is given by the time integral of $\sin^2 \theta(t)$, approxi-

mated in all simulations by the average of $\sin^2 \theta_i$ over all n time steps t_i

$$\sin^2 \theta_{eff} = \left(\sum_{i=1}^n \sin^2 \theta_i \right) / n \quad (2.2)$$

$$\theta_i = \arctan \frac{\omega_1(t_i)}{\Omega_{AFP}(t_i)}. \quad (2.3)$$

θ_{eff} is the effective tilt angle with the following meaning: in a *Gedanken-experiment* we assume a static spin-lock field, where magnetization remains at an angle θ_{eff} . Such a spin would show the same relaxation behaviour as magnetization that follows the effective field from $+z$ to $-z$.

Application of a spin-lock field changes the relaxation properties of spins. Magnetization relaxes towards its steady-state value for $t \rightarrow \infty$. Under free precession conditions, the steady-state corresponds to the equilibrium value σ^{eq} , which is zero for I_x and I_y magnetization and one for I_z . The steady-state value during spin-lock, however, differs from the equilibrium value.

The following equations describe the spin dynamics of magnetization in a spin-lock field [27]:

$$\frac{d\sigma(t)}{dt} = (\mathbf{L} - \mathbf{R}) \sigma(t) + \mathbf{R} (\sigma(t) - \sigma^{eq}) \quad (2.4)$$

$$\sigma(t) = e^{\mathbf{L}t} (\sigma(0) - \sigma^\infty) + \sigma^\infty \quad (2.5)$$

$\sigma(t)$ is the time-dependent density matrix, σ^∞ and σ^{eq} are the steady-state and the equilibrium density matrices, respectively, given by

$$\sigma(t) = \begin{pmatrix} M_x(t) \\ M_y(t) \\ M_z(t) \end{pmatrix} \quad \sigma^\infty = \begin{pmatrix} M_x(\infty) \\ M_y(\infty) \\ M_z(\infty) \end{pmatrix} \quad \sigma^{eq} = \begin{pmatrix} 0 \\ 0 \\ 1 \end{pmatrix}. \quad (2.6)$$

The Liouvillian matrix \mathbf{L} and the relaxation matrix \mathbf{R} are given by

$$\mathbf{L} = \begin{pmatrix} -R_2 & -\omega_I & 0 \\ \omega_I & -R_2 & -\omega_{1x} \\ 0 & \omega_{1x} & -R_1 \end{pmatrix} \quad (2.7)$$

$$\mathbf{R} = \begin{pmatrix} -R_2 & 0 & 0 \\ 0 & -R_2 & 0 \\ 0 & 0 & -R_1 \end{pmatrix} \quad (2.8)$$

with longitudinal relaxation rate R_1 , transverse relaxation rate R_2 , spin Larmor frequency ω_I , spin-lock field from x ω_{1x} .

σ^∞ can be calculated from $\frac{d\sigma(t)}{dt} = 0$ to $\sigma^\infty = \mathbf{L}^{-1} \mathbf{R} \sigma^{eq}$. Simulations demonstrate that σ^∞ can be assumed by good approximation to be zero for all spin-locked magnetization components.

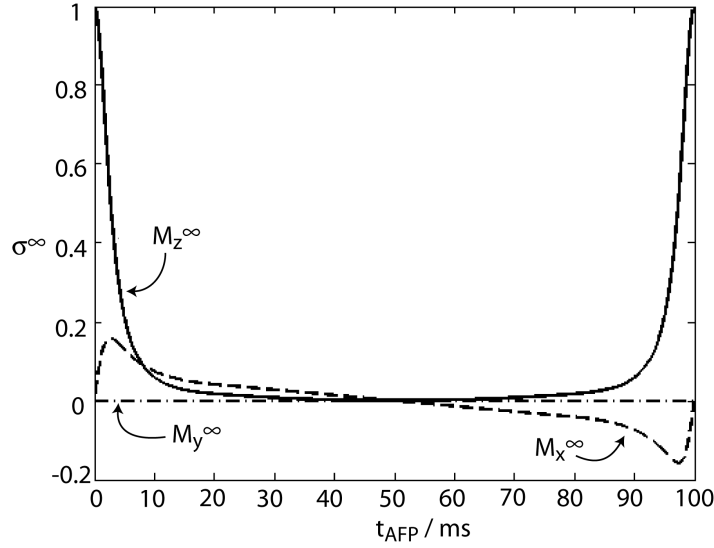


Figure 2.3: All components of σ^∞ during an AFP pulse.

2.2 Numerical Treatment of AFP Pulses

A numerical simulation of magnetization during an AFP pulse amounts to solving the following equation for each time step $\tau = t_i - t_{i-1}$ during the AFP pulse resulting in a multi-step calculation

$$\sigma(t_i) = e^{-\mathbf{L}\tau} \sigma(t_{i-1}) \quad (2.9)$$

For an isolated spin S system without J-coupling, cross-correlated relaxation and chemical/conformational exchange, $\sigma(t)$ and the Liouvillian-matrix \mathbf{L} are given by equations (2.6) and (2.7). A matrix extension, however, is necessary for a full description when the spin S is coupled to a spin I, e.g. ^{15}N in a protein coupled to ^1H . Also CSA-DD cross correlation has to be considered, resulting in the following matrices, where J is the scalar coupling constant and $G_{x/z}$ the transverse and longitudinal CSA-DD cross-correlated relaxation rate, respectively:

$$\mathbf{L} = - \begin{pmatrix} R_{2S} & \omega_S & \omega_{1y} & G_x & J & 0 \\ -\omega_S & R_{2S} & \omega_{1x} & -J & G_x & 0 \\ -\omega_{1y} & -\omega_{1x} & R_{1S} & 0 & 0 & -G_z \\ G_x & J & 0 & R_{2S} + R_{1I} & \omega_S & \omega_{1y} \\ -J & G_x & 0 & -\omega_S & R_{2S} + R_{2I} & \omega_{1x} \\ 0 & 0 & -G_z & -\omega_{1y} & -\omega_{1x} & R_{1S} + R_{1I} \end{pmatrix} \quad (2.10)$$

$$\sigma(t) = \begin{pmatrix} S_x(t) \\ S_y(t) \\ S_z(t) \\ S_x I_z(t) \\ S_y I_z(t) \\ S_z I_z(t) \end{pmatrix} \quad (2.11)$$

Yet another matrix extension is necessary for systems that undergo chemical exchange between two species A and B. \mathbf{L} and $\sigma(t)$ are then given by:

$$\mathbf{L} = - \begin{pmatrix} \mathbf{A} & \mathbf{B} \\ \mathbf{C} & \mathbf{D} \end{pmatrix} \quad (2.12)$$

$$\mathbf{A} = \begin{pmatrix} R_{2S}^A + k_{AB} & \omega_{SA} & \omega_{Ay} & G_x & J & 0 \\ -\omega_{SA} & R_{2S}^A + k_{AB} & \omega_{Ax} & -J & G_x & 0 \\ -\omega_{Ay} & -\omega_{Ax} & R_{1S}^A + k_{AB} & 0 & 0 & -G_z \\ G_x & J & 0 & R_{2S}^A + R_{1I}^A + k_{AB} & \omega_{SA} & \omega_{Ay} \\ -J & G_x & 0 & -\omega_{SA} & R_{2S}^A + R_{1I}^A + k_{AB} & \omega_{Ax} \\ 0 & 0 & -G_z & -\omega_{Ay} & -\omega_{Ax} & R_{1S}^A + R_{1I}^A + k_{AB} \end{pmatrix}$$

$$\mathbf{B} = \begin{pmatrix} -k_{BA} & 0 & 0 & 0 & 0 & 0 \\ 0 & -k_{BA} & 0 & 0 & 0 & 0 \\ 0 & 0 & -k_{BA} & 0 & 0 & 0 \\ 0 & 0 & 0 & -k_{BA} & 0 & 0 \\ 0 & 0 & 0 & 0 & -k_{BA} & 0 \\ 0 & 0 & 0 & 0 & 0 & -k_{BA} \end{pmatrix}$$

$$\mathbf{C} = \begin{pmatrix} -k_{AB} & 0 & 0 & 0 & 0 & 0 \\ 0 & -k_{AB} & 0 & 0 & 0 & 0 \\ 0 & 0 & -k_{AB} & 0 & 0 & 0 \\ 0 & 0 & 0 & -k_{AB} & 0 & 0 \\ 0 & 0 & 0 & 0 & -k_{AB} & 0 \\ 0 & 0 & 0 & 0 & 0 & -k_{AB} \end{pmatrix}$$

$$\mathbf{D} = \begin{pmatrix} R_{2S}^B + k_{BA} & \omega_{SB} & \omega_{By} & G_x & J & 0 \\ -\omega_{SB} & R_{2S}^B + k_{BA} & \omega_{Bx} & -J & G_x & 0 \\ -\omega_{By} & -\omega_{Bx} & R_{1S}^B + k_{BA} & 0 & 0 & -G_z \\ G_x & J & 0 & R_{2S}^B + R_{1I}^B + k_{BA} & \omega_{SB} & \omega_{By} \\ -J & G_x & 0 & -\omega_{SB} & R_{2S}^B + R_{1I}^B + k_{BA} & \omega_{Bx} \\ 0 & 0 & -G_z & -\omega_{By} & -\omega_{Bx} & R_{1S}^B + R_{1I}^B + k_{BA} \end{pmatrix}$$

$$\sigma(t) = \begin{bmatrix} S_{ax} & S_{ay} & S_{az} & S_{ax}I_{az} & S_{ay}I_{az} & S_{az}I_{az} \\ S_{bx} & S_{by} & S_{bz} & S_{bx}I_{bz} & S_{by}I_{bz} & S_{bz}I_{bz} \end{bmatrix}'. \quad (2.13)$$

k_{AB} and k_{BA} are related to the exchange-rate constant k_{ex} by

$$k_{AB} = p_B k_{ex} \quad (2.14)$$

$$k_{BA} = p_A k_{ex} \quad (2.15)$$

$$k_{ex} = k_{AB} + k_{BA} \quad (2.16)$$

where p_A and p_B are the populations of species A and B, respectively.

The effective spin-lock relaxation rate can be calculated to

$$R_{1\rho} = \frac{1}{t_{AFP}} \ln \frac{M_z(0)}{M_z(t_{AFP})} \quad (2.17)$$

$M_z(0)$ and $M_z(t_{AFP})$ are the z-components of the magnetization at $t = 0$ and at the end of the AFP pulse ($t = t_{AFP}$), respectively. Since a typical AFP pulse consists of 1000-10000 time steps, a stepwise calculation of spin dynamics is quite time consuming. However, there are two possibilities to increase the computational speed:

Krylov subspace method

The exponential expression

$$\sigma(t_{i+1}) = e^{\mathbf{L}\tau} \sigma(t_i) \quad (2.18)$$

can be approximated by $\sigma(t_{i+1}) = \sum_{n=0}^{\infty} \frac{(\mathbf{L}\tau)^n \sigma(t_i)}{n!}$, where $\tau = t_{i+1} - t_i$. This can decrease computing time, if the propagator converges within a small number of iterative steps n (for slow to intermediate exchange five to six steps are usually sufficient, fast exchange might need up to 15).

Baker-Campbell-Hausdorff (BCH) theory[28]

The expression to be evaluated is

$$\sigma(t) = \exp(\mathbf{L}_n \tau) \dots \exp(\mathbf{L}_3 \tau) \exp(\mathbf{L}_2 \tau) \exp(\mathbf{L}_1 \tau) \sigma(0). \quad (2.19)$$

It is computationally less expensive to replace a product of two matrixexponentials by one matrixexponential constructed from the two exponentials. The BCH relation states:

$$e^{\mathbf{A}} e^{\mathbf{B}} = \exp \left(\mathbf{A} + \mathbf{B} - \frac{1}{2} [\mathbf{B}, \mathbf{A}] + \frac{1}{12} ([\mathbf{B}, [\mathbf{B}, \mathbf{A}]] + [[\mathbf{B}, \mathbf{A}], \mathbf{A}] + \dots) \right) \quad (2.20)$$

In Liouvillian space four time steps can be combined to a first-order average Liouvillian:

$$\begin{aligned} \mathbf{L}(4\tau) &\approx \underbrace{(\mathbf{L}_1 + \mathbf{L}_2 + \mathbf{L}_3 + \mathbf{L}_4)}_{\mathbf{L}^0} \tau \dots \\ &\dots - \underbrace{\frac{1}{2} ([\mathbf{L}_2, \mathbf{L}_1] + [\mathbf{L}_3, \mathbf{L}_1] + [\mathbf{L}_3, \mathbf{L}_2] + [\mathbf{L}_4, \mathbf{L}_1] + [\mathbf{L}_4, \mathbf{L}_2] + [\mathbf{L}_4, \mathbf{L}_3])}_{\mathbf{L}^1} \tau^2. \end{aligned} \quad (2.21)$$

Simulations show no observable deviations between the density matrices obtained using the above approximation and the exact solutions.

2.3 Analytical Treatment of AFP Pulses

A heteronuclear, J-coupled IS system with the AFP pulse acting on S can be described by the following Hamiltonian in the doubly rotating frame[29, 30]:

$$\mathbf{H}_I = 2\pi J I_z S_z + \Omega_{AFP}(t_i) S_z + \omega_1(t_i) S_x. \quad (2.22)$$

The Hamiltonian can be diagonalized by rotation into a tilted frame (with the tilt angle corresponding to the angle between the static magnetic field and the effective field that is given at every time step by $\theta(t) = \arctan\left(\frac{\omega_1(t)}{\Omega_{AFP}(t)}\right)$):

$$\mathbf{H}_I' = \mathbf{U} \mathbf{H}_I \mathbf{U}^{-1} \quad (2.23)$$

$$\mathbf{U} = \exp(i\theta S_y) \quad (\text{for a field from y direction}) \quad (2.24)$$

$$\begin{aligned} \mathbf{H}_I' &= 2\pi J S_z' I_z c_\theta - 2\pi J S_x' I_z s_\theta + \\ &\quad S_z' (\Omega_{AFP}(t_i) c_\theta + \omega_1(t_i) s_\theta) + \\ &\quad \underbrace{S_x' (\omega_1(t_i) c_\theta - \Omega_{AFP}(t_i) s_\theta)}_{=0} \end{aligned} \quad (2.25)$$

$$c_\theta = \cos \theta = \frac{\Omega_{AFP}(t_i)}{\sqrt{\Omega_{AFP}(t_i)^2 + \omega_1(t_i)^2}} \quad (2.26)$$

$$s_\theta = \sin \theta = \frac{\omega_1(t_i)}{\sqrt{\Omega_{AFP}(t_i)^2 + \omega_1(t_i)^2}} \quad (2.27)$$

(the prime indicates a product operator in the tilted frame). In contrast to Zwahlen's *et al.* [29] treatment of adiabatic pulses during INEPT steps, simulations have shown that the nonsecular part of the Hamiltonian in the tilted frame (proportional to $S_x' I_z$) cannot be neglected for narrow sweep widths, as recommended for ^{15}N . In this case substantial deviations can occur if this term is neglected and exchange is considered in the calculation. For

larger sweep widths as for ^1H nuclei on the other hand, the $S'_x I_z$ -term can be safely neglected. The effect of neglecting the nonsecular term can be demonstrated by the comparison of $R_{1\rho}$ values for a broad range of $\sin^2 \theta_{\text{eff}}$.

Figure 2.4 shows results yielded by numerical simulation, analytical treatment, and analytical treatment neglecting the $S'_x I_z$ -term for a system undergoing two-site exchange. An example for the time evolution of the six product operator terms that result from an analytical treatment (compare figure 2.7) are shown in figures 2.5 and 2.6 for initial magnetization of $S_z=1$ with all other terms being zero.

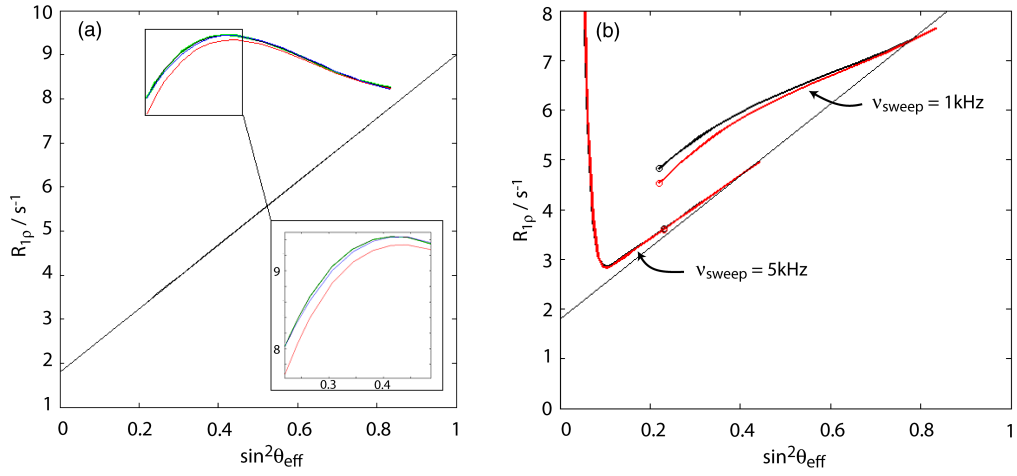


Figure 2.4: (a) Simulation of ^{15}N - $R_{1\rho}$ with the exchange parameters $k_{\text{ex}} = 1000 \text{ s}^{-1}$, $p_B = 10\%$, $\Delta\omega = 2 \text{ ppm}$. ν_{sweep} was set to 1 kHz . Green: numerical simulation, black: full analytical simulation, red: analytical simulation neglecting the $S'_x I_z$ -term, blue: equation (1.8). (b) $\Delta\omega = 1 \text{ ppm}$. ν_{sweep} are 1 kHz and 5 kHz . For the circled data point a full time evolution of all product operator terms can be seen in figures 2.5 and 2.6. The color coding is as in (a).

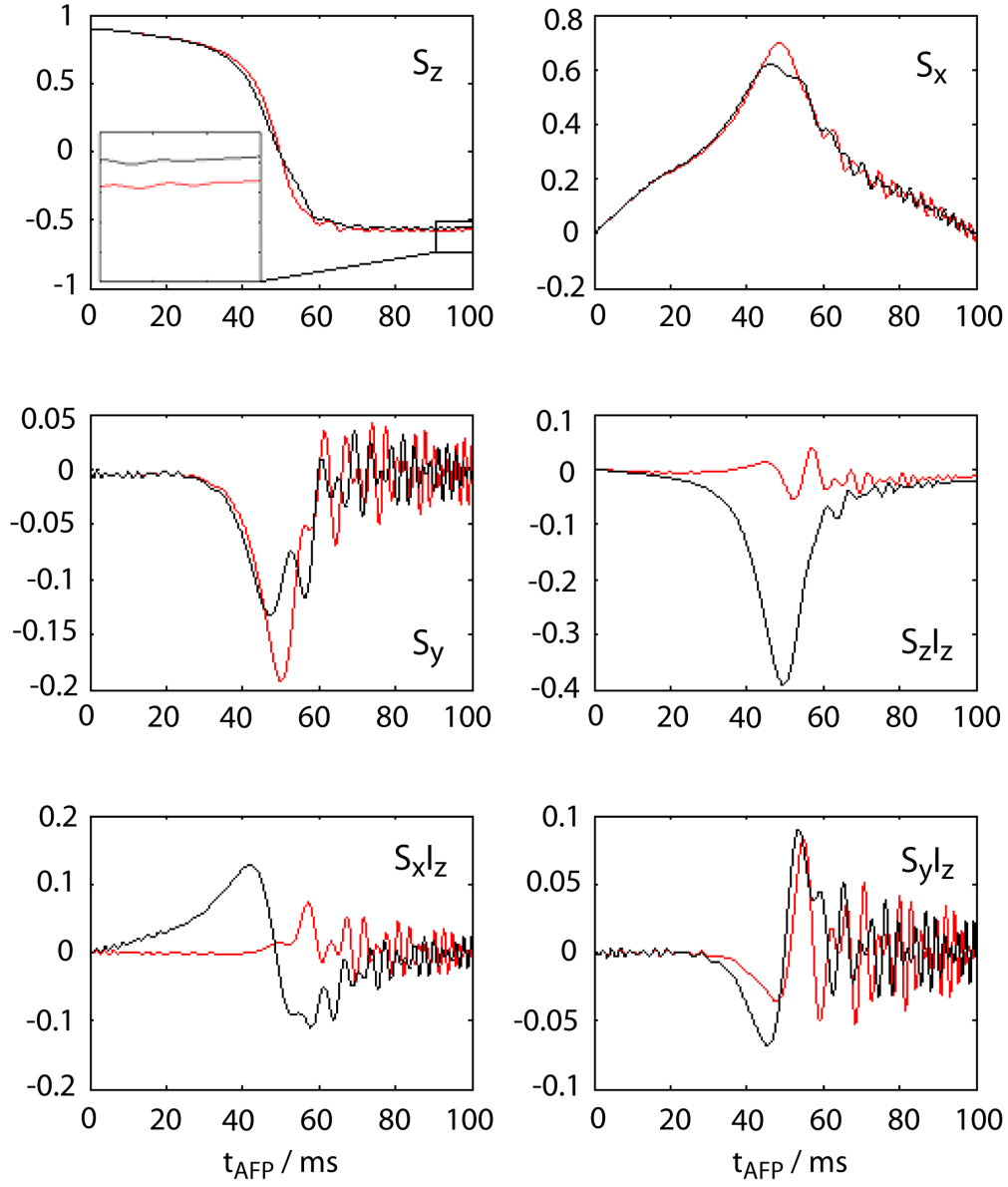


Figure 2.5: Full time evolution of all product operator terms. Exchange parameters $k_{ex} = 1000\text{s}^{-1}$, $p_B = 10\%$, $\Delta\varpi = 1\text{ppm}$. ν_{sweep} is 1kHz and ω_1 as 80Hz. Note the different scaling on the y-axes. Black: full analytical simulation, red: analytical simulation neglecting the $S'_x I_z$ -term.

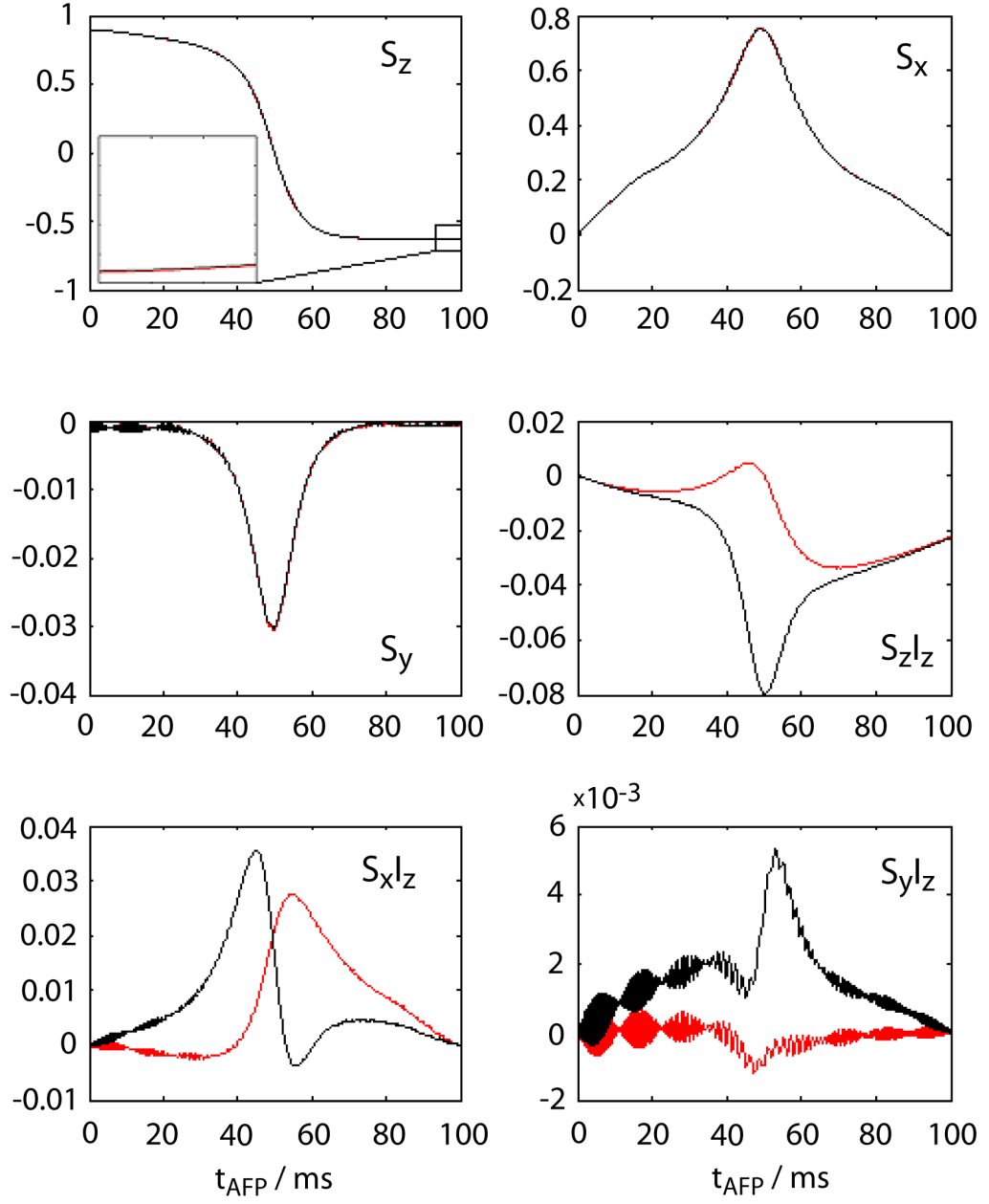


Figure 2.6: Full time evolution of all product operator terms. Exchange parameters $k_{ex} = 1000\text{s}^{-1}$, $p_B = 10\%$, $\Delta\varpi = 1\text{ppm}$. ν_{sweep} is as 5kHz and ω_1 as 425Hz. Note the different scaling on the y-axes. Black: full analytical simulation, red: analytical simulation neglecting the $S'_x I_z$ -term. The insert is scaled as in figure 2.5.

The computation is split in two parts: (I) the coherent and (II) the relaxation part. **(I)** The density matrix is calculated in a step-wise manner (equivalently to the numerical method) incorporating all terms of eq. (2.26)

1. Rotation of the density matrix into the tilted frame by the equation

$$\sigma(t_i)' = \mathbf{U}\sigma(t_i)\mathbf{U}^{-1} \quad (2.28)$$

2. Calculation of the next time step using the tilted-frame Hamiltonian

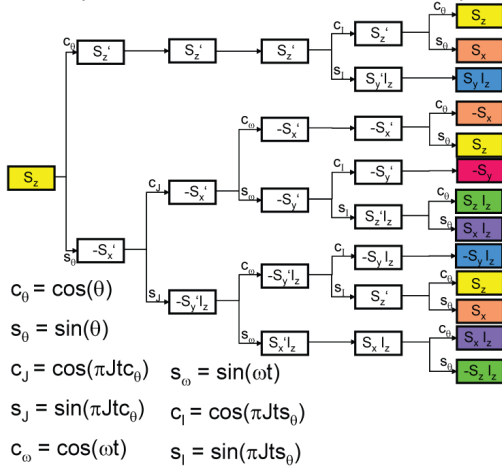
$$\sigma(t_{i+1})' = \exp(-i\mathbf{H}'_{i+1})\sigma(t_i)\exp(i\mathbf{H}'_{i+1}) \quad (2.29)$$

3. Rotation back into the doubly rotating frame

$$\sigma(t_{i+1}) = \mathbf{U}^{-1}\sigma(t_{i+1})'\mathbf{U} \quad (2.30)$$

First Step

1) $-S_y$ 2a) $S_z'l_z$ 2b) S_z' 2c) $-S_x'l_z$ 3) S_y



$$A_1 = A_0 (c_\theta^2 c_1 + s_\theta^2 c_J c_\omega + s_\theta c_\theta s_J s_\omega) \quad \text{Yellow box } S_z$$

$$B_1 = A_0 (c_\theta s_\theta c_1 - s_\theta c_\theta c_J c_\omega + s_\theta^2 s_J s_\omega) \quad \text{Orange box } S_x$$

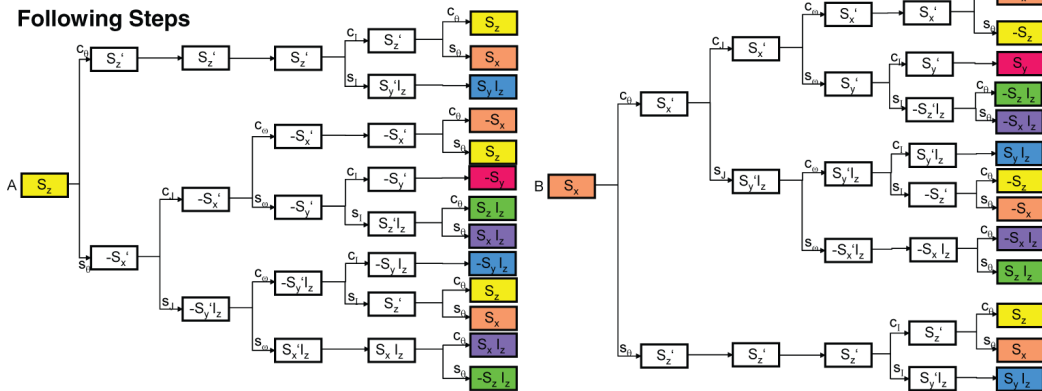
$$C_1 = A_0 (-s_\theta c_J c_\omega) \quad \text{Pink box } S_y$$

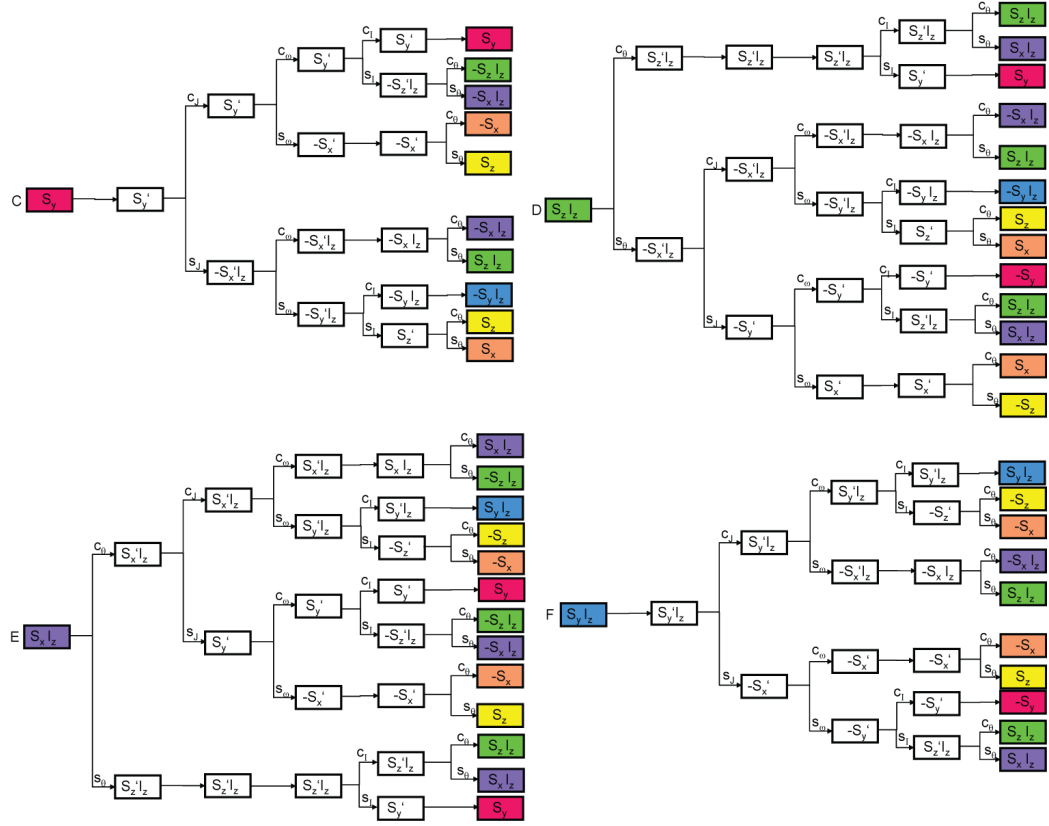
$$D_1 = A_0 (-s_\theta^2 s_J s_\omega + s_\theta c_\theta s_J c_\omega) \quad \text{Green box } 2S_z'l_z$$

$$E_1 = A_0 (c_\theta s_\theta s_J s_\omega + s_\theta^2 s_J c_\omega) \quad \text{Purple box } 2S_x'l_z$$

$$F_1 = A_0 (-s_\theta c_J s_\omega + c_\theta s_J) \quad \text{Blue box } 2S_y'l_z$$

Following Steps





	S_z A_i	S_x B_i	S_y C_i	$S_z I_z$ D_i	$S_x I_z$ E_i	$S_y I_z$ F_i
S_z A_{i+1}	$C_0^2 C_1 + S_0^2 C_J C_\omega + S_0 C_0 S_J S_J C_\omega$	$C_0 S_0 C_1 - C_0 S_0 C_J C_\omega + C_0^2 S_J S_J C_\omega$	$S_0 C_J S_\omega + C_0 S_J S_J S_\omega$	$-S_0^2 S_J S_\omega + C_0 S_0 S_J C_J S_\omega$	$C_0 S_0 S_J S_\omega - C_0^2 S_J C_J S_\omega$	$S_0 S_J C_\omega - C_0 S_J C_J C_\omega$
S_x B_{i+1}	$C_0 S_0 C_1 - C_0 S_0 C_J C_\omega + S_0^2 S_J S_J C_\omega$	$C_0^2 C_J C_\omega + S_0^2 C_1 - C_0 S_0 S_J S_J C_\omega$	$-C_0 C_J S_\omega + S_0 S_J S_J S_\omega$	$C_0 S_0 S_J S_\omega + S_0^2 S_J C_J S_\omega$	$-C_0^2 S_J S_\omega - S_0 C_0 S_J C_J S_\omega$	$-C_0 S_J C_\omega - S_0 S_J C_J C_\omega$
S_y C_{i+1}	$-S_0 C_1 C_J S_\omega$	$C_0 C_1 C_J S_\omega$	$C_1 C_J C_\omega$	$-S_0 C_J S_J C_\omega + C_0 S_J$	$C_0 C_J S_J C_\omega + S_0 S_J$	$-C_1 S_J S_\omega$
$S_z I_z$ D_{i+1}	$-S_0^2 S_J S_\omega + S_0 C_0 S_J C_J S_\omega$	$C_0 S_0 S_J S_\omega - C_0^2 C_J S_J S_\omega$	$S_0 S_J C_\omega - C_0 S_J C_J C_\omega$	$C_0^2 C_1 + S_0^2 C_J C_\omega + C_0 S_0 S_J S_J C_\omega$	$C_0 S_0 C_1 - C_0 S_0 C_J C_\omega - C_0^2 S_J S_J C_\omega$	$S_0 C_J S_\omega + C_0 S_J S_J S_\omega$
$S_x I_z$ E_{i+1}	$C_0 S_0 S_J S_\omega + S_0^2 S_J C_J S_\omega$	$-C_0^2 S_J S_\omega - C_0 S_0 S_J C_J S_\omega$	$-C_0 S_J C_\omega - S_0 S_J C_J C_\omega$	$C_0 S_0 C_1 - C_0 S_0 C_J C_\omega + S_0^2 S_J S_J C_\omega$	$C_0^2 C_J C_\omega + S_0^2 C_1 - S_0 C_0 S_J S_J C_\omega$	$-C_0 C_J S_\omega + S_0 S_J S_J S_\omega$
$S_y I_z$ F_{i+1}	$-S_0 C_J S_J C_\omega + C_0 S_J$	$C_0 C_J S_J C_\omega + S_0 S_J$	$-C_1 S_J S_\omega$	$-S_0 C_J C_J S_\omega$	$C_0 C_J C_J S_\omega$	$C_1 C_J C_\omega$

Figure 2.7: Magnetization transfer during an AFP time step.

The density matrix for $t = 0$ corresponds to S_z magnetization, i.e. in the first calculation step only this magnetization component has to be considered. During the first step S_x , S_y , $S_x I_z$, $S_y I_z$, and $S_z I_z$ are generated by the AFP. It is shown in figure 2.7 that the magnetization subspace is entirely covered by these operators.

(II) This treatment, however, includes only J-coupling and chemical shift evolution (i.e. coherent evolution). Neither relaxation nor chemical exchange nor CSA-DD cross correlation are explicitly considered. In order to include them, after every time step CSA-DD cross correlation, relaxation, and chemical exchange are introduced utilizing the analytical solution for the following mathematical problem:

$$\frac{dM(t)}{dt} = \mathbf{A}M_0 \quad (2.31)$$

$$\mathbf{A} = \begin{pmatrix} a & b \\ c & d \end{pmatrix} \quad (2.32)$$

where \mathbf{A} represents a certain relaxation mechanism. In order to solve the above differential equation \mathbf{A} has to be diagonalized, i.e.

$$\frac{dM(t)}{dt} = \mathbf{A}M_0 = \mathbf{U}\mathbf{U}^{-1}\mathbf{A}\mathbf{U}\mathbf{U}^{-1}M_0 = \mathbf{U}\mathbf{D}\mathbf{U}^{-1}M_0 \quad (2.33)$$

$$M(t) = \mathbf{U} \exp(\mathbf{D}t) \mathbf{U}^{-1} M_0. \quad (2.34)$$

\mathbf{U} is the normalized matrix of *Eigenvectors*. Calculation of the *Eigenvalues* λ

$$\begin{vmatrix} a - \lambda & b \\ c & d - \lambda \end{vmatrix} = 0 \quad (2.35)$$

$$(a - \lambda)(d - \lambda) - bc = 0 \quad (2.36)$$

$$\lambda^2 - \lambda(a + d) + (ad - bc) = 0 \quad (2.37)$$

$$\lambda_{1,2} = \frac{1}{2} \left(a + d \pm \sqrt{(a + d)^2 - 4(ad - bc)} \right) \quad (2.38)$$

gives the *Eigenvectors*

$$(a - \lambda)x_1 + bx_2 = 0 \quad (2.39)$$

$$cx_1 + (d - \lambda)x_2 = 0 \quad (2.40)$$

$$\Rightarrow x_1 = 1 \quad x_2 = -\frac{a - \lambda}{b}. \quad (2.41)$$

resulting in the matrix of *Eigenvectors* $\begin{pmatrix} 1 & 1 \\ -\frac{a-\lambda_1}{b} & -\frac{a-\lambda_2}{b} \end{pmatrix}$ which can be normalized to

$$\mathbf{U} = \begin{pmatrix} \frac{1}{\sqrt{1+\left(\frac{a-\lambda_1}{b}\right)^2}} & \frac{1}{\sqrt{1+\left(\frac{a-\lambda_2}{b}\right)^2}} \\ -\frac{a-\lambda_1}{b\sqrt{1+\left(\frac{a-\lambda_1}{b}\right)^2}} & -\frac{a-\lambda_2}{b\sqrt{1+\left(\frac{a-\lambda_2}{b}\right)^2}} \end{pmatrix} = \begin{pmatrix} u_{11} & u_{12} \\ u_{21} & u_{22} \end{pmatrix} \quad (2.42)$$

$$\mathbf{U}^{-1} = \frac{1}{u_{11}u_{22} - u_{12}u_{21}} \begin{pmatrix} u_{22} & -u_{12} \\ -u_{21} & u_{11} \end{pmatrix}. \quad (2.43)$$

Diagonalization of a matrix is essential for the calculation of the matrix-exponential, because only for diagonal matrixes

$$\mathbf{D} = \begin{pmatrix} d_{11}t & 0 \\ 0 & d_{22}t \end{pmatrix} = \begin{pmatrix} \lambda_1 t & 0 \\ 0 & \lambda_2 t \end{pmatrix} \quad (2.44)$$

the following equation holds

$$\exp(\mathbf{D}t) = \begin{pmatrix} e^{d_{11}t} & 0 \\ 0 & e^{d_{22}t} \end{pmatrix} = \begin{pmatrix} e^{\lambda_1 t} & 0 \\ 0 & e^{\lambda_2 t} \end{pmatrix} = \begin{pmatrix} L_1 & 0 \\ 0 & L_2 \end{pmatrix} \quad (2.45)$$

with $\lambda_{1,2}$ being the *Eigenvalues* of the matrix. The magnetization after a time step t is therefore calculated by

$$\begin{aligned} M(t) &= \mathbf{U} \exp(\mathbf{D}t) \mathbf{U}^{-1} M_0 \quad (2.46) \\ &= \frac{1}{x_{11}x_{22} - x_{12}x_{21}} \begin{pmatrix} x_{11} & x_{12} \\ x_{21} & x_{22} \end{pmatrix} \begin{pmatrix} L_1 & 0 \\ 0 & L_2 \end{pmatrix} \begin{pmatrix} x_{22} & -x_{12} \\ -x_{21} & x_{11} \end{pmatrix} \begin{pmatrix} M_A^0 \\ M_B^0 \end{pmatrix} \\ &= \frac{1}{x_{11}x_{22} - x_{12}x_{21}} \begin{pmatrix} x_{11}L_1 & x_{12}L_2 \\ x_{21}L_1 & x_{22}L_2 \end{pmatrix} \begin{pmatrix} x_{22} & -x_{12} \\ -x_{21} & x_{11} \end{pmatrix} \begin{pmatrix} M_A^0 \\ M_B^0 \end{pmatrix} \\ &= \frac{1}{x_{11}x_{22} - x_{12}x_{21}} \begin{pmatrix} x_{11}x_{22}L_1 - x_{12}x_{21}L_2 & -x_{11}x_{12}L_1 + x_{12}x_{11}L_2 \\ x_{21}x_{22}L_1 - x_{21}x_{22}L_2 & -x_{21}x_{12}L_1 + x_{11}x_{22}L_2 \end{pmatrix} \begin{pmatrix} M_A^0 \\ M_B^0 \end{pmatrix} \end{aligned}$$

In particular longitudinal components of the density matrix are affected by:

- Longitudinal relaxation and exchange between S_z -terms

$$\mathbf{A} = \begin{pmatrix} -R_{1,S} - k_{ab} & k_{ba} \\ k_{ab} & -R_{1,S} - k_{ba} \end{pmatrix} \quad M_0 = \begin{pmatrix} S_{z,A} \\ S_{z,B} \end{pmatrix} \quad (2.47)$$

- Longitudinal relaxation and exchange between $S_z I_z$ -terms

$$\begin{aligned} \mathbf{A} &= \begin{pmatrix} -R_{1,S} - R_{1,I} - k_{ab} & k_{ba} \\ k_{ab} & -R_{1,S} - R_{1,I} - k_{ba} \end{pmatrix} \\ M_0 &= \begin{pmatrix} S_z I_{z,A} \\ S_z I_{z,B} \end{pmatrix} \end{aligned} \quad (2.48)$$

- CSA-DD cross-correlation $S_z \leftrightarrow S_z I_z$ for both states A and B

$$\mathbf{A} = \begin{pmatrix} 0 & -G_z \\ -G_z & 0 \end{pmatrix} \quad M_0 = \begin{pmatrix} S_z \\ S_z I_z \end{pmatrix} \quad (2.49)$$

Equivalently, transverse components are treated using:

- Transverse relaxation and exchange between S_x - or S_y -terms

$$\mathbf{A} = \begin{pmatrix} -R_{2,S} - k_{ab} & k_{ba} \\ k_{ab} & -R_{2,S} - k_{ba} \end{pmatrix} \quad M_0 = \begin{pmatrix} S_{x,A} \\ S_{x,B} \end{pmatrix} \\ M_0 = \begin{pmatrix} S_{y,A} \\ S_{y,B} \end{pmatrix} \quad (2.50)$$

- Transverse relaxation and exchange between $S_x I_z$ - or $S_y I_z$ -terms

$$\mathbf{A} = \begin{pmatrix} -R_{2,S} - R_{2,I} - k_{ab} & k_{ba} \\ k_{ab} & -R_{2,S} - R_{2,I} - k_{ba} \end{pmatrix} \quad (2.51)$$

$$M_0 = \begin{pmatrix} S_x I_{z,A} \\ S_x I_{z,B} \end{pmatrix} \\ M_0 = \begin{pmatrix} S_y I_{z,A} \\ S_y I_{z,B} \end{pmatrix} \quad (2.52)$$

- CSA-DD cross-correlation $S_x \leftrightarrow S_x I_z$ or $S_y \leftrightarrow S_y I_z$ for both exchanging states A and B

$$\mathbf{A} = \begin{pmatrix} 0 & G_x \\ G_x & 0 \end{pmatrix} \quad M_0 = \begin{pmatrix} S_x \\ S_x I_z \end{pmatrix} \\ M_0 = \begin{pmatrix} S_y \\ S_y I_z \end{pmatrix} \quad (2.53)$$

Chapter 3

NOE and ROE Effects

3.1 Introduction

The nuclear Overhauser effect (NOE) [31] is a transfer of magnetization that does not occur through bonds but through space. This relaxation mechanism is triggered by neighbouring dipoles, i.e. NMR-active spins, and is therefore often referred to as dipole-dipole relaxation. NOE measurements are used primarily for structure determination since it allows the extraction of distance information. In recent years a number of NMR experiments based on NOE and/or ROE have been developed (STD [32], INPHARMA [33], SALMON [34]) that provide information about protein-ligand complexes in the form of binding modes and relative orientation.

A 1D NOE experiment consists of a selective 180° pulse followed by a mixing time τ_m and the read-out pulse. During τ_m the following magnetization transfer occurs:

$$-I_{1z} \xrightarrow{\tau_m} -\sum_{k=1}^K a_{1k} I_{kz}.$$

This means, the magnetization is transferred from spin 1 to all other spins ($2, 3, \dots, K-1, K$) that are close in space (close means at a distance less than approx. 5\AA). a_{1k} represents the fraction of magnetization transferred from the 1st to the kth spin. The experiment is set up as a difference experiment with and without the first pulse. This leads to subtraction of all resonances that are not inverted and thus results in a simplified spectrum where only the peak of the source spin and the enhanced signals of its NOE-partners are visible.

Extension to a two-dimensional experiment is straightforward [35]: after an initial 90° hard pulse followed by the evolution time, a second 90° pulse brings the magnetization along z . At this point the mixing time is implemented fol-

lowed by the read-out pulse. Such a NOESY experiment gives a 2D spectrum with a conventional 1D H-spectrum on the diagonal and cross-peaks between dipolar coupled spin.

However, the spins do not have to be longitudinal in order to transfer magnetization. In a ROESY (rotating-frame nuclear Overhauser spectroscopy) experiment a spin-lock field is applied during the mixing time [36]. In both cases magnetization transfer (considering two spins) before the mixing time is given by [37]:

$$\begin{aligned} I_{1z} \xrightarrow{90_x^\circ} -I_{1y} \xrightarrow{t_1} & -I_{1y} \cos(\omega t_1) \cos(\pi J t_1) + 2I_{1x}I_{2z} \cos(\omega t_1) \sin(\pi J t_1) \\ & + I_{1x} \sin(\omega t_1) \cos(\pi J t_1) + 2I_{1y}I_{2z} \sin(\omega t_1) \sin(\pi J t_1) \\ \xrightarrow{90_x^\circ} & -I_{1z} \cos(\omega t_1) \cos(\pi J t_1) - 2I_{1x}I_{2y} \cos(\omega t_1) \sin(\pi J t_1) \\ & + I_{1x} \sin(\omega t_1) \cos(\pi J t_1) - 2I_{1z}I_{2y} \sin(\omega t_1) \sin(\pi J t_1) \end{aligned}$$

In a NOESY all terms except I_{1z} are experimentally suppressed with phase cycling or pulse field gradients. In a ROESY a spin-lock field from x with spin-lock angle θ is applied at this point. All y -operators are thereby dephased by rf-inhomogeneity and do not have to be considered. x and z operators are now transformed into the tilted-frame by rotation along $-I_y$, i.e. $\exp(i\theta_1 I_y) B \exp(-i\theta_1 I_y)$:

$$\begin{aligned} & -I_{1z} \cos(\omega t_1) \cos(\pi J t_1) + I_{1x} \sin(\omega t_1) \cos(\pi J t_1) \\ \xrightarrow{\text{tilting frame}} & -(I'_{1z} \cos \theta_1 - I'_{1x} \sin \theta_1) \cos(\omega t_1) \cos(\pi J t_1) \\ & + (I'_{1x} \cos \theta_1 + I'_{1z} \sin \theta_1) \sin(\omega t_1) \cos(\pi J t_1) \end{aligned}$$

Only the I'_z terms commute with the spin-lock Hamiltonian in the tilted frame ($\mathbf{H}' = \omega_1 I'_z$ ignoring scalar coupling). During τ_m cross-relaxation occurs

$$-I'_{1z} \cos(\omega t_1 + \theta_1) \cos(\pi J t_1) \xrightarrow{\tau_m} -\sum_{k=1}^K a_{1k} I'_{kz} \cos(\omega t_1 + \theta_1) \cos(\pi J t_1).$$

Transformation back into the rotating (not tilted) frame and the application of the read-out pulse yields

$$\begin{aligned} & -\sum_{k=1}^K a_{1k} (I_{kz} \cos \theta_k + I_{kx} \sin \theta_k) \cos(\omega t_1 + \theta_1) \cos(\pi J t_1) \\ \xrightarrow{90_x^\circ} & \sum_{k=1}^K a_{1k} (I_{ky} \cos \theta_k - I_{kx} \sin \theta_k) \cos(\omega t_1 + \theta_1) \cos(\pi J t_1). \end{aligned}$$

For like spins NOE (σ_{NOE}) and ROE (σ_{ROE}) as well as auto-relaxation (R_1) and transverse relaxation (R_2), NOE and ROE enhancements (η_{NOE}, η_{ROE}) are given by [37]

$$\sigma_{NOE} = \frac{\mu_0^2 \hbar^2 \gamma_H^4}{64\pi^2 r^6} [-J(0) + 6J(2\omega_0)] \quad (3.1)$$

$$\sigma_{ROE} = \frac{\mu_0^2 \hbar^2 \gamma_H^4}{64\pi^2 r^6} [2J(0) + 3J(2\omega_0)] \quad (3.2)$$

$$R_1 = \frac{\mu_0^2 \hbar^2 \gamma_H^4}{64\pi^2 r^6} [J(0) + 3J(\omega_0) + 6J(2\omega_0)] \quad (3.3)$$

$$R_2 = \frac{\mu_0^2 \hbar^2 \gamma_H^2}{64\pi^2 r_{HH}^6} (5/2J(0) + 9/2J(\omega_0) + 3J(2\omega_0)) \quad (3.4)$$

$$\eta_{NOE} = \frac{\sigma_{NOE}}{R_1} = \frac{-J(0) + 6J(2\omega_0)}{J(0) + 3J(\omega_0) + 6J(2\omega_0)} \quad (3.5)$$

$$\eta_{ROE} = \frac{\sigma_{ROE}}{R_1} = \frac{2J(0) + 3J(2\omega_0)}{J(0) + 3J(\omega_0) + 6J(2\omega_0)} \quad (3.6)$$

with vacuum permeability μ_0 , reduced Planck constant \hbar , ^1H gyromagnetic ratio γ_H and the ^1H Larmor frequency ω_0 . $J(\omega)$ is the spectral density at frequency ω and is commonly defined by the Lipari-Szabo model free approach [38, 39]

$$J(\omega) = \frac{2}{5} \frac{\tau_c}{1 + \omega^2 \tau_c^2}. \quad (3.7)$$

This equation holds in the absence of local motion. τ_c is the rotational correlation time. Therefore equations (3.5) and (3.6) can be recast as a function of τ_c (which depends on the size of the molecule, the viscosity of the solvent, and the temperature) as well as the spectrometer frequency.

$$\eta_{NOE} = \frac{-1 + \frac{6}{1+4\omega_0^2 \tau_c^2}}{1 + \frac{3}{1+\omega_0^2 \tau_c^2} + \frac{6}{1+4\omega_0^2 \tau_c^2}} \quad (3.8)$$

$$\eta_{ROE} = \frac{2 + \frac{3}{1+\omega_0^2 \tau_c^2}}{1 + \frac{3}{1+\omega_0^2 \tau_c^2} + \frac{6}{1+4\omega_0^2 \tau_c^2}} \quad (3.9)$$

In the context of my thesis there are several features of NOE and ROE enhancement important (see also figure 3.1):

- For large molecules (like proteins) in the spin diffusion limit ($\omega_0 \tau_c \gg 1$) NOE and ROE differ in sign. As a consequence, if longitudinal and transverse cross relaxation are mixed, the effects partially cancel out. Maximum NOE enhancement is -100%, maximum ROE enhancement is 200%.

- For small molecules in the extreme narrowing limit ($\omega_0\tau_c \ll 1$) NOE and ROE enhancements are of the same sign and magnitude (50%).
- σ_{NOE} as well as η_{NOE} are zero for $\omega_0\tau_c = 1.12$.

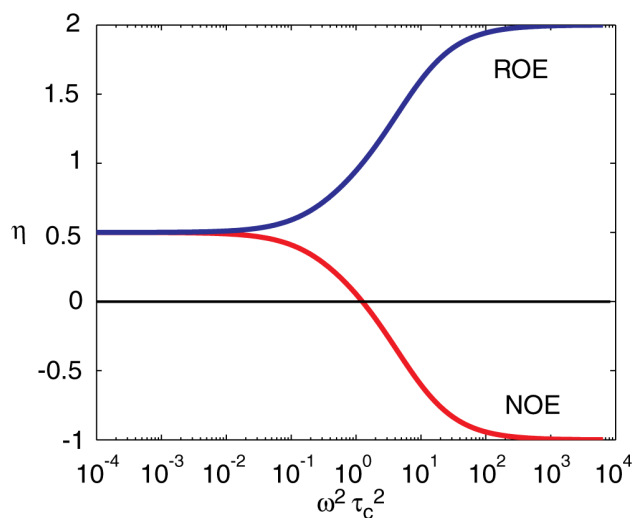


Figure 3.1: NOE and ROE enhancement vs $\omega^2\tau_c^2$. Note the logarithmic scale on the y-axis.

3.2 AFP in NOESY

Application of an AFP pulse during the NOESY mixing time leads to the simultaneous presence of NOE and ROE effects. Their respective weights are time-dependent (i.e. they go from purely longitudinal to purely transverse cross-relaxation and back in the course of the pulse), but its net effect can be expressed by the effective tilt angle θ_{eff} . Effective cross-relaxation between two spins i and j is given by [37]

$$\sigma_{eff}^{i,j} = \sigma_{NOE} \cos \theta_{i,eff} \cos \theta_{j,eff} + \sigma_{ROE} \sin \theta_{i,eff} \sin \theta_{j,eff} \quad (3.10)$$

$$= \frac{\sin \theta_{i,eff} \sin \theta_{j,eff}}{\sin^2 \theta} (\sigma_{NOE} \cos^2 \theta + \sigma_{ROE} \sin^2 \theta) \quad (3.11)$$

$$\theta_{eff} = \arctan \sqrt{\tan \theta_{i,eff} \tan \theta_{j,eff}} \quad (3.12)$$

θ_{eff} increases with the power of the applied spin-lock field as the magnetization vector spends a larger fraction of the total pulse duration in the transverse plane.

In the slow tumbling regime ($\omega_0 \tau_c > \sqrt{5/2}$), NOE and ROE display different signs. This means that there is an angle θ_0 , for which the two effects cancel.

$$\sigma_{eff}^{i,j} = \frac{\sin \theta_{i,eff} \sin \theta_{j,eff}}{\sin^2 \theta} (\sigma_{NOE} \cos^2 \theta + \sigma_{ROE} \sin^2 \theta) = 0 \quad (3.13)$$

$$\frac{\sigma_{NOE}}{\sigma_{ROE}} = -\tan^2 \theta_0 \quad (3.14)$$

For slowly tumbling molecules $\frac{\sigma_{NOE}}{\sigma_{ROE}}$ is $-\frac{1}{2}$, which results in a θ_0 of 35.26° . In the fast tumbling regime, on the other hand, NOE and ROE enhancement are virtually the same, and the enhancement does not depend on $\sin^2 \theta_{eff}$.

Figure 3.2 shows the processes during an AFP-NOESY. In a free ligand in solution NOE and ROE enhancement are of the same magnitude and sign. Therefore a signal enhanced by cross-relaxation is in all cases positive with respect to a negative inverted signal and shows no $\sin^2 \theta_{eff}$ dependence. Upon addition of a protein, a ligand that binds reversibly to it, shows macromolecular cross-relaxation behaviour for the duration of binding, which corresponds to an overall increase in cross-relaxation with the NOE changing sign. This results in a strong $\sin^2 \theta_{eff}$ dependence with the signals being negative initially, when mostly NOE enhancement takes place. The zero crossing angle θ^0 depends on parameters such as protein concentration but, more importantly, on internal mobility and spin-diffusion effects, with the latter depending on the proton density in the binding pocket.

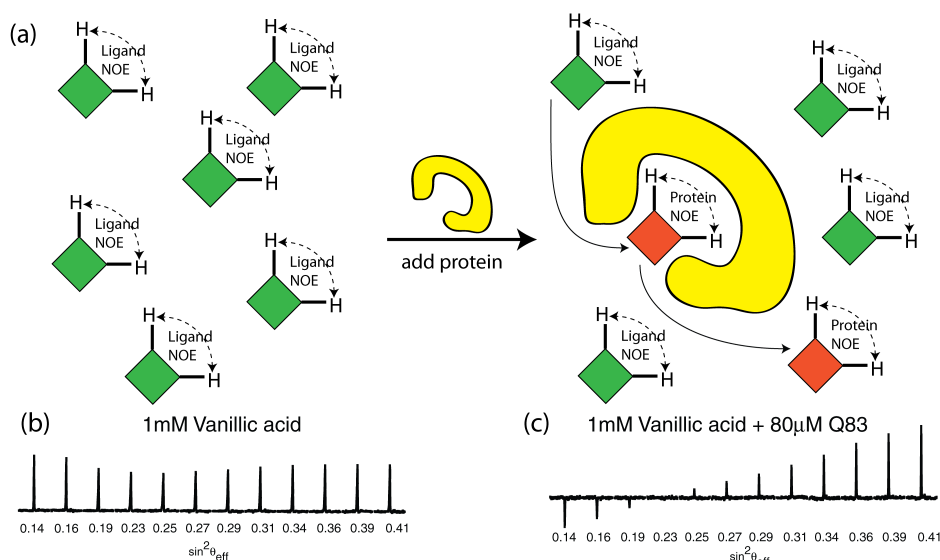


Figure 3.2: Schematic representation of the processes during an AFP-NOESY. The cross-relaxation between two ligand protons is modulated by reversible binding to a protein. Note that peak positions remain unchanged since the ligand is in large excess with respect to the added protein.

3.2.1 AFP-NOESY Experiments

The experiments were conducted generally in a 1D manner. The pulse sequence is given in figure 3.3.

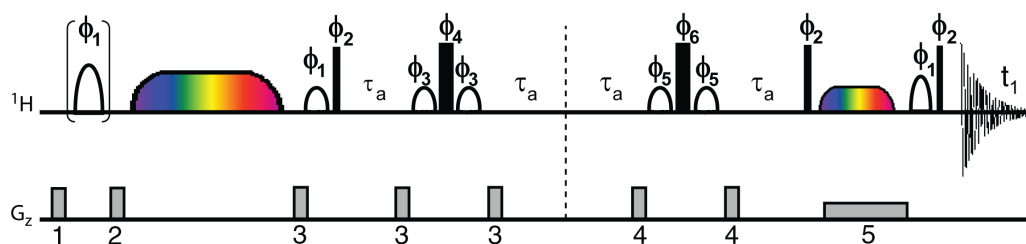


Figure 3.3: Pulse scheme for measuring a 1D NOESY with an AFP during mixing time. For further details see Supporting Information of Paper I.

A 2D version (figure 3.4) was measured in order to obtain a distribution of zero crossing angles in non-ideal spin systems, as they are affected by internal mobility and spin diffusion. In particular, if at a given protein concentration the zero-crossing angles of two enhanced signals differ significantly, it can be

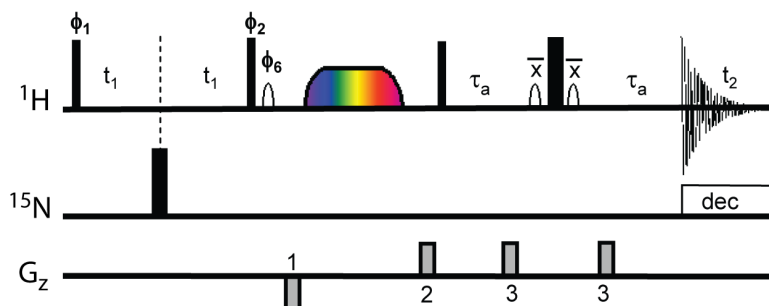


Figure 3.4: Pulse scheme for measuring a 2D NOESY with an AFP during mixing time. Phase cycle: $\phi_1 = x, 2(-x), x, y, 2(-y), y$; $\phi_2 = 2(x), 2(-x), 2(y), 2(-y)$; $\phi_6 = -x, 2(x), -x, -y, 2(y), -y$; receiver $x, -x$.

either due to internal mobility that results in a $\sin^2 \theta^0$ smaller than expected or due to spin-diffusion that gives a $\sin^2 \theta^0$ larger than expected.

We recorded a 2D AFP-NOESY on the quail lipocalin Q83. The measurements show as expected negative cross peaks for small effective tilt angles (referenced to negative diagonal peaks). With increasing tilt angle, the cross peaks lose intensity, cross zero and become positive for large tilt angles. The histogram of zero passage tilt angles (figure 3.5) clearly shows a broad distribution around the theoretical θ^0 value of 35.3° , with significant deviations toward both sides.

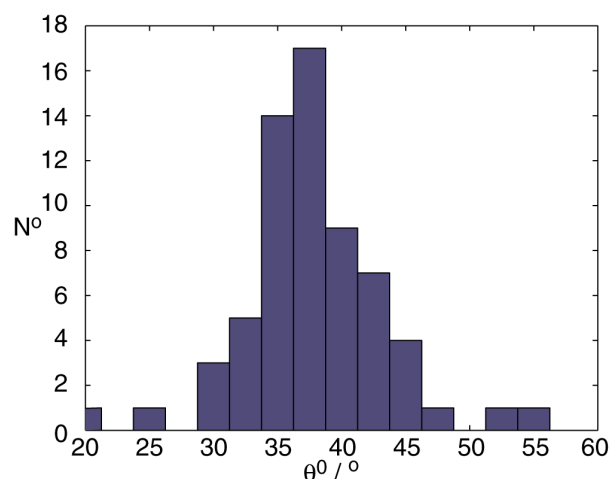


Figure 3.5: A histogram of 66 cross-peaks from a 2D AFP-NOESY of the Q83-Enterobactin system at 37°C . Out of 80 signals analysed, 14 show no zero-crossing while the rest shows θ^0 -values between 20 and 55° .

While internal mobility reduces the effective correlation time relevant for the time modulation of the internuclear vector and leads to a zero passage at smaller tilt angles, spin diffusion causes the opposite effect and often leads to larger zero passage tilt angles. Spin-diffusion affects a proton during an AFP-NOESY sequence in a way that magnetization enhancement due to cross-relaxation fades out resulting either in the lack of zero-crossing upon switching from the NOE to the ROE regime or in zero-crossing angles θ^0 larger than 35.3° . Simulations of such spin-diffusion effects and internal mobility confirm experimental findings.

3.2.2 The Effect of Internal Mobility

Simulations of AFP-NOESY effects carried out in the framework of this thesis are based on solving the Liouvillian equation numerically. General simulation procedures have been introduced in chapter 2.2 while a more detailed description of this particular method can be found in Supporting Information of Paper I. All simulations shown here compute intensities normalized with respect to the inverted signal (Δ_{NOE}).

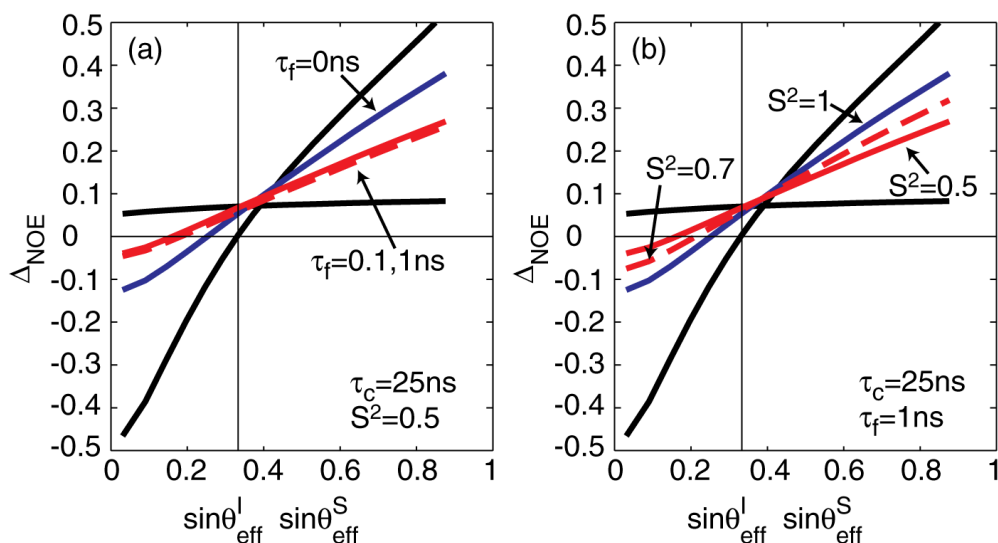


Figure 3.6: The black lines represent intensities obtained in the absence of local motion for a fast and a slowly tumbling molecule, respectively. (a) The effect of τ_f on the $\sin^2 \theta$ -dependence. $\tau_f = 0$ (blue), 0.1 ns (red, dashed), 1 ns (red, solid). The AFP was 400 ms with 10 kHz frequency sweep and 10% ramping at both ends. (b) The effect of S^2 . The AFP parameters are the same as in (a).

Figure 3.6 shows that internal mobility results in zero-crossing angles $\theta^0 < 35.3^\circ$. To calculate the effect of internal mobility we employed instead of eq. (3.7) (see Supporting Information of Paper I) an extended expression for the spectral density function $J(\omega)$ where local motions are not neglected

$$J(\omega) = \frac{2}{5} \left(\frac{S^2 \tau_c}{1 + \omega^2 \tau_c^2} + \frac{(1 - S^2) \tau}{1 + \omega^2 \tau^2} \right) \quad (3.15)$$

with $\tau = \tau_c \tau_f / (\tau_c + \tau_f)$ where τ_f is the correlation time of the faster motion. The time constant representing internal mobility, τ_f , has to be at least one order of magnitude smaller than the overall correlation time τ_c . In the absence of internal motion $S^2 = 1$, and eq. 3.15 reduces to eq. 3.7. In the case where the internal mobility is isotropic, $S^2 = 0$. For realistic scenarios $S^2 \geq 0.5$ can be assumed. In well defined secondary structure elements order parameters are typically around 0.8.

3.2.3 The Effect of Spin Diffusion

We have measured AFP-NOESY of the system $\text{NAD}^-/4\% \text{ADH}$ (see fig. 3.7). Both ribose H1 protons (I) were inverted, resulting in four resolved cross-peaks in the aromatic region corresponding to the indicated positions 1-4 in fig. 3.7(a). Simulations indicate that no zero-crossing should be observed for this system, a pattern observed for cross-peaks 2 and 3 of NAD^- . However, two resonances start with negative enhancements at low $\sin^2 \theta_{eff}$, one of them showing a defined zero-crossing angle while the other one is approaching. This indicated that both protons 1 and 4 are affected by spin-diffusion due to a higher proton density in the immediate surrounding. Similar results have been obtained for a different system (AMP/ADH), which is discussed in detail in Paper I.

Results of the simulations of spin-diffusion on the AFP-NOESY profile are shown in fig. 3.8. Spin diffusion is introduced in the calculation by extending the Liouvillian matrix by N spins (A_1, A_2, \dots, A_N) connecting spins I (inverted) and S in the following way:

$$\begin{aligned} I_x &\xleftrightarrow{ROE_{IA}} A_{i,x} \xleftrightarrow{ROE_{SA}} S_x \\ I_y &\xleftrightarrow{ROE_{IA}} A_{i,y} \xleftrightarrow{ROE_{SA}} S_y \\ I_z &\xleftrightarrow{NOE_{IA}} A_{i,z} \xleftrightarrow{NOE_{SA}} S_z \end{aligned}$$

A higher proton density in the surrounding of I and S results also in a larger transverse relaxation rate. In order to account for this effect, R_2^0 is

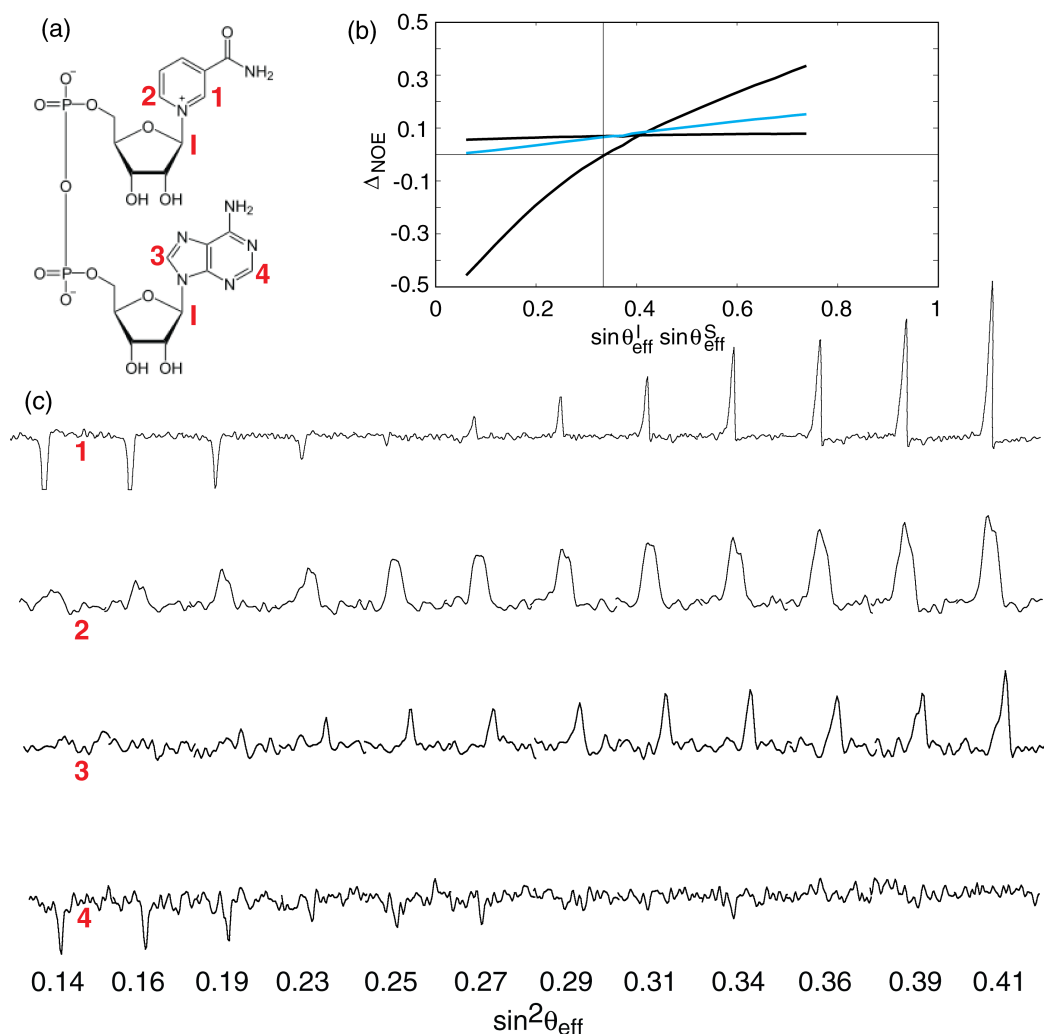


Figure 3.7: (a) Structure of NAD⁺. (b) Simulation of the AFP-NOESY with $\tau_c^{\text{lig}} = 0.3\text{ns}$, $\tau_c^{\text{prot}} = 33\text{ns}$ for the free ligand and the protein (black) and the ligand in solution assuming that 4% of the ligand is in the bound state and that the exchange rate constant is in a regime representing reversible binding ($k_{\text{ex}} = 1000\text{s}^{-1}$). (c) AFP-NOESY traces for NAD⁺ in solution with 4% ADH. H1 of the sugars were selectively inverted. Further information see text.

increased in a physically meaningful manner. It becomes apparent that spin-diffusion results in a shift of the zero-crossing angle towards higher $\sin^2\theta$ values. When a critical proton density is reached, zero-crossing is no longer observed.

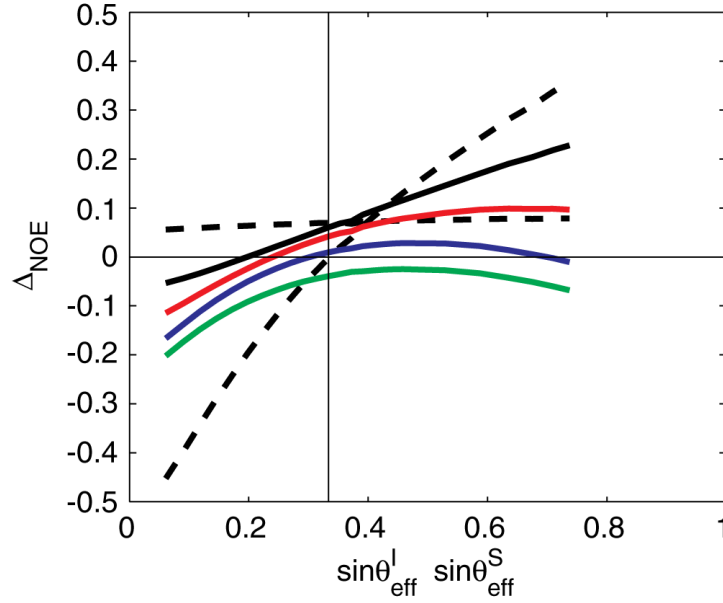


Figure 3.8: Simulation of the effect of spin diffusion on the AFP-NOESY profile. The behavior of a free ligand and a ligand with only macromolecular cross-relaxation properties are shown by the dashed lines with $\tau_c^{lig} = 0.3\text{ns}$, $\tau_c^{prot} = 30\text{ns}$. The solid lines show the AFP-NOESY profile of a ligand in solution with 10% protein. Black: no spin diffusion. Spin diffusion is simulated by adding N spins connecting I and S over one step. To account for the increased transverse relaxation rate when the ligand is surrounded by a high proton density, R_2^0 is multiplied by a . Red: $N=2$, $a=1$. Blue: $N=5$, $a=2$. Green: $N=15$, $a=5$.

3.2.4 The Effect of J-coupling

In a small ligand the inverted spin I and the NOE/ROE enhanced spin S are frequently J-coupled. Since I and S are like spins, strong coupling has to be assumed. Simulations of the effect of J-coupling have been performed using the full Liouvillian matrix (considering dipole-dipole effects only and neglecting CSA terms) for two spins ($N=2$), which is a $4^N \times 4^N = 16 \times 16$ matrix, and, correspondingly, the full density matrix [40]:

$$\sigma(t) = \begin{bmatrix} E/2 & I_x & I_y & I_z & S_x & S_y & S_z & 2I_x S_z \\ 2I_y S_z & 2I_z S_x & 2I_z S_y & 2I_x S_x & 2I_x S_y & 2I_y S_x & 2I_y S_y & 2I_z S_z \end{bmatrix}' \quad (3.16)$$

$$\mathbf{L} = \begin{pmatrix} 0 & 0 & 0 & 0 & 0 & 0 & 0 & 0 & 0 & 0 & 0 & 0 & 0 & 0 & 0 \\ 0 & R_{2I} & \omega_I & 0 & \mu & 0 & 0 & 0 & \pi J & 0 & -\pi J & 0 & 0 & 0 & 0 \\ 0 & -\omega_I & R_{2I} & \omega_x & 0 & \mu & 0 & -\pi J & 0 & \pi J & 0 & 0 & 0 & 0 & 0 \\ -2M_I & 0 & -\omega_x & R_{1I} & 0 & 0 & \sigma & 0 & 0 & 0 & 0 & 0 & \pi J & -\pi J & 0 \\ 0 & \mu & 0 & 0 & R_{2S} & \omega_S & 0 & 0 & -\pi J & 0 & \pi J & 0 & 0 & 0 & 0 \\ 0 & 0 & \mu & 0 & -\omega_S & R_{2S} & \omega_x & \pi J & 0 & -\pi J & 0 & 0 & 0 & 0 & 0 \\ -2M_S & 0 & 0 & \sigma & 0 & -\omega_x & R_{1S} & 0 & 0 & 0 & 0 & 0 & -\pi J & \pi J & 0 \\ 0 & 0 & \pi J & 0 & 0 & -\pi J & 0 & \rho_I^a & \omega_I & \mu^a & 0 & 0 & -\omega_x & 0 & 0 \\ 0 & -\pi J & 0 & 0 & -\pi J & 0 & 0 & -\omega_I & \rho_I^a & 0 & \mu^a & 0 & 0 & 0 & -\omega_x \\ 0 & 0 & -\pi J & 0 & 0 & \pi J & 0 & \mu^a & 0 & \rho_S^a & \omega_S & 0 & 0 & -\omega_x & 0 \\ 0 & \pi J & 0 & 0 & -\pi J & 0 & 0 & 0 & \mu^a & -\omega_S & \rho_S^a & 0 & 0 & 0 & -\omega_x \\ 0 & 0 & 0 & 0 & 0 & 0 & 0 & 0 & 0 & 0 & 0 & \lambda^{xx} & \omega_S & \omega_I & \mu^{xxyy} \\ 0 & 0 & 0 & -\pi J & 0 & 0 & \pi J & \omega_x & 0 & 0 & 0 & -\omega_S & \lambda^{xy} & \mu^{xyyx} & \omega_I \\ 0 & 0 & 0 & \pi J & 0 & 0 & -\pi J & 0 & 0 & \omega_x & 0 & -\omega_I & \mu^{xyyx} & \lambda^{yx} & \omega_S \\ 0 & 0 & 0 & 0 & 0 & 0 & 0 & 0 & \omega_x & 0 & \omega_x & \mu^{xyyx} & -\omega_I & -\omega_S & \lambda^{yy} \\ 0 & 0 & 0 & 0 & 0 & 0 & 0 & 0 & -\omega_x & 0 & -\omega_x & \mu^{xxzz} & 0 & 0 & \mu^{yyzz} \end{pmatrix} \quad (3.17)$$

with

$$M_I = R_{1I}M_{I0} + \sigma M_{S0} \quad (3.18)$$

$$M_S = R_{1I}M_{S0} + \sigma M_{I0} \quad (3.19)$$

$$R_{2I} = R_{2S} = F[5/2J(0) + 9/2J(\omega) + 3J(2\omega)] \quad (3.20)$$

$$R_{1I} = R_{1S} = F[J(0) + 3J(\omega) + 6J(2\omega)] \quad (3.21)$$

$$\mu = F[2J(0) + 3J(2\omega)] \quad (3.22)$$

$$\sigma = F[-J(0) + 6J(2\omega)] \quad (3.23)$$

$$\rho_I^a = \rho_S^a = F[5/2J(0) + 3/2J(\omega) + 3J(2\omega)] \quad (3.24)$$

$$\mu^a = F[2J(0)] \quad (3.25)$$

$$\lambda^{xy} = \lambda^{yx} = F[J(0) + 3J(\omega) + 3J(2\omega)] \quad (3.26)$$

$$\lambda^{xx} = \lambda^{yy} = F[3J(\omega) + 3J(2\omega)] \quad (3.27)$$

$$\rho_{IS}^2 = F[6J(\omega)] \quad (3.28)$$

$$\mu^{xyyx} = F[-J(0) + 3J(2\omega)] \quad (3.29)$$

$$\mu^{xxyy} = F[-3J(2\omega)] \quad (3.30)$$

$$\mu^{xxzz} = \mu^{yyzz} = [-3J(\omega)] \quad (3.31)$$

$$J(\omega) = \frac{2}{5} \frac{\tau_c}{1 + \omega^2 \tau_c^2}$$

$$F = \frac{\mu_0^2 \hbar^2 \gamma^4}{64 \pi^2 r^6} \quad (3.32)$$

The effect of strong J-coupling between the irradiated and the enhanced signal is illustrated in figure 3.9(a). It affects enhancement at large $\sin^2 \theta_{eff}$ values where transverse cross-relaxation dominates resulting in a loss of intensity. In the extreme case of a very large J-coupling constant, the intensity can even become zero and ultimately change sign. In addition, in a model where the selectively inverted spin is dipolar-coupled to a spin, which is in turn J-coupled to a third spin, has been considered. The effect of this is less pronounced than for J-coupled source and enhanced spins, as can be seen from figure 3.9(b). The simulation required the extension of the Liouvillian matrix to completely describe a three-spin system (64x64 matrix).

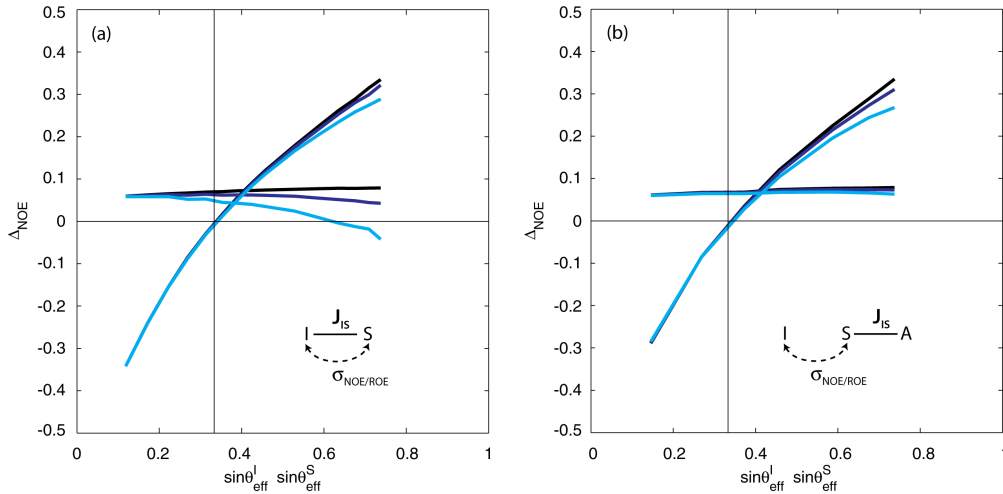


Figure 3.9: The effect of direct and indirect coupling on the enhanced signal for free and bound ligand. (a) The inverted spin is both dipolar-coupled and J-coupled to the enhanced spin. (b) The inverted spin is dipolar coupled to the enhanced spin, which is J-coupled to a third spin. For both plots: $J=0$ (black), 4Hz (blue) and 7Hz (cyan). Distance between source and enhanced spin is 3\AA . $\tau_c^{\text{lig}} = 0.3\text{ns}$, $\tau_c^{\text{prot}} = 33\text{ns}$, $t_{AFP} = 400\text{ms}$, $\nu_{sweep} = 10\text{kHz}$ with 10% ramping.

Chapter 4

Measurement of the Sign of $\Delta\omega$

The NMR spectrum of a protein undergoing chemical exchange between a highly populated ground state G and a low populated excited state E is dominated by the conformation of the major state. The minor state is by all means invisible for NMR since the population is usually very low. However, in many cases the excited state has biological significance and therefore obtaining the structure is vital [41, 42]. A number of highly sophisticated pulse sequences have been developed to probe the excited state, the most fundamental one being CPMG relaxation dispersion. Its utility is severalfold. First, populations of exchanging conformers can be obtained along with rates of exchange [20], so that in cases where experiments are performed as a function of temperature and/or pressure it is possible to generate a detailed one-dimensional energy landscape for the system under study [43, 44]. Second, absolute values of chemical shift differences between exchanging states, $|\Delta\omega|$, are extracted from fits of dispersion profiles. In cases where the sign of $|\Delta\omega|$ is available, the chemical shifts of the excited states can be obtained, thus allowing structure determination of the excited state. Several approaches for obtaining the signs of the chemical shift differences have been developed. The one most commonly used for heteronuclei coupled to a proton was suggested by Skrynnikov *et al.* [16] and is referred to as the H(S/M)QC method. The peak positions in the indirect dimensions of HSQC and HMQC data-sets recorded at several static magnetic fields are compared to isolate the sign information for ^{15}N and ^{13}C values. A second approach, termed CEESY [17], is based on very similar principles except that the sign information is encoded in relative peak intensities of a pair of data-sets. This approach has been applied to obtain the sign of ^{15}N and $^1\text{H}^{\text{N}}$ values. Finally, a third method measures selective $\text{R}_{1\rho}$ relaxation rates as a function of spin-lock offset [18, 19, 45, 46, 47], which can be a sensitive reporter of sign information as well. Another approach to extract sign information for $^1\text{H}^{\text{N}}$ compares zero-quantum and double-quantum

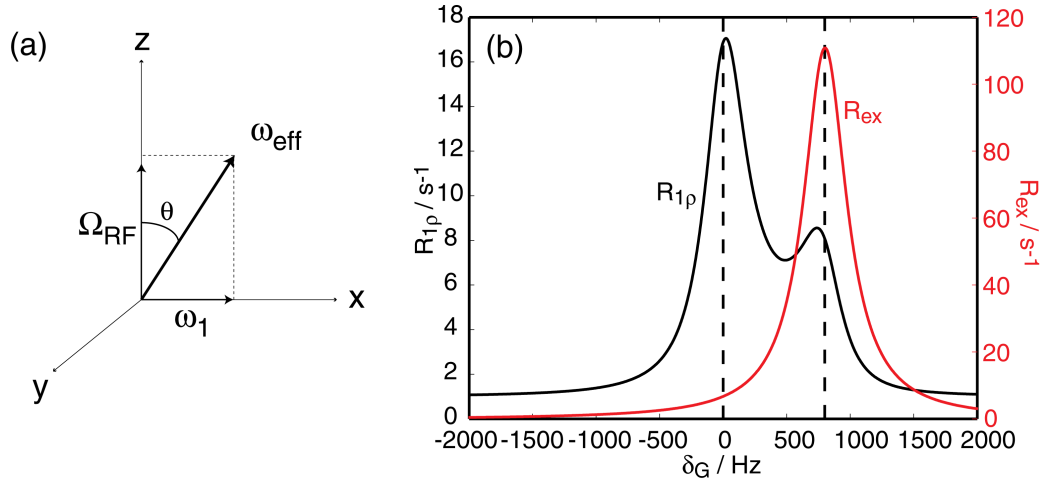


Figure 4.1: (a) Coordinate system in the spin-lock frame. (b) Offset dependence of R_{ex} and $R_{1\rho}$.

$^1\text{H}^N$ - ^{15}N dispersion profiles, where the sign for $^1\text{H}^N$ relative to the sign of ^{15}N can be obtained [48, 49]. The drawbacks of this method are that (a) the sign of ^{15}N has to be known and (b) that $|\Delta\omega(^{15}\text{N})|$ has to be large enough to see a clear difference in the dispersion profiles.

For an exchange reaction between a highly populated ground state (G) and a low populated excited state (E), Trott and Palmer [22] have shown that the relaxation rate in the spin-lock rotating frame, $R_{1\rho}$, is given by eq. (1.9)

$$R_{1\rho} = R_1 \cos^2 \theta + (R_2^0 + R_{ex}) \sin^2 \theta$$

$$R_{ex} = \frac{p_A p_B \Delta\omega^2 k_{ex}}{\omega_{eff}^2 + k_{ex}^2} = \frac{p_A p_B \delta^2 k_{ex}}{(\delta_G + \Delta\omega)^2 + \omega_1^2 + k_{ex}^2}$$

The maximum in R_{ex} occurs when the spin-lock field is on-resonance with the frequency of the minor state (see figure 4.1). The global maximum in $R_{1\rho}$ occurs when the spin-lock is on-resonance with the frequency of the major state (i.e. $\delta_G = 0$, therefore $\sin^2 \theta = 1$ and $\cos^2 \theta = 0$ and $R_2^0 + R_{ex} > R_1$). However, there is a second maximum at the offset of the minor state. Thus by recording a pair of $R_{1\rho}$ decay curves with $\delta_G \approx \pm\Delta\omega$ the sign of $\Delta\omega$ can be determined, since $R_{1\rho}$ -values recorded for $\delta_G = -\Delta\omega$ will be larger than those for $\delta_G = \Delta\omega$.

Experimental details are given in Papers II and III for different nuclei ($^1\text{H}^\alpha$, $^{13}\text{C}^\alpha$, $^1\text{H}^N$). The monoexponential fit of signal intensity *vs* spin-lock

delay allows the extraction of $R_{1\rho}^+$ and $R_{1\rho}^-$. In many cases, the difference in the two relaxation curves is obvious and the sign can be extracted easily. However, Student t-test and f-test statistics were applied in order to check whether the difference in relaxation rates is significant (details in Paper III).

Chapter 5

Summary - Zusammenfassung

5.1 Paper I: NOESY-AFP

English. We have developed a method that allows us to investigate protein-ligand binding using cross-relaxation experiments in combination with adiabatic fast passage (AFP) pulses. Cross-relaxation is a widely used mechanism yielding valuable parameters for structural studies since it can be used to probe the surroundings of any NMR-active nucleus (predominantly protons) within a 5\AA radius. AFP pulses distinguish themselves by their ease of implementation and general advantages, like negligible offset-dependence and a perfect inversion profile. The combination of cross-relaxation and AFP pulses allows us to gain information about the binding epitope including properties such as internal mobility or spin diffusion, which is a direct measure for the surrounding proton density. Epitope mapping provides relevant information for drug development and optimization. We were able to apply this method successfully to several protein-ligand systems (Q83-Vanillic acid, ADH-AMP, ADH-NADH).

Deutsch. Wir haben eine Methode entwickelt, die dazu dient, die Bindung eines Liganden an ein Protein zu untersuchen. Die Messung basiert auf Cross-Relaxation und *adiabatic fast passage* (AFP) Pulsen. Cross-Relaxation ist ein Mechanismus, der wertvolle Informationen für Strukturuntersuchungen liefert. Er kann bei NMR-aktiven Kernen (vorwiegend Protonen) angewandt werden, um deren Umgebung innerhalb eines 5\AA Radius zu studieren. AFP Pulse zeichnen sich durch ihre einfache Handhabung sowie ihre geringe Offset-Abhängigkeit und ihr perfektes Inversionsprofil aus. Die Kombination von Cross-Relaxation und AFP erlaubt es uns, Informationen über die Bindungstasche sowie Daten über interne Mobilität oder Spin Diffusion zu

erhalten, die ein direkter Parameter für die umgebende Protonendichte ist. Die Untersuchung der Bindungstasche und der Wechselwirkungen zwischen Liganden und Proteinen kann äußerst relevante Informationen für Medikamentenentwicklung und -optimierung liefern. Wir konnten diese Methode erfolgreich an verschiedenen Systemen testen (Q83-Vanillinsäure, ADH-AMP, ADH-NADH).

5.2 Papers II and III: Sign of $\Delta\omega$

English. Protein dynamics are involved in many important biological processes, e.g. binding, folding, allostery, molecular recognition and catalysis. Typically, a highly populated conformer exchanges with a low populated, transiently formed state, which is in many cases the biologically relevant one. This excited state can be studied in detail by NMR spectroscopy. CPMG measurements yield the magnitude of $\Delta\omega$, i.e. the chemical shift of the minor species with respect to the chemical shift of the major species, and thus half the information necessary for the reconstruction of the spectrum of the excited state which leads to the determination of its structure. A second method has to be applied in order to obtain the sign of $\Delta\omega$. We have developed an experiment that allows us to measure the sign of $\Delta\omega$ for various NMR-active nuclei. It is based on the spin-lock relaxation rate $R_{1\rho}$. The main advantages of this method with respect to the most commonly used methods for sign determination (H(S/M)QC or the comparison of zero-quantum and double quantum dispersion profiles) are (a) it does not require the $\Delta\omega$ of the coupled nucleus to be different from zero and (b) it works not only for heteronuclei (as does the H(S/M)QC method), but can easily be applied to $^1\text{H}^\alpha$ and $^1\text{H}^N$. The high reliability of this method has been tested on the Abp1p-Ark1p protein-ligand system, where the correct $\Delta\omega$'s including the signs were available.

Deutsch. Proteindynamik ist in viele wichtige biologische Prozesse involviert, wie z.B. Bindung, Faltung, Allosterie, molekulare Erkennung und Katalyse. Typischerweise tauscht ein hoch populierter Grundzustand mit einem gering populierten, sog. angeregten Zustand aus, der wiederum in vielen Fällen von hoher biologischer Relevanz ist. Er kann mittels NMR Spektroskopie genau untersucht werden. CPMG Messungen liefern den Absolutwert von $\Delta\omega$, d.h. die Position der Signale des gering populierten Zustands relativ zu den Signalen des Grundzustands, und daher die eine Hälfte der Information, die nötig ist, um das Spektrum des angeregten Zustandes zu rekonstruieren und damit seine Struktur zu bestimmen. Eine zweite Methode muss angewandt

werden, um das Vorzeichen von $\Delta\omega$ zu erfahren. Wir haben ein Experiment entwickelt, um das Vorzeichen von $\Delta\omega$ für mehrere NMR-aktive Kerne zu messen. Es basiert auf der spin-lock Relaxationsrate $R_{1\rho}$. Die großen Vorteile dieser Methode im Vergleich mit den gebräuchlichsten Methoden (H(S/M)QC oder der Vergleich von Null- und Doppelquanten-Dispersionen) sind, (a) dass das $\Delta\omega$ des gekoppelten Kerns nicht von Null verschieden sein muss und (b) dass sie nicht nur für Heterokerne (wie die H(S/M)QC Methode) sondern auch für $^1\text{H}^\alpha$ und $^1\text{H}^N$ funktioniert. Die hohe Zuverlässigkeit dieser Methode wurde am Protein-Liganden System Abp1p-Ark1p getestet, von dem die korrekten Werte für $\Delta\omega$ und deren Vorzeichen bekannt sind.

Appendix A

Product Operator Formalism

The most commonly used formalism for the description of pulse sequences description are product operators [50]. They are highly suitable for simulations since they can be used intuitively and give the exact pathways of magnetization transfer due to, for instance, shift evolution, J-coupling or relaxation. Product operator transformations can basically be reduced to matrix calculations. A magnetization component B undergoes a transformation due to a certain mechanism represented by the product operator A in the following way:

$$e^{-i\theta A} B e^{i\theta A} = B \cos \theta + C \sin \theta. \quad (\text{A.1})$$

C can be calculated from the following cyclic commutation relationship:

$$[A, B] = iC. \quad (\text{A.2})$$

Exchanging A and B leads to sign change of C . In this simple manner chemical shift evolution, J-coupling, and the effect of radiofrequency pulses can be calculated in a straightforward way. For a two spin system (I and S) the following commutation relations apply [37]

$$[I_x, I_y] = iI_z \quad (\text{A.3})$$

$$[I_\alpha, 2I_\beta S_\gamma] = 2[I_\alpha, I_\beta] S_\gamma \quad (\text{A.4})$$

$$[2I_\alpha S_\gamma, 2I_\beta S_\epsilon] = [I_\alpha, I_\beta] \delta_{\gamma\epsilon} \quad (\text{A.5})$$

$\alpha, \beta, \gamma, \epsilon$ can assume the values x, y, z i.e. the magnetization components; $\delta_{\gamma\epsilon}$ is the Kronecker delta. Relationship (A.3) can be intuitively understood by using the right-handed coordinate system. The right hand thumb shows along axis of the first operator (I_x) and by the rotation of the other fingers it can be seen that I_y transforms to I_z . In the following, mechanisms are related to their pertinent product operators.

Chemical Shift Evolution. $\mathcal{H}_{cs} = \omega I_z$

$$[I_z, I_x] = iI_y \quad (\text{A.6})$$

$$[I_z, I_y] = -iI_x \quad (\text{A.7})$$

$$[I_z, I_z] = 0 \quad (\text{A.8})$$

Weak J-coupling. $\mathcal{H}_J = 2\pi J I_z S_z$

$$[2I_z S_z, I_x] = i2I_y S_z \quad (\text{A.9})$$

$$[2I_z S_z, I_y] = -i2I_x S_z \quad (\text{A.10})$$

$$[2I_z S_z, I_z] = 0 \quad (\text{A.11})$$

Strong J-coupling. $\mathcal{H}_J = 2\pi J(I_x S_x + I_y S_y + I_z S_z)$

$$[2I_x S_x, I_x] = 0 \quad (\text{A.12})$$

$$[2I_x S_x, I_y] = i2I_z S_x \quad (\text{A.13})$$

$$[2I_x S_x, I_z] = -i2I_y S_x \quad (\text{A.14})$$

$$[2I_y S_y, I_x] = -i2I_z S_y \quad (\text{A.15})$$

$$[2I_y S_y, I_y] = 0 \quad (\text{A.16})$$

$$[2I_y S_y, I_z] = i2I_x S_y \quad (\text{A.17})$$

The equations for $I_z S_z$ are given above (weak J-coupling).

Pulse from x-axis. $\mathcal{H}_x = \theta I_x$

$$[I_x, I_x] = 0 \quad (\text{A.18})$$

$$[I_x, I_y] = iI_z \quad (\text{A.19})$$

$$[I_x, I_z] = -iI_y \quad (\text{A.20})$$

Pulse from y-axis. $\mathcal{H}_y = \theta I_y$

$$[I_y, I_x] = iI_z \quad (\text{A.21})$$

$$[I_y, I_y] = 0 \quad (\text{A.22})$$

$$[I_y, I_z] = iI_x \quad (\text{A.23})$$

CSA-DD cross correlation. CSA-DD cross correlation is a relaxation mechanism and therefore computed using double commutators:

$$\left[\frac{2}{\sqrt{6}} I_z, \left[\frac{2}{\sqrt{6}} I_z S_z, B \right] \right] \quad (\text{A.24})$$

$$\left[-\frac{1}{2} I^+, \left[\frac{1}{2} I^- S_z, B \right] \right] \quad (\text{A.25})$$

$$\left[-\frac{1}{2} I^-, \left[-\frac{1}{2} I^+ S_z, B \right] \right] \quad (\text{A.26})$$

The consequence for various operators, i.e. magnetization components, is listed in table A.1. Summing it up, I_x is transferred to $I_x S_z$, I_y to $I_y S_z$, I_z to $-I_z S_z$ and *vice versa*.

Table A.1: Product operator transformation during CSA-DD cross correlation.

B	(A.24)	(A.25)	(A.26)	Sum
I_x	$\frac{2}{3} I_x S_z$	$-\frac{1}{8} I_x S_z - \frac{i}{8} I_y S_z$	$-\frac{1}{8} I_x S_z + \frac{i}{8} I_y S_z$	$\frac{5}{12} I_x S_z$
I_y	$\frac{2}{3} I_y S_z$	$\frac{i}{8} I_x S_z - \frac{1}{8} I_y S_z$	$-\frac{i}{8} I_x S_z - \frac{1}{8} I_y S_z$	$\frac{5}{12} I_y S_z$
I_z	0	$-\frac{1}{4} I_z S_z$	$-\frac{1}{4} I_z S_z$	$-\frac{1}{2} I_z S_z$
$I_x S_z$	$\frac{1}{6} I_x$	$-\frac{1}{32} I_x - \frac{i}{32} I_y$	$-\frac{1}{32} I_x + \frac{i}{32} I_y$	$\frac{5}{48} I_x$
$I_y S_z$	$\frac{1}{6} I_y$	$\frac{i}{32} I_x - \frac{1}{32} I_y$	$-\frac{i}{32} I_x - \frac{1}{32} I_y$	$\frac{5}{48} I_y$
$I_z S_z$	0	$-\frac{1}{16} I_z$	$-\frac{1}{16} I_z$	$-\frac{1}{8} I_z$

Appendix B

Relaxation in the Rotating Frame

In the tilted rotating frame the relaxation rate is given by the average of transverse and longitudinal relaxation rates. For the description of relaxation in the rotating frame two spins I and S can be treated as like spins in the presence of a spin-lock field. The following double commutators have to be calculated [37]:

$$[\mathbf{A}, [\mathbf{A}, I'_z]] = \frac{(5I_x + 4S_x) \sin \theta_I}{24} + \frac{(I_z - S_z) \cos \theta_I}{6} \quad (\text{B.1})$$

$$[\mathbf{B}^*, [\mathbf{B}, I'_z]] = [\mathbf{B}, [\mathbf{B}^*, I'_z]] = -\frac{(2I_x + 2S_x + 2I^-) \sin \theta_I}{8} - \frac{I_z \cos \theta_I}{8} \quad (\text{B.2})$$

$$[\mathbf{C}^*, [\mathbf{C}, I'_z]] = [\mathbf{C}, [\mathbf{C}^*, I'_z]] = -\frac{I^- \sin \theta_I}{8} - \frac{(I_z + S_z) \cos \theta_I}{8} \quad (\text{B.3})$$

with

$$\mathbf{A} = \frac{2}{\sqrt{6}} I_z S_z - \frac{1}{2\sqrt{6}} I^- S^+ - \frac{1}{2\sqrt{6}} I^+ S^- \quad (\text{B.4})$$

$$\mathbf{B} = -\frac{1}{2} I_z S^+ - \frac{1}{2} I^+ S_z \quad (\text{B.5})$$

$$\mathbf{B}^* = \frac{1}{2} I_z S^- + \frac{1}{2} I^- S_z \quad (\text{B.6})$$

$$\mathbf{C} = \frac{1}{2} I^+ S^+ \quad (\text{B.7})$$

$$\mathbf{C}^* = \frac{1}{2} I^- S^- \quad (\text{B.8})$$

$$I'_z = I_x \sin \theta_I + I_z \sin \theta_I \quad (\text{B.9})$$

$$S'_z = S_x \sin \theta_S + S_z \sin \theta_S \quad (\text{B.10})$$

In order to calculate the autorelaxation rate of I , equations (B.1)-(B.3) are premultiplied by I'_z and the trace is calculated to

$$\langle I'_z | (B.1) \rangle = \frac{5}{24} \sin^2 \theta_I + \frac{1}{12} \cos^2 \theta_I \quad (B.11)$$

$$\langle I'_z | (B.2) \rangle = -\frac{3}{16} \sin^2 \theta_I - \frac{1}{8} \cos^2 \theta_I \quad (B.12)$$

$$\langle I'_z | (B.3) \rangle = \frac{1}{8} \sin^2 \theta_I + \frac{1}{4} \cos^2 \theta_I \quad (B.13)$$

The operators **A**, **B**, and **C** give rise to $J(0)$, $J(\omega)$, and $J(2\omega)$ terms, respectively. This results in an autorelaxation rate of:

$$\begin{aligned} R_{1\rho} &= \frac{1}{48} [(2 \cos^2 \theta_I + 5 \sin^2 \theta_I) J(0) + (6 \cos^2 \theta_I + 9 \sin^2 \theta_I) J(\omega) + \\ &\quad (12 \cos^2 \theta_I + 6 \sin^2 \theta_I) J(2\omega)] = \\ &= R_{1I} \cos^2 \theta_I + R_{2I} \sin^2 \theta_I \end{aligned} \quad (B.14)$$

Analogously, the cross-relaxation rate is calculated by premultiplying equations (B.1)-(B.3) by S'_z and forming the trace.

$$\langle S'_z | (B.1) \rangle = \frac{1}{6} \sin \theta_S \sin \theta_I - \frac{1}{12} \cos \theta_S \cos \theta_I \quad (B.15)$$

$$\langle S'_z | (B.2) \rangle = -\frac{1}{8} \sin \theta_S \sin \theta_I \quad (B.16)$$

$$\langle S'_z | (B.3) \rangle = \frac{1}{4} \cos \theta_S \cos \theta_I \quad (B.17)$$

The cross-relaxation rate is then given by

$$\begin{aligned} \sigma_{eff} &= \frac{1}{24} [(-\cos \theta_S \cos \theta_I + 2 \sin \theta_S \sin \theta_I) J(0) + 3 \sin \theta_S \sin \theta_I J(\omega) + \\ &\quad 6 \cos \theta_S \cos \theta_I J(2\omega)] = \\ &= \sigma_{NOE} \cos \theta_S \cos \theta_I + \sigma_{ROE} \sin \theta_S \sin \theta_I \end{aligned} \quad (B.18)$$

Bibliography

- [1] M. Kainosho, T. Torizawa, Y. Iwashita, T. Terauchi, A. M. Ono, and P. Guentert. Optimal isotope labelling for NMR protein structure determinations. *Nature*, 440:52–57, 2006.
- [2] M. Pfuhl and P. C. Driscoll. Protein nuclear magnetic resonance spectroscopy in the new millennium. *Phil. Trans. R. Soc. Lond. A*, 358:513–545, 2000.
- [3] K. H. Gardner and L. E. Kay. The use of ^2H , ^{13}C , ^{15}N multidimensional NMR to study the structure and dynamics of proteins. *Annu. Rev. Biophys. Biomol. Struct.*, 27:357–406, 1998.
- [4] R. Lichtenecker, M. L. Ludwiczek, W. Schmid, and R. Konrat. Simplification of Protein NOESY Spectra Using Bioorganic Precursor Synthesis and NMR Spectral Editing. *J. Am. Chem. Soc.*, 126:5348–5349, 2004.
- [5] N. K. Goto, K. H. Gardner, G. A. Mueller, R. C. Willis, and L. E. Kay. A robust and cost-effective method for the production of Val, Leu, Ile (δ 1) methyl-protonated ^{15}N -, ^{13}C -, ^2H -labeled proteins. *J. Biomol. NMR*, 13:369–374, 1999.
- [6] A. Mittermaier and L. E. Kay. New Tools Provide New Insights in NMR Studies of Protein Dynamics. *Science*, 312:224–228, 2006.
- [7] L.E. Kay. NMR studies of protein structure and dynamics. *J. Magn. Reson.*, 173:193–207, 2005.
- [8] R. Sprangers and L.E. Kay. Quantitative dynamics and binding studies of the 20S proteasome by NMR. *Nature*, 445:618–622, 2007.
- [9] A. Velyvis, Y.R. Yang, H.K. Schachman, and L.E. Kay. A solution NMR study showing that active site ligands and nucleotides directly perturb the allosteric equilibrium in spartate transcarbamoylase. *PNAS*, 104:8815–8820, 2007.

-
- [10] A. G. Palmer III. NMR Characterization of the Dynamics of Biomacromolecules. *Chem. Rev.*, 104:3623–3640, 2004.
- [11] P. Guentert. Structure calculation of biological macromolecules from NMR data. *Quarterly Reviews of Biophysics*, 31:145–237, 1998.
- [12] C.A.E.M. Spronk, S.B. Nabuurs, A. Krieger, G. Vried, and G.W. Vuister. Validation of protein structures derived by NMR spectroscopy. *Prog. Nucl. Magn. Reson. Spectr.*, 45:315–337, 2004.
- [13] H. Y. Carr and E. M. Purcell. Effects of Diffusion on Free Precession in Nuclear Magnetic Resonance Experiments. *Phys. Rev.*, 94:630–638, 1954.
- [14] S. Meiboom and D. Gill. Modified Spin-Echo Method for Measuring Nuclear Relaxation Times. *Rev. Sci. Instrum.*, 29:688–691, 1958.
- [15] M. Tollinger, N. R. Skrynnikov, F. A. A. Mulder, J. D. Forman-Kay, and L. E. Kay. Slow Dynamics in Folded and Unfolded States of an SH3 Domain. *J. Am. Chem. Soc.*, 123:11341–11352, 2001.
- [16] N.R. Skrynnikov, F.W. Dahlquist, and L.E. Kay. Reconstructing NMR spectra of invisible excited protein states using HSQC and HMQC experiments. *J. Am. Chem. Soc.*, 124:12352–12360, 2002.
- [17] H. van Ingen, G.W. Vuister, S. Wijmenga, and M. Tessari. CEESY: characterizing the conformation of unobservable protein states. *J. Am. Chem. Soc.*, 128:3856–3857, 2006.
- [18] D.M. Korzhnev, V.Y. Orekhov, F.W. Dahlquist, and L.E. Kay. Off-resonance R1rho relaxation outside of the fast exchange limit: an experimental study of a cavity mutant of T4 lysozyme. *J. Biomol. NMR*, 26:39–48, 2003.
- [19] R. Auer, P. Neudecker, D.R. Muhandiram, P. Lundstrom, D.F. Hansen, R. Konrat, and L.E. Kay. Measuring the signal of $^1\text{H}(\alpha)$ chemical shift differences between ground and excited protein states by off-resonance spin-lock R(1rho) NMR spectroscopy. *J. Am. Chem. Soc.*, 131:10832–10833, 2009.
- [20] A. G. Palmer III, C. D. Kroenke, and J. P. Loria. Nuclear Magnetic Resonance Methods for Quantifying Microsecond-to-Millisecond Motions in Biological Macromolecules. *Methods Enzymol.*, 339:204–238, 2001.

-
- [21] T. J. Swift and R. E. Connick. NMR-Relaxation Mechanisms of O17 in Aqueous Solutions of Paramagnetic Cations and the Lifetime of Water Molecules in the First Coordinate Sphere. *J. Chem. Phys.*, 37:307–320, 1962.
- [22] O. Trott and A. G. III Palmer. R1rho Relaxation outside of the Fast-Exchange Limit. *J. Magn. Reson.*, 154:157–160, 2002.
- [23] O. Trott, D. Abergel, and A. G. III Palmer. An average-magnetization analysis of R1rho relaxation outside of the fast exchange limit. *Mol. Phys.*, 101:753–763, 2003.
- [24] E. Kupce and R. Freeman. Adiabatic Pulses for Wideband Inversion and Broadband Decoupling. *J. Magn. Reson., Series A*, 115:273–276, 1995.
- [25] A. Abragam. *The Principles of Nuclear Magnetism*. Clarendon Press, Oxford, UK, 1986.
- [26] J.M. Boehlen and G. Bodenhausen. Experimental Aspects of Chirp NMR Spectroscopy. *J. Magn. Reson. Ser. A*, 102:293–301, 1993.
- [27] I. Burghardt, R. Konrat, B. Boulat, S. J. F. Vincent, and G. Bodenhausen. Measurement of cross relaxation between two selected nuclei by synchronous nutation of magnetization in nuclear magnetic resonance. *J. Chem. Phys.*, 98:1721–1736, 1993.
- [28] R. R. Ernst, G. Bodenhausen, and A. Wokaun. *Principles of Nuclear Magnetic Resonance in One and Two Dimensions*. Oxford University Press, Oxford, UK, 1990.
- [29] C. Zwaahlen, P. Legault, S. J. F. Vincent, J. Greenblatt, R. Konrat, and L. E. Kay. Methods for Measurement of Intermolecular NOEs by Multinuclear NMR Spectroscopy: Application to a Bacteriophage λ N-Peptide/boxB RNA Complex. *J. Am. Chem. Soc.*, 119:6711–6721, 1997.
- [30] C. Zwaahlen, S. J. F. Vincent, and L. E. Kay. Analytical Description on the Effect of Adiabatic Pulses on IS, I2S, and I3S Spin Systems. *J. Magn. Reson.*, 130:169–175, 1998.
- [31] D. Neuhaus and M.P. Williamson. *The Nuclear Overhauser Effect in Structural and Conformational Analysis*. Verlag Chemie, New York, USA, 1989.

- [32] M. Mayer and B. Meyer. Characterization of Ligand Binding by Saturation Transfer Difference NMR Spectroscopy. *Angew. Chem. Int. Ed.*, 38:1784–1788, 1999.
- [33] V.M. Sánchez-Pedregal, M. Reese, J. Meiler, M.J.J. Blommers, and C. Griesinger. The INPHARMA Method: Protein-Mediated Interligand NOEs for Pharmacophore Mapping. *Angew. Chem. Int. Ed.*, 44:4172–4175, 2005.
- [34] C. Ludwig, P.J.A. Michiels, X. Wu, K.L. Kavanagh, E. Pilka, A. Jansson, U. Oppermann, and U.L. Guenther. SALMON: Solvent Accessibility, Ligand binding, and Mapping of ligand Orientation by NMR Spectroscopy. *J. Med. Chem.*, 51:1–3, 2008.
- [35] J. Jeener, B.H. Meier, P. Bachmann, and R.R. Ernst. Investigation of exchange processes by two-dimensional NMR spectroscopy. *J. Chem. Phys.*, 71:4546–4553, 1979.
- [36] A.A. Bothner-By, R.L. Stephens, J.-M. Lee, C.D. Warren, and R.W. Jeankoz. Structure determination of a tetrasaccharide: transient nuclear Overhauser effects in the rotating frame. *J. Am. Chem. Soc.*, 106:811–813, 1984.
- [37] J. Cavanagh, W. J. Fairbrother, A. G. III Palmer, and N. J. Skelton. *Protein NMR Spectroscopy: Principles and Practice*. Academic Press, San Diego, USA, 1996.
- [38] G. Lipari and A. Szabo. Model-Free Approach to the Interpretation of Nuclear Magnetic Resonance Relaxation in Macromolecules. 1. Theory and Range of Validity. *J. Am. Chem. Soc.*, 104:4546–4559, 1982.
- [39] G. Lipari and A. Szabo. Model-Free Approach to the Interpretation of Nuclear Magnetic Resonance Relaxation in Macromolecules. 1. Analysis of Experimental Results. *J. Am. Chem. Soc.*, 104:4559–4570, 1982.
- [40] P. Allard, M. Helgstrand, and T. Hard. A Method for Simulation of NOESY, ROESY, and Off-Resonance ROESY Spectra. *J. Magn. Reson.*, 129:19–29, 1997.
- [41] P. Vallurupalli, P.F. Hansen, and L.E. Kay. Structures of invisible, excited protein states by relaxation dispersion NMR spectroscopy. *PNAS*, 105:11766–11771, 2008.

-
- [42] D.F. Hansen, P. Vallurupalli, and L.E. Kay. Using relaxation dispersion NMR spectroscopy to determine structures of excited, invisible protein states. *J. Biomol. NMR*, 41:113–120, 2008.
- [43] D.M. Korzhnev, X. Salvatella, M. Vendruscolo, A.A. Di Nardo, A.R. Davidson, C.M. Dobson, and L.E. Kay. Low-populated folding intermediates of Fyn SH3 characterized by relaxation dispersion NMR. *Nature*, 430:586–590, 2004.
- [44] D.M. Korzhnev, I. Bezsonova, F. Evanics, N. Taulier, Z. Zhou, Y. Bai, T.V. Chalikian, R.S. Prosser, and L.E. Kay. Probing the transition state ensemble of a protein folding reaction by pressure-dependent NMR relaxation dispersion. *J. Am. Chem. Soc.*, 128:5262–5269, 2006.
- [45] D.M. Korzhnev, V.Y. Orekhov, and L.E. Kay. Off-resonance R(1rho) NMR studies of exchange dynamics in proteins with low spin-lock fields: an application to a Fyn SH3 domain. *J. Am. Chem. Soc.*, 127:713–721, 2005.
- [46] A.L. Hansen, E.N. Nikolova, A. Casiano-Negroni, and Al-Hashimi H.M. Extending the range of microsecond-to-millisecond chemical exchange detected in labeled and unlabeled nucleic acids by selective R(1rho) NMR spectroscopy. *J. Am. Chem. Soc.*, 131:3818–3819, 2009.
- [47] F. Massi, E. Johnson, C. Wang, M. Rance, and A.G. III Palmer. NMR R1 rho rotating-frame relaxation with weak radio frequency fields. *J. Am. Chem. Soc.*, 126:2247–2256, 2004.
- [48] K. Kloiber and R. Konrat. Differential multiple-quantum relaxation arising from cross-correlated time-modulation of isotropic chemical shifts. *J. Biomol. NMR*, 18:33–42, 2000.
- [49] V.Y. Orekhov, D.M. Korzhnev, and L.E. Kay. Double- and zero-quantum NMR relaxation dispersion experiments sampling millisecond time scale dynamics in proteins. *J. Am. Chem. Soc.*, 126:1886–1891, 2004.
- [50] P. Guentert. Symbolic NMR Product Operator Calculation. *Int. J. Quantum Chem.*, 106:344–350, 2006.

I

Pharmacophore Mapping via Cross-Relaxation during Adiabatic Fast Passage

Renate Auer, Karin Kloiber, Andrea Vavrinska, Leonhard Geist, Nicolas Coudeville, and Robert Konrat*

Department of Structural and Computational Biology, Max F. Perutz Laboratories, University of Vienna, Campus Vienna Biocenter 5, A-1030 Vienna, Austria

Received November 30, 2009; E-mail: Robert.Konrat@univie.ac.at

NMR spectroscopy has become an indispensable tool in chemical biology, drug discovery, and structural genomics relevant to pharmaceutical and biotech industries.¹ To date, a broad range of experiments is available to screen for or to analyze protein–ligand interactions. Broadly speaking, these experiments are either exploiting NOE effects (transferred NOE, STD, pumped NOE, waterLOGSY)² or, alternatively, exploiting changes of chemical shifts (most importantly ¹⁹F based detection scheme, such as FAXS³) or molecular weights (PFG diffusion measurements).⁴ Most recently, fragment-based drug design (FBDD) has demonstrated great potential in indicating valuable lead compounds for drug discovery as it allows for a better coverage of the available chemical space.⁵ In early stages of the FBDD process often medium-to-weak binders are encountered, and thus reliable and sensitive detection techniques are crucial. It will be in this area that NMR spectroscopy will find most of its future applications as it not only is a very sensitive detection technique but also provides additional information about binding modes and orientations of bound ligands. Several experiments have thus been developed in the recent past, INPHARMA⁶ and SALMON,⁷ which exploit structural and dynamical information provided by the Nuclear Overhauser effect (NOE)⁸ and rotating frame Overhauser effect (ROE).⁹

Here we introduce a novel NMR experiment, AFP-NOESY, which measures homonuclear (¹H–¹H) cross-relaxation rates (NOEs and ROEs) during adiabatic fast passage (AFP) and demonstrate its suitability for the examination of protein ligand interactions and ligand binding epitope (pharmacophore) mapping. Our experiment involves adiabatic fast passage radio frequency (RF) pulses with a parabolic phase modulation leading to a linear frequency sweep through a very large spectral window.¹⁰ In addition to its well-established applications for broad band spin inversion and/or heteronuclear decoupling, the original AFP concept has been exploited for measuring heteronuclear spin lock relaxation rates.¹¹ In contrast to conventional AFP schemes the RF field intensity is not small compared to the frequency sweep range but of comparable strength and thus leads to significant contributions of transverse relaxation to the effective spin lock relaxation rate.¹¹ Here we present an extension of the methodology to studies of protein–ligand complexes. The pulse sequence is essentially a conventional NOESY experiment in which the original longitudinal NOESY mixing period is replaced by the AFP RF pulse (an outline of the pulse sequence is given in the Supporting Information (SI)). The adiabatic spin-lock frame is shown in Figure 1. During adiabatic fast passage cross-relaxation between spins *i* and *j* occurs and the rate (σ_{ij}) is given by $\sigma_{ij} = \sigma_{\text{NOE}} \cos^2 \theta_{\text{eff}} + \sigma_{\text{ROE}} \sin^2 \theta_{\text{eff}}$. For a macromolecule (protein) devoid of internal mobility a passage through zero occurs at a tilt angle of $\theta = 35.3^\circ$,⁹ while small molecules (ligands) show no $\sin^2 \theta$ dependence (see SI). If a ligand binds to the protein, an increase of the effective cross-relaxation rate and a pronounced dependence of the cross-relaxation rate on the effective tilt angle will be observed.

Typical results for an adiabatic spin-lock cross-relaxation experiment are shown in Figure 2, where we monitored the binding of vanillic

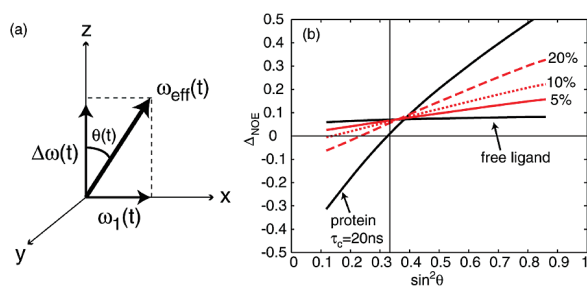


Figure 1. (a) Adiabatic spin-lock frame with offset $\Delta\omega(t)$, r.f. field $\omega_1(t)$, effective field $\omega_{\text{eff}}(t)$, and the angle $\theta(t)$ between offset and effective field. The time integral of $\sin^2 \theta(t)$ yields an effective tilt angle. The frequency of the adiabatic pulse is swept over a certain range thereby introducing a time dependent offset. Provided the adiabaticity condition ($d\theta/dt \ll \omega_{\text{eff}}$)¹⁰ is fulfilled, the magnetization can be assumed to follow the effective field leading to a perfect inversion at the end of the pulse. (b) Changes in intensity of the NOE-enhanced signal of interest due to effective cross-relaxation from a selectively inverted signal simulated for a rigid macromolecule, e.g. a protein, and a small molecule in the extreme narrowing limit, i.e. a free ligand, as a function of the (effective) tilt angle. Upon binding to the protein (red) the effective correlation time of the ligand increases and (after dissociation) the signal of the free ligand shows protein-like behavior. Examples are given for 5% (solid), 10% (dotted), and 20% (dashed) of free ligand with macromolecular behavior.

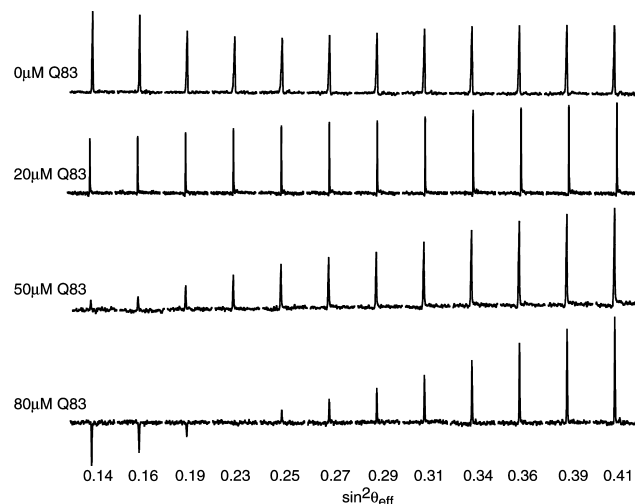


Figure 2. Selective 1d AFP-NOESY spectra for a complex formed between vanillic acid (VA, = 4-hydroxy-3-methoxybenzoic acid) and the lipocalin protein Q83. The NOE between 3-OCH₃ protons and H₂ of VA is measured as a function of AFP spin lock power and protein concentration. Experimental conditions were as follows: ¹H Larmor frequency: 500 MHz; AFP delay: 400 ms; concentrations: VA 1 mM; Q83: (top to bottom) 0, 20, 50, and 80 μM. In the free form (top) the extreme narrowing condition holds (thus leading to a flat profile), whereas in the bound state the macromolecular cross-relaxation dominates.

acid to quail lipocalin Q83 (157 residues, 18 kDa).¹² The data clearly demonstrate the sensitivity of the AFP-NOESY method to probe

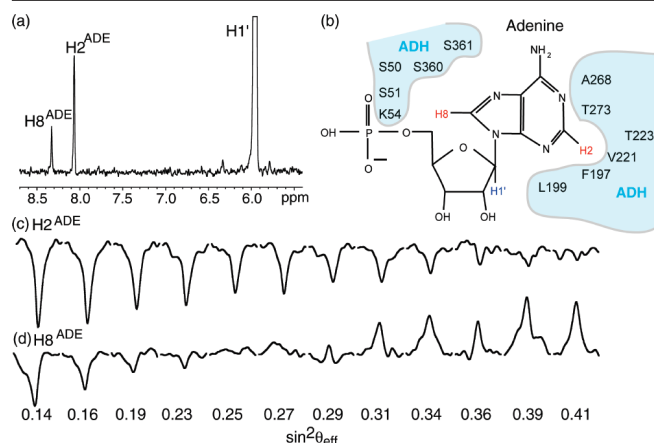


Figure 3. (a) Part of the 1D ^1H NMR spectrum of AMP. (b) Schematic representation of AMP contacts to ADH. (c–d) Experimental AFP cross-relaxation rates of the AMP-ADH complex, recorded with 400 ms mixing time (concentrations: AMP: 1 mM; ADH: 40 μM). The ribose proton $\text{H1}'$ proton was selectively inverted and acted as the source for magnetization transfer to H2^{ADE} (c) and H8^{ADE} (d). Experimental conditions are given in the Supporting Information.

protein ligand binding processes. At low protein concentration the extreme narrowing condition prevails and the effective cross-relaxation rate is nearly independent of the RF spin lock power, whereas at higher protein concentrations the effective cross-relaxation rate shows a profile typical for a rigid macromolecule. As expected, the experimental results correspond nicely with numerical simulations (see Figure 1b).

It is well-known that internal mobility and/or spin diffusion effects can alter the tilt angle profile of rotating-frame cross-relaxation rates.¹³ While internal mobility reduces the effective correlation time relevant for the time modulation of the internuclear vector and leads to a zero passage at smaller tilt angles, spin diffusion causes the opposite effect and often leads to larger zero passage tilt angles. We have investigated the influence of spin diffusion effects by recording 2D AFP-NOESY on the quail lipocalin Q83 (SI). Unambiguous evidence for the relevance of spin diffusion was observed. The histogram of zero passage tilt angles θ_0 clearly shows a broad distribution around the theoretical θ_0 value of $\sim 35.3^\circ$, with significant deviations toward both sides. Higher temperatures slightly alleviate spin diffusion effects (by reducing the effective correlation time). Although the observed spin diffusion effects impair a quantitative analysis of the protein AFP cross-relaxation data in terms of intramolecular dynamics, it offers a potentially rich source of information for pharmacophore mapping. In the past, protein ligand spin diffusion effects were considered problematic for the interpretation of transferred NOE measurements, and therefore experiments have been developed to quench these indirect pathways and extract reliable cross-relaxation rates devoid of spin diffusion.¹⁴ Here these indirect relaxation pathways are actively exploited to extract structural information about ligand binding modes.

An example for experimental pharmacophore mapping is given in Figure 3. Selective AFP cross-relaxation rates were measured for the AMP/ADH and NAD^+ /ADH (Alcohol Dehydrogenase from *S. cerevisiae*) protein complexes. The sugar proton $\text{H1}'$ was chosen as the NOE source spin. At the chosen molar ratio intraligand NOEs are dominated by the bound state and amplitude profiles typical for macromolecules are to be expected. Interestingly, however, only the cross-relaxation rate between $\text{H1}'$ and H8 showed an amplitude profile typical for a rigid macromolecule. Conversely, for the NOE between $\text{H1}'$ and H2 a clear indication of indirect spin diffusion pathways was observed. This suggests that H8 is most likely exposed to the solvent,

whereas H2 is embedded in a ^1H dipolar coupling network and buried in a hydrophobic binding cleft. The 3D structure of AMP/ADH nicely corroborates the findings (see SI). Similar results were found for the NAD^+ /ADH complex (zero crossing of H8^{ADE} and no zero crossing of H2^{ADE} due to spin diffusion; data not shown).

In summary, we were able to show that AFP-NOESY allows us to probe protein ligand interactions and provides detailed information about pharmacophores which will be useful for rational drug design programs. Although STD was suggested as a tool for epitope mapping, its quantitative interpretation is less straightforward. However, the pronounced differences of zero-crossing angles for H2 and H8 in Figure 3 suggest application of the AFP-NOESY method for refined analysis of protein–ligand interaction sites by quantification of proton densities for evaluation of docking models. Given the high sensitivity we anticipate widespread applications in fragment-based drug design programs, particularly as the methodology provides valuable information about potential sites for ligand extensions and/or decoration.

Acknowledgment. R.A. is a recipient of a DOC-fORTE-fellowship, and K.K. of an APART-fellowship of the Austrian Academy of Sciences. This work was partly supported by Grants (P20549-N19 and SFB17 to R.K.) and via generous start-up funding from the Austrian Science Fund (FWF) (to R.K.).

Supporting Information Available: Pulse scheme, the structure of the AMP/ADH complex, simulation details, and spin diffusion effects in Q83 are given. This material is available free of charge via the Internet at <http://pubs.acs.org>.

References

- (1) Pellecchia, M.; Bertini, I.; Cowburn, D.; Dlavit, C.; Giralto, E.; Jahnke, W.; James, T. L.; Hoamns, S. W.; Kessler, H.; Luchinat, C.; Meyer, B.; Oschkinat, H.; Peng, J.; Schwalbe, H.; Siegal, G. *Nat. Rev. Drug Discovery* **2008**, *7*, 738–745.
- (2) (a) Balam, P.; Bothner-By, A.; Breslow, E. *J. Am. Chem. Soc.* **1972**, *94*, 4017–4018. (b) Balam, P.; Bothner-By, A.; Dadok, J. *J. Am. Chem. Soc.* **1972**, *94*, 4015–4017. (c) Mayer, M.; Meyer, B. *Angew. Chem., Int. Ed.* **1999**, *38*, 1784–1788. (d) Chen, A.; Shapiro, M. *J. Am. Chem. Soc.* **1998**, *120*, 10258–10259. (e) Dalvit, C.; Pevarello, P.; Tato, M.; Veronesi, M.; Vulpetti, A.; Sundstroem, M. *J. Biomol. NMR* **2000**, *18*, 65–68.
- (3) (a) Dalvit, C. *Prog. NMR Spectrosc.* **2007**, *51*, 243–27. (b) Dalvit, C.; Fagnerness, P. E.; Hadden, D. T.; Sarver, R. W.; Stockman, B. J. *J. Am. Chem. Soc.* **2003**, *125*, 7696–7703.
- (4) Lin, M.; Shapiro, M. *J. Org. Chem.* **1996**, *61*, 7617–7619.
- (5) (a) Jhoti, H. *Nat. Biotechnol.* **2005**, *23*, 184–186. (b) Erlanson, D. A. *Curr. Opin. Biotechnol.* **2006**, *17*, 643–652. (c) De Kloe, G. E.; Bailey, D.; Leurs, R.; De Esch, I. J. P. *Drug Discov. Today* **2009**, *14*, 630–646.
- (6) Sanchez-Pedregal, V. M.; Reese, M.; Meiler, J.; Blommers, M. J. J.; Griesinger, C.; Carlomagno, T. *Angew. Chem., Int. Ed.* **2005**, *44*, 4172–4175.
- (7) (a) Ludwig, C.; Michiels, P. J. A.; Wu, X.; Kavanagh, K. L.; Pilka, E.; Jansson, A.; Oppermann, U.; Günther, U. *J. Med. Chem.* **2008**, *51*, 1–3. (b) Ludwig, C.; Michiels, P. J. A.; Lodi, A.; Ride, J.; Bunce, C.; Günther, U. *ChemMedChem* **2008**, *3*, 1371–1376.
- (8) (a) Macura, S.; Ernst, R. R. *Mol. Phys.* **1980**, *41*, 95. (b) Neuhaus, D.; Williamson, M. P. *The Nuclear Overhauser Effect in Structural and Conformational Analysis*; Verlag Chemie: New York, 1989. (c) Ernst, R. R.; Bodenhausen, G.; Wokaun, A. *Principle of Nuclear Magnetic Resonance in One and Two Dimensions*; Oxford University Press: Oxford, 1987.
- (9) (a) Bothner-By, A. A.; Stevens, R. L.; Lee, J. T.; Warren, C. D.; Jeanloz, R. W. *J. Am. Chem. Soc.* **1994**, *106*, 811–813. (b) Desvaux, H.; Berthault, P.; Birlirakis, N.; Goldman, M. *J. Magn. Reson. A* **1994**, *108*, 219–229. (c) Desvaux, H.; Berthault, P.; Birlirakis, N. *Chem. Phys. Lett.* **1995**, *233*, 545–549. (d) Desvaux, H.; Berthault, P. *Prog. NMR Spectrosc.* **1999**, *35*, 295–340.
- (10) (a) Abragam, A. *The Principles of Nuclear Magnetism*; Oxford University Press: Oxford, 1983. (b) Boehlen, J. M.; Bodenhausen, G. *J. Magn. Reson., Ser. A* **1993**, *102*, 293–301. (c) Kupce, E.; Freeman, R. J. *J. Magn. Reson., Ser. A* **1996**, *118*, 299–303.
- (11) Konrat, R.; Tollinger, M. *J. Biomol. NMR* **1999**, *13*, 213–221.
- (12) Hartl, M.; Matt, T.; Schüler, W.; Siemeister, G.; Kontaxis, G.; Klobner, K.; Konrat, R.; Bister, K. *J. Mol. Biol.* **2003**, *333*, 33–4.
- (13) Schleucher, J.; Wijmenga, S. J. *J. Am. Chem. Soc.* **2002**, *124*, 5881–89.
- (14) (a) Zwaalen, C.; Vincent, S. J. F.; Di Bari, L.; Levitt, M.; Bodenhausen, G. *J. Am. Chem. Soc.* **1994**, *116*, 362–368. (b) Vincent, S. J. F.; Zwaalen, C.; Bodenhausen, G. *J. Biomol. NMR* **1996**, *7*, 169–172. (c) Vincent, S. J. F.; Zwaalen, C.; Post, C. B.; Burgner, J. W.; Bodenhausen, G. *Proc. Natl. Acad. Sci. U.S.A.* **1997**, *94*, 4383–4388.

JA910098S

Supporting Information

**Pharmacophore Mapping via
Cross-Relaxation during Adiabatic
Fast Passage**

Renate Auer, Karin Kloiber, Andrea Vavrinska,
Leonhard Geist, Nicolas Coudevylle and Robert Konrat

1 1D AFP-NOESY Pulse Sequence

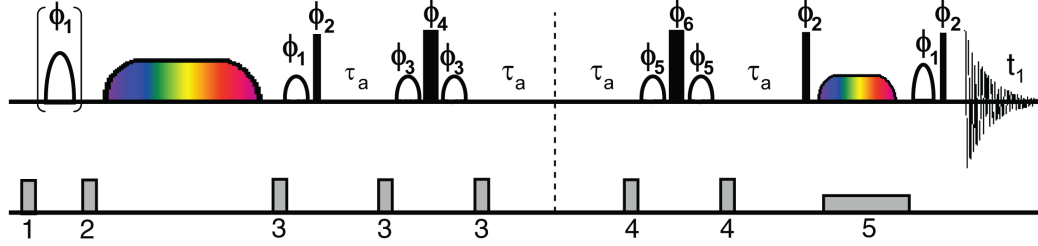


Figure S1: AFP-NOESY pulse scheme for measuring 1d selective cross-relaxation (NOE/ROE) in small molecules. The sequence is based on conventional NOESY sequences but has an adiabatic fast passage (AFP) pulse during the mixing time. The narrow/wide solid pulses have flip angles of $90^\circ/180^\circ$. All shaped pulses except for the first one are water-selective. The first pulse selectively inverts the signal it is on-resonance with. In every other scan the same pulse is applied 50kHz off-resonance in order to have the same conditions for on-the-fly spectrum subtraction (note the phase cycle of the selective inversion pulse and of the receiver). The first AFP applied immediately after the selective inversion pulse substitutes the conventional NOESY mixing time. It has a length of 400ms and the frequency is set at the beginning of the pulse at 5kHz downfield and is swept during the entire length of the pulse linearly over 10kHz in upfield direction. Pulse powers up to 2.0kHz and 10% sinusoidal/cosinusoidal apodization at the beginning/end are used. Water suppression is performed with two WATERGATE elements with τ_a set to 2.74ms. The second AFP (30ms, $\nu_{sweep}=20\text{kHz}$, $\nu_1=1.1\text{kHz}$) is used to suppress zero quantum coherences that arise between coupled spins [1]. The phase cycle is set to: $\phi_1 = 2(-x), 2(x), 2(-y), 2(y)$; $\phi_2 = 2(x), 2(-x), 2(y), 2(-y)$; $\phi_3 = 8(-x), 8(x), 8(-y), 8(y)$; $\phi_4 = 8(x), 8(-x), 8(y), 8(-y)$; $\phi_5 = 32(-x), 32(x), 32(-y), 32(y)$; $\phi_6 = 32(x), 32(-x), 32(y), 32(-y)$; receiver $2[2(x, -x, -x, x, y, -y, y, y), 2(-x, x, x, -x, -y, y, y, -y)], 2[2(-x, x, x, -x, -y, y, y, -y), 2(x, -x, -x, x, y, -y, y, y)]$. Gradient strength and durations are (ms, G/cm): G1=(0.4/36.5), G2=(0.4/27.5), G3=(0.45/18.3), G4=(1/18.3), G5=(30/2.4).

2 AMP as embedded in ADH

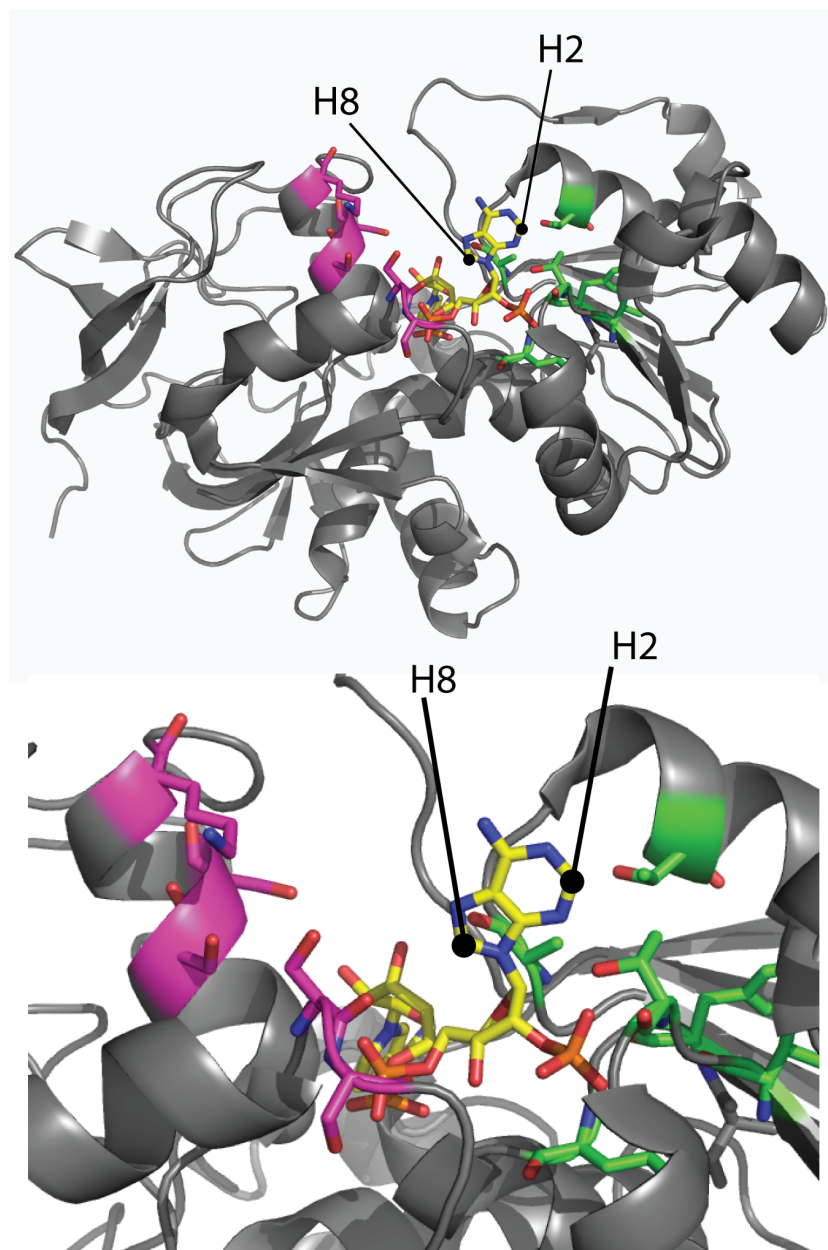


Figure S2: Structure of ADH with AMP. The hydrophilic residues are given in magenta, the hydrophobic in green. PDB identification number 1P0F.

3 Cross-Relaxation during Spin-Lock

Including an AFP during the NOESY mixing time allows the introduction of a magnetic field that can be described by an effective angle θ_{eff} with respect to the z-axis. Transverse and longitudinal cross relaxation rates are mixed and according to θ_{eff} and the effective cross-relaxation rate for two spins i and j is given by [2]

$$\sigma_{eff}^{i,j} = \sigma_{NOE} \cos \theta_i \cos \theta_j + \sigma_{ROE} \sin \theta_i \sin \theta_j \quad (1)$$

$$\theta_i = \arctan \frac{\omega_1}{\Omega} \quad (2)$$

$$\theta = \arctan \sqrt{\tan \theta_i \tan \theta_j} \quad (3)$$

$$\sigma_{eff}^{i,j} = \frac{\sin \theta_i \sin \theta_j}{\sin^2 \theta} (\sigma_{NOE} \cos^2 \theta + \sigma_{ROE} \sin^2 \theta) \quad (4)$$

In the slow tumbling regime ($\omega_0 \tau_c > \sqrt{5/2}$), NOE and ROE have different sign, i.e. an angle θ_0 exists, for which the two effects cancel each other out.

$$\sigma_{eff}^{i,j} = \frac{\sin \theta_i \sin \theta_j}{\sin^2 \theta} (\sigma_{NOE} \cos^2 \theta + \sigma_{ROE} \sin^2 \theta) = 0 \quad (5)$$

$$\frac{\sigma_{NOE}}{\sigma_{ROE}} = -\tan^2 \theta^0 \quad (6)$$

In the slow tumbling regime (i.e. large $\omega^2 \tau_c^2$) $\frac{\sigma_{NOE}}{\sigma_{ROE}}$ is $-\frac{1}{2}$ (see figure S3 and compare eq. 14 and 15), which results in a θ^0 of 35.26° .

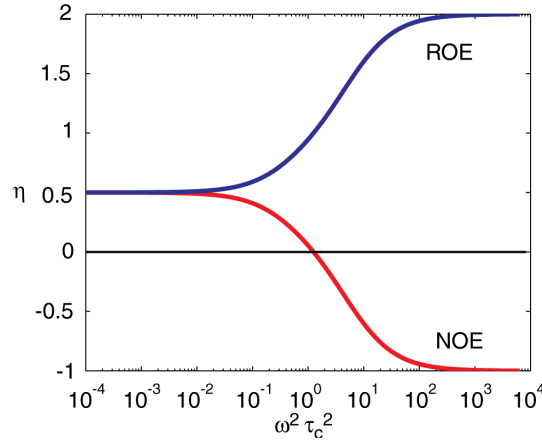


Figure S3: NOE and ROE enhancement $\eta = \sigma_{NOE/ROE}/R_1$ vs $\omega^2 \tau_c^2$. Note the logarithmic scale.

4 Simulation of Nuclear Overhauser Effect during a Spin-Lock

For the simulation of Nuclear Overhauser Effect (NOE) and Rotating Frame Overhauser Effect (ROE) between two like, uncoupled spins I and S at a distance r_{IS} during an adiabatic fast passage (AFP) pulse a longitudinal starting magnetization M_0 is assumed. The end magnetization M_n is calculated iteratively: the total time of the AFP t_{AFP} is divided into n time intervals Δt (that have to be small compared to t_{AFP}) and the magnetization is calculated for every time point $t_{i+1} = t_i + \Delta t$ by solving the following Liouvillian equation until $t_{i+1} = t_{AFP}$ [3][4]

$$M_{i+1} = \exp(-\mathbf{L}_i \Delta t) M_i. \quad (7)$$

with

$$M_i = [E/2 \quad I_x \quad I_y \quad I_z \quad S_x \quad S_y \quad S_z]' \quad (8)$$

$$\mathbf{L}_i = \begin{bmatrix} 0 & 0 & 0 & 0 & 0 & 0 & 0 & 0 \\ 0 & R_2^I & \omega_I & 0 & \sigma_{ROE} & 0 & 0 & 0 \\ 0 & -\omega_I & R_2^I & \omega_x & 0 & \sigma_{ROE} & 0 & 0 \\ -2M_I & 0 & -\omega_x & R_1^I & 0 & 0 & \sigma_{NOE} & 0 \\ 0 & \sigma_{ROE} & 0 & 0 & R_2^S & \omega_S & 0 & 0 \\ 0 & 0 & \sigma_{ROE} & 0 & -\omega_S & R_2^S & \omega_x & 0 \\ -2M_S & 0 & 0 & \sigma_{NOE} & 0 & -\omega_x & R_1^S & 0 \end{bmatrix}_i \quad (9)$$

the longitudinal relaxation rate R_1 , the transverse relaxation rate R_2 , the longitudinal cross-relaxation rate σ_{NOE} , the transverse cross-relaxation rate σ_{ROE} , Larmor frequencies ω_I and ω_S , spin-lock frequency along x ω_x and

$$M_I = R_1^I M_{I0} + \sigma_{NOE} M_{S0} \quad (10)$$

$$M_S = R_1^S M_{S0} + \sigma_{NOE} M_{I0} \quad (11)$$

M_0 is equilibrium magnetization. Although the following equations hold for all spins, we assume from now on $I=^1\text{H}$ and $S=^1\text{H}$. R_1 , R_2 , σ_{NOE} and σ_{ROE} are calculated using the Lipari-Szabo model-free approach [5][6]

$$R_1 = \frac{\mu_0^2 \hbar^2 \gamma_H^2}{64\pi^2 r_{HH}^6} (J(0) + 3J(\omega_H) + 6J(2\omega_H)) \quad (12)$$

$$R_2 = \frac{\mu_0^2 \hbar^2 \gamma_H^2}{64\pi^2 r_{HH}^6} (5/2J(0) + 9/2J(\omega_H) + 3J(2\omega_H)) \quad (13)$$

$$\sigma_{NOE} = \frac{\mu_0^2 \hbar^2 \gamma_H^2}{64\pi^2 r_{HH}^6} (-J(0) + 6J(2\omega_H)) \quad (14)$$

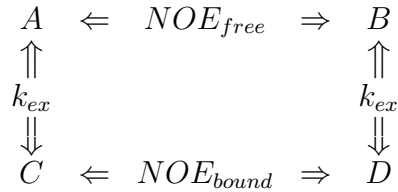
$$\sigma_{ROE} = \frac{\mu_0^2 \hbar^2 \gamma_H^2}{64\pi^2 r_{HH}^6} (2J(0) + 3J(2\omega_H)) \quad (15)$$

with vacuum permeability μ_0 , reduced Planck constant \hbar and ^1H gyromagnetic ratio γ_H . The spectral density function $J(\omega)$ is defined as

$$J(\omega) = \frac{2}{5} \frac{S^2 \tau_c}{(1 + \omega^2 \tau_c^2)}. \quad (16)$$

An AFP pulse is swept linearly over a defined frequency range, introducing a time-dependence in ω_I and ω_S . The amplitude is increased from 0 to the maximum value in the first 10% of the pulse length using a sine shape build-up, and decreased to 0 in the last 10% using a cosine-shape, thus introducing a time-dependence in ω_x .

For a system where a ligand reversibly binds to a protein, the matrix can be easily extended to describe a four-spin system that is connected in the following manner:



in which A and B are two spins in the ligand connected by cross-relaxation. They exchange with the bound state (C and D). The cross-relaxation rates differ significantly, since A and B behave as small molecules and C and D show big-molecule-behaviour. ROE and NOE enhancement depend on molecule size (see figure S3). For small molecules (i.e. the ligand) NOE and ROE enhancement are the same (50%), for large molecules NOE enhancement is negative (100%) while ROE enhancement stays positive but increases to 200%. In a small molecule the enhancement is virtually independent of the AFP field strength during the mixing time, since NOE enhancement, that

prevails for weak field strengths, and ROE enhancement, that prevails for strong field strengths, are of the same size. The profile of the enhancement vs AFP field strength is therefore flat. If the small compound reversibly binds to a macromolecule, it will - in the bound state - experience cross-relaxation of a large molecule. The profile of the enhancement is then strongly field-dependent. Thus this method is suitable for binding studies and epitope mapping.

Figure S4 is a simulation that shows the behaviour of a free ligand, of a protein, as well as a ligand reversibly binding to a protein. As can be seen clearly, a protein with 25ns correlation time fullfills the condition $\sigma_{ROE} = -2\sigma_{NOE}$ and $\theta^0 = 35.3^\circ$. A shorter correlation time results in a smaller zero-crossing angle. Increasing the protein concentration results in an increase of the proportion of free ligand with protein-like cross-relaxation properties, i.e. the zero-crossing angle is being pushed towards its limit of 35.3° . However, under no circumstances values of θ^0 larger than 35.3° can be reached in a two-spin system.

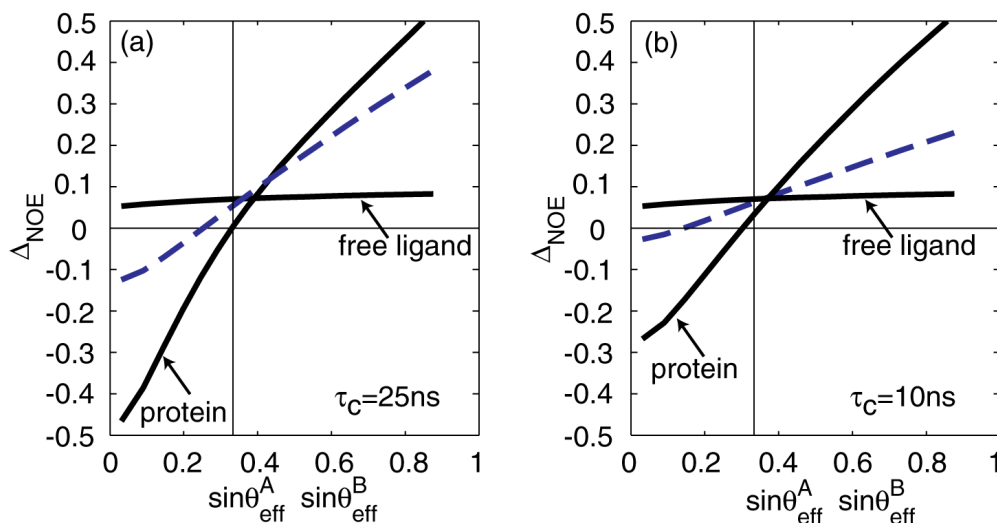


Figure S4: Simulation of NOE/ROE of a free ligand and a free protein with (a) $\tau_c = 25\text{ns}$ and (b) $\tau_c = 10\text{ns}$. The dashed line shows the expected behaviour of a ligand in the presence of a protein to which it binds reversibly. It is assumed that the ligand spends 20% of the time bound to the protein. For the simulations a 400ms AFP with 10000Hz frequency sweep and 10% ramping at both ends was assumed. The inverted signal and the signal, enhanced by cross-relaxation, were at 1.5 and -1.5 ppm, respectively.

The AFP parameters can be chosen freely within the hardware require-

ments. A certain offset-dependence is expected according to simulations (see figure S5). It can be circumvented by using larger frequency sweeps, which as a drawback require stronger fields in order to reach higher $\sin^2 \theta$ values.

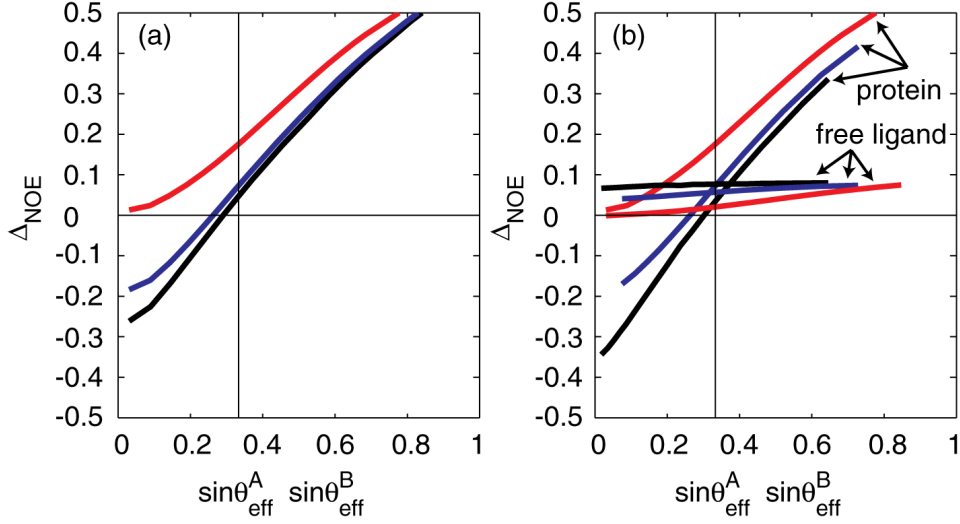


Figure S5: Behaviour of a free protein with a 10ns correlation time. (a) AFP parameters were $t_{AFP} = 400\text{ms}$, $\nu_{sweep} = 10000\text{Hz}$ and 10% ramping at both ends. The position of inverted signal/enhanced signal is 0/3ppm (black), 0/5ppm (blue) and -5/5ppm (red) at 500MHz. Offset dependence can be seen clearly. (b) The effect of larger frequency sweeps on a system with the inverted signal at -5 and the enhanced signal at 5ppm. $\nu_{sweep} = 10000\text{Hz}$ (red), 20000Hz (blue), 70000Hz (black). The free ligand behaviour is also shown ('horizontal' lines). All other parameters are as in (a). Larger frequency sweeps reduce the offset-dependence, since the two spins become more and more similar as can be seen from their respective $\sin \theta$ -values.

5 Spin-diffusion Effects

Spin-diffusion affects a proton during an AFP-NOESY sequence in a way that magnetization enhancement due to cross-relaxation fades out resulting either in the lack of zero-crossing upon switching from the NOE to the ROE regime or in zero-crossing angles θ^0 larger than 35.3° . Simulations of such spin-diffusion effects confirm experimental findings. Figure S6 shows the distribution of zero-crossing angles of a number of cross-peaks in a 2d AFP-NOESY version. Out of 80 signals analysed, 14 show no zero-crossing while the rest shows θ^0 -values between 20 and 55° .

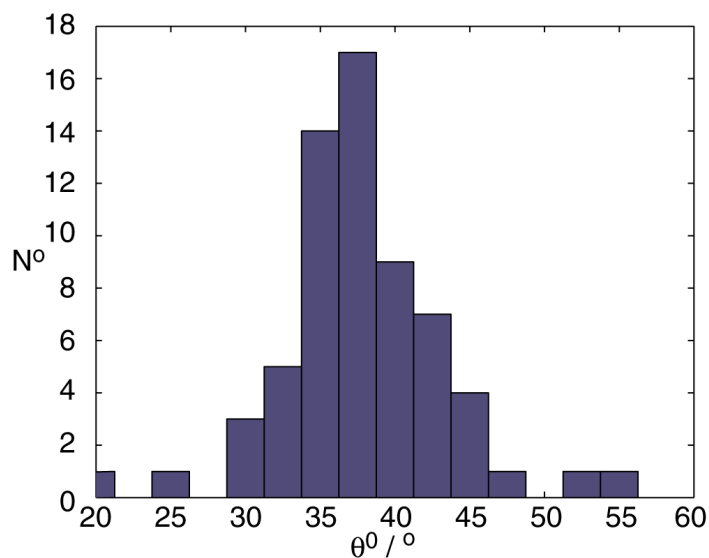


Figure S6: A histogram of 66 cross-peaks from a 2d AFP-NOESY of the Q83-Enterobactin system at 37°C .

References

- [1] M. J. Thrippleton and J. Keeler. Elimination of Zero-Quantum Interference in Two-Dimensional NMR Spectra. *Angew. Chem. Int. Ed. Engl.*, 42:3938–3941, 2003.
- [2] J. Cavanagh, W. J. Fairbrother, A. G. III Palmer, and N. J. Skelton. *Protein NMR Spectroscopy: Principles and Practice*. Academic Press, San Diego, USA, 1996.
- [3] P. Allard, M. Helgstrand, and T. Hard. A Method for Simulation of NOESY, ROESY, and Off-Resonance ROESY Spectra. *J. Magn. Reson.*, 129:19–29, 1997.
- [4] M. H. Levitt and L. Di Bari. The Homogeneous Master Equation and the Manipulation of Relaxation Networks. *Bull. Magn. Reson.*, 16:94–114, 1994.
- [5] G. Lipari and A. Szabo. Model-Free Approach to the Interpretation of Nuclear Magnetic Resonance Relaxation in Macromolecules. 1. Theory and Range of Validity. *J. Am. Chem. Soc.*, 104:4546–4559, 1982.
- [6] G. Lipari and A. Szabo. Model-Free Approach to the Interpretation of Nuclear Magnetic Resonance Relaxation in Macromolecules. 1. Analysis of Experimental Results. *J. Am. Chem. Soc.*, 104:4559–4570, 1982.

II

Measuring the Signs of $^1\text{H}^\alpha$ Chemical Shift Differences Between Ground and Excited Protein States by Off-Resonance Spin-Lock $R_{1\rho}$ NMR SpectroscopyRenate Auer,^{†,‡} Philipp Neudecker,[‡] D. Ranjith Muhandiram,[‡] Patrik Lundström,^{‡,§}
D. Flemming Hansen,[‡] Robert Konrat,[†] and Lewis E. Kay^{*,‡}*Department of Structural and Computational Biology, Max F. Perutz Laboratories, University of Vienna, Campus-Vienna-Biocenter 5, A-1030 Vienna, Austria, Departments of Molecular Genetics, Biochemistry, and Chemistry, University of Toronto, Toronto, Ontario, Canada M5S 1A8, and Molecular Biotechnology/IFM, Linköping University, SE-581 83 Linköping, Sweden*

Received May 27, 2009; E-mail: kay@pound.med.utoronto.ca

Protein dynamics are of fundamental importance for many biological processes, including folding, binding, catalysis, and molecular recognition.^{1,2} Often these dynamics involve conformational rearrangements whereby a highly populated conformer exchanges with one or more low-populated, transiently formed states. Such states can be of functional significance and hence are of interest for detailed study, although their low populations and short lifetimes render them “invisible” to many of the techniques of structural biology. In cases where the exchange occurs on the millisecond time scale with excited states populated at 0.5% or higher, Carr–Purcell–Meiboom–Gill (CPMG) relaxation dispersion NMR spectroscopy is a sensitive technique for characterizing the kinetics and thermodynamics of the exchange process.³ Structural information is also forthcoming in the form of the absolute values of the chemical shift differences between probes in the ground and excited states ($\Delta\omega$). The signs of the shift differences and hence the chemical shifts of the excited state, $\tilde{\omega}_E$, can be obtained in many cases by a comparison of peak positions in HSQC/HMQC data sets recorded at a number of static magnetic fields.⁴ To date, isotopic labeling strategies and NMR experiments that exploit these labeling approaches have been developed for the measurement of backbone ^{15}N , $^1\text{H}^\text{N}$, $^{13}\text{C}^\alpha$, and ^{13}CO signed $\Delta\tilde{\omega}$ values as well as $^1\text{H}^\alpha$ and $^{13}\text{C}^\beta$ $|\Delta\tilde{\omega}|$ values.^{5–10} We are particularly interested in $^1\text{H}^\alpha$ $\tilde{\omega}_E$ values, since the $^1\text{H}^\alpha$ chemical shift is sensitive to both secondary and tertiary structure¹¹ and thus provides important restraints in structure calculations for the excited state. In principle, the sign of $^1\text{H}^\alpha$ $\Delta\tilde{\omega}$ could be obtained from analysis of $^1\text{H}^\alpha$ – $^{13}\text{C}^\alpha$ double- and zero-quantum CPMG relaxation dispersion profiles once the sign of $^{13}\text{C}^\alpha$ $\Delta\tilde{\omega}$ is known, as is currently done in the case of $^1\text{H}^\text{N}$ (see refs 12 and 13). In practice, this would require protein samples with isolated $^1\text{H}^\alpha$ and $^{13}\text{C}^\alpha$ spins, and such samples would be challenging to produce. Herein we describe an alternative and very simple approach in which off-resonance $^1\text{H}^\alpha$ decay rates under conditions of spin-locking, $R_{1\rho}$, are measured via one-dimensional spectroscopy using very weak spin-lock fields. Comparison of a pair of decay curves measured with the radio-frequency field applied on opposite sides of the ground-state peak provides the necessary sign information. The utility of the methodology is first established using an exchanging system for which the signed $\Delta\tilde{\omega}$ values are available, and subsequently, an application to the A39V/N53P/V55L Fyn SH3 domain is presented, in which an on-pathway folding intermediate converts with the folded state.¹⁴

For an exchange reaction between a ground state (G) and an excited state (E) (i.e., $\text{G} \rightleftharpoons \text{E}$, with rate constants $k_{\text{G} \rightarrow \text{E}}$ and $k_{\text{E} \rightarrow \text{G}}$) in which the G population is much greater than the E population (i.e., $p_{\text{G}} \gg p_{\text{E}}$), Trott and Palmer¹⁵ have shown that $R_{1\rho}$ is given by

$$R_{1\rho} = R_1 \cos^2 \theta + (R_2 + R_{\text{ex}}) \sin^2 \theta \quad (1)$$

where R_1 and R_2 are longitudinal and intrinsic transverse relaxation rates, respectively, and R_{ex} is the exchange contribution to $R_{1\rho}$, given by

$$R_{\text{ex}} = \frac{p_{\text{E}} \Delta\omega^2 k_{\text{ex}}}{\omega_{\text{E,eff}}^2 + k_{\text{ex}}^2} = \frac{p_{\text{E}} \Delta\omega^2 k_{\text{ex}}}{(\delta_{\text{G}} + \Delta\omega)^2 + \omega_1^2 + k_{\text{ex}}^2} \quad (2)$$

In eqs 1 and 2, ω_1 is the strength of the applied field (rad/s), $\delta_{\text{G}} = \Omega_{\text{G}} - \Omega_{\text{SL}}$ and $\delta_{\text{E}} = \Omega_{\text{E}} - \Omega_{\text{SL}}$ are resonance offsets from the spin-lock (SL) carrier for the G and E states, respectively, $\theta = \arctan(\omega_1/\delta_{\text{G}})$, $\omega_{\text{E,eff}}^2 = \omega_1^2 + \delta_{\text{E}}^2$, $\Delta\omega = \Omega_{\text{E}} - \Omega_{\text{G}}$, and $k_{\text{ex}} = k_{\text{G} \rightarrow \text{E}} + k_{\text{E} \rightarrow \text{G}}$. Because the maximum in R_{ex} occurs when the spin-lock field is resonant with the frequency of the minor state (eq 2), recording a pair of $R_{1\rho}$ decay curves with $\delta_{\text{G}} \approx \pm\Delta\omega$ allows the sign of $\Delta\omega$ to be determined, since $R_{1\rho}$ values recorded for $\delta_{\text{G}} = -\Delta\omega$ will be larger than those for $\delta_{\text{G}} = \Delta\omega$.

Figure 1 illustrates the one-dimensional NMR pulse scheme that has been developed to measure the signs of $^1\text{H}^\alpha$ $\Delta\tilde{\omega}$ values. The sequence is similar to one previously developed by Korzhnev et al.¹⁶ for studies of exchange in proteins by ^{15}N off-resonance $R_{1\rho}$ and a subsequent experiment by Hansen et al.¹⁷ quantifying ^{13}C $R_{1\rho}$ values in nucleic acids and closely follows previously developed schemes for measuring ^1H relaxation rates in proteins.¹⁸ Two-dimensional NMR experiments have also been proposed,^{19,20} but the present approach is very efficient when only a subset of residues (those for which $\Delta\tilde{\omega} \neq 0$) must be queried and when very weak spin-lock fields are desired. In the present case, selective Hartmann–Hahn magnetization transfer²¹ between $^1\text{H}^\alpha$ and $^{13}\text{C}^\alpha$ (a to b in Figure 1) of a chosen residue and subsequently from $^{13}\text{C}^\alpha$ back to $^1\text{H}^\alpha$ (c to d) is used so R_{ρ} values can be measured from a one-dimensional ^1H spectrum containing in general only the peak of interest. For the uniformly ^{13}C - and fractionally ^2H -labeled samples used [in both these experiments and those measuring $|\Delta\tilde{\omega}|$ (ref 10a)], simulation and experiment have established that a 130–150 Hz continuous-wave field ($\omega_{1,\text{CW}}/2\pi$) ensures excellent transfer without losses due to $^{13}\text{C}^\alpha$ – ^{13}CO or $^{13}\text{C}^\alpha$ – $^{13}\text{C}^\beta$ couplings

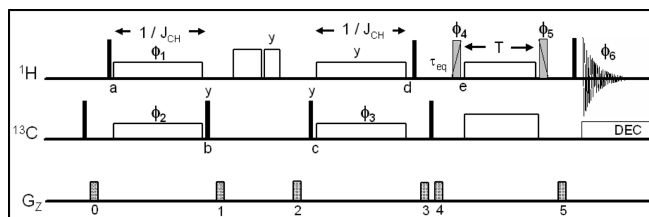


Figure 1. Pulse scheme for measuring $^1\text{H}^\alpha$ off-resonance $R_{1\rho}$ relaxation rates in proteins. All of the solid pulses have flip angles of 90° and are applied along the x axis, unless indicated otherwise. ^1H pulses of phase ϕ_4/ϕ_5 (shaded pulses) are applied with a flip angle θ for which $\tan \theta = \omega_1/\delta_{\text{G}}$, where δ_{G} and ω_1 are optimized as described in the text. See the SI for details.

[†] University of Vienna.[‡] University of Toronto.[§] Linköping University.

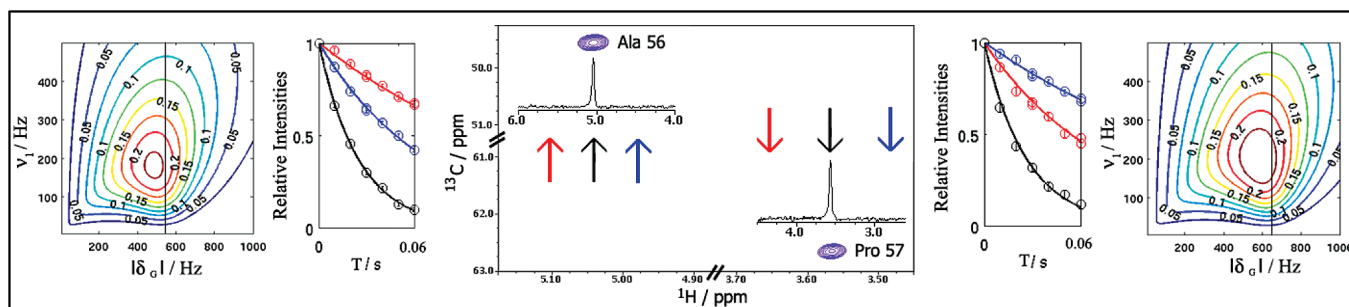


Figure 2. $R_{1\rho}$ decay curves for Ala56 and Pro57 of the A39V/N53P/V55L Fyn SH3 domain (800 MHz), with the spin-lock carrier positioned downfield (red), on-resonance (black), or upfield (blue) of the position of the major-state peak. Each point of each decay profile was recorded in 6 min (room temperature probe head), giving a total measurement time of 0.9 h for each curve (9 points, including a pair of repeats). Contour plots of $\Delta(\delta_G, \nu_1)$ (where $\nu_1 = \omega_1/2\pi$) simulated for 800 MHz are also shown; the vertical line indicates $|\delta_G| = |\Delta\omega|$. The sample (1 mM protein dissolved in D_2O) was prepared with 50% D_2O supplemented with 1 g/L $^{15}NH_4Cl$ and 3 g/L [$^{13}C_6, ^2H_7$]-glucose as the sole nitrogen and carbon sources, respectively, as described previously.¹⁰

and with essentially no excitation of spins resonating at frequencies outside of a window extending beyond $\pm\omega_{1,CW}$ from the $^1H/^13C$ carriers. The $^1H^\alpha$ magnetization at point e is subsequently locked along its effective field for a time T , during which relaxation occurs as $I = I_0 \exp(-R_{1\rho}T)$, prior to recording the spectrum.

As a test of the method, we used an Abp1p SH3 domain-ligand exchanging system with only a small mole fraction of added ligand, as described previously.²² In this case, the ground state is the apo form of the protein, and the signs of the previously measured $^1H^\alpha \Delta\tilde{\omega}$ values¹⁰ can be obtained using the pulse scheme in Figure 1 and subsequently compared with the “correct” signs from chemical shift values measured directly in the spectra of the apo and fully ligand-bound domains. Previous $^1H^\alpha$ CPMG dispersion measurements at 25 °C established that $k_{ex} = 300 \text{ s}^{-1}$ and $p_E = 6\%$, with $\Delta\tilde{\omega}$ in the range 0.05–0.55 ppm for 17 residues.¹⁰

For each of these residues, values of δ_G and ω_1 were chosen on the basis of k_{ex} , p_E , and residue-specific $|\Delta\tilde{\omega}|$ values from CPMG measurements using a grid search that maximized

$$\Delta = \left| \exp(-R_{1\rho}^+ T) - \exp(-R_{1\rho}^- T) \right| \quad (3)$$

where $T = 50 \text{ ms}$ and, according to eqs 1 and 2,

$$R_{1\rho}^\pm = R_1 \cos^2 \theta + \left(R_2 + \frac{p_E \Delta\omega^2 k_{ex}}{(\pm\delta_G + |\Delta\omega|)^2 + \omega_1^2 + k_{ex}^2} \right) \sin^2 \theta \quad (4)$$

and the optimum δ_G and ω_1 values were subsequently used in the experiments. Notably, although Δ depends on R_1 and R_2 , the position of the maximum does not. For 14 of the 17 residues, the signs of $\Delta\tilde{\omega}$ ($|\Delta\tilde{\omega}| \geq 0.05 \text{ ppm}$) could be determined correctly, while for the remaining three, the $R_{1\rho}$ values for $\delta_G \approx \pm\Delta\omega$ were not sufficiently different to establish the sign [see the Supporting Information (SI)]. Not surprisingly, the $\Delta\tilde{\omega}$ values for these residues were small (0.01–0.03 ppm).

Encouraged by these results on a test system, we next turned to the A39V/N53P/V55L Fyn SH3 domain,¹⁴ for which $k_{ex} = 780 \text{ s}^{-1}$ and $p_E = 1.4\%$ (20 °C). $^1H^\alpha R_{1\rho}$ values were measured for 24 residues, and the sign of $\Delta\tilde{\omega}$ was unambiguously determined for 19 of them ($\Delta\tilde{\omega} \geq 0.17 \text{ ppm}$; see the SI). Figure 2 shows $R_{1\rho}$ decay curves (along with an on-resonance measurement) for residues Ala56 and Pro57. The larger $R_{1\rho}$ value when the irradiating field was applied upfield of the peak from the major conformer of Ala56 indicates that $\Delta\omega = \Omega_E - \Omega_G$ is negative; conversely, the sign of $\Delta\tilde{\omega}$ for Pro57 must be positive. As expected from eq 1, the decay curve for the on-resonance spin-lock case (black) was always below those generated when the spin-lock was applied off-resonance.

Figure 2 also shows contour plots of Δ (eq 3) used to generate the optimized experimental δ_G and ω_1 values.

In summary, we have presented a simple method for measuring the signs of $^1H^\alpha \Delta\tilde{\omega}$ values, allowing the determination of $^1H^\alpha$ chemical shifts of invisible, excited conformers. It is anticipated that these shifts will be important restraints for defining conformational ensembles characterizing intermediates that are both transiently formed and short-lived but nevertheless play important roles in biological function.

Acknowledgment. R.A. is a recipient of a DOC-fORTE Fellowship of the Austrian Academy of Sciences. P.N. and D.F.H. are recipients of postdoctoral fellowships from the Canadian Institutes of Health Research (CIHR). This work was supported by a grant from the CIHR. L.E.K. holds a Canada Research Chair in Biochemistry.

Supporting Information Available: Relaxation curves for all of the measured residues in the proteins studied, tables of $^1H^\alpha \Delta\tilde{\omega}$ values, simulations of decay profiles for different offsets and ω_1 values, and additional pulse sequence information. This material is available free of charge via the Internet at <http://pubs.acs.org>.

References

- (1) Karplus, M.; Kuriyan, J. *Proc. Natl. Acad. Sci. U.S.A.* **2005**, *102*, 6679.
- (2) Henzler-Wildman, K.; Kern, D. *Nature* **2007**, *450*, 964.
- (3) Palmer, A. G.; Kroenke, C. D.; Loria, J. P. *Methods Enzymol.* **2001**, *339*, 204.
- (4) Skrynnikov, N. R.; Dahlquist, F. W.; Kay, L. E. *J. Am. Chem. Soc.* **2002**, *124*, 12352.
- (5) Hansen, D. F.; Vallurupalli, P.; Kay, L. E. *J. Biomol. NMR* **2008**, *41*, 113.
- (6) Hansen, D. F.; Vallurupalli, P.; Lundström, P.; Neudecker, P.; Kay, L. E. *J. Am. Chem. Soc.* **2008**, *130*, 2667.
- (7) Ishima, R.; Baber, J.; Louis, J. M.; Torchia, D. A. *J. Biomol. NMR* **2004**, *29*, 187.
- (8) Ishima, R.; Torchia, D. *J. Biomol. NMR* **2003**, *25*, 243.
- (9) Loria, J. P.; Rance, M.; Palmer, A. G. *J. Am. Chem. Soc.* **1999**, *121*, 2331.
- (10) (a) Lundström, P.; Hansen, D. F.; Vallurupalli, P.; Kay, L. E. *J. Am. Chem. Soc.* **2009**, *131*, 1915. (b) Lundström, P.; Lin, H.; Kay, L. E. *J. Biomol. NMR* **2009**, in press.
- (11) Wishart, D. S.; Case, D. A. *Methods Enzymol.* **2001**, *338*, 3.
- (12) Kloiber, K.; Konrat, R. *J. Biomol. NMR* **2000**, *18*, 33.
- (13) Korzhnev, D. M.; Neudecker, P.; Mittermaier, A.; Orekhov, V. Y.; Kay, L. E. *J. Am. Chem. Soc.* **2005**, *127*, 15602.
- (14) Neudecker, P.; Zarrine-Afsar, A.; Choy, W. Y.; Muhandiram, D. R.; Davidson, A. R.; Kay, L. E. *J. Mol. Biol.* **2006**, *363*, 958.
- (15) Trott, O.; Palmer, A. G. *J. Magn. Reson.* **2002**, *154*, 157.
- (16) Korzhnev, D. M.; Orekhov, V. Y.; Kay, L. E. *J. Am. Chem. Soc.* **2005**, *127*, 713.
- (17) Hansen, A. L.; Nikolova, E. N.; Casiano-Negroni, A.; Al-Hashimi, H. M. *J. Am. Chem. Soc.* **2009**, *131*, 3818.
- (18) Boulat, B.; Bodenhausen, G. *J. Biomol. NMR* **1993**, *3*, 335.
- (19) Korzhnev, D. M.; Orekhov, V. Y.; Dahlquist, F. W.; Kay, L. E. *J. Biomol. NMR* **2003**, *26*, 39.
- (20) Massi, F.; Johnson, E.; Wang, C.; Rance, M.; Palmer, A. G. *J. Am. Chem. Soc.* **2004**, *126*, 2247.
- (21) Pelupessy, P.; Chiapparini, E. *Concepts Magn. Reson.* **2000**, *12*, 103.
- (22) Vallurupalli, P.; Hansen, D. F.; Stollár, E. J.; Meirovitch, E.; Kay, L. E. *Proc. Natl. Acad. Sci. U.S.A.* **2007**, *104*, 18473.

JA904315M

Supporting information for

Measuring the Signs of $^1\text{H}^\alpha$ Chemical Shift Differences Between Ground and Excited Protein States by Off-Resonance Spin-Lock $\text{R}_{1\rho}$ NMR Spectroscopy

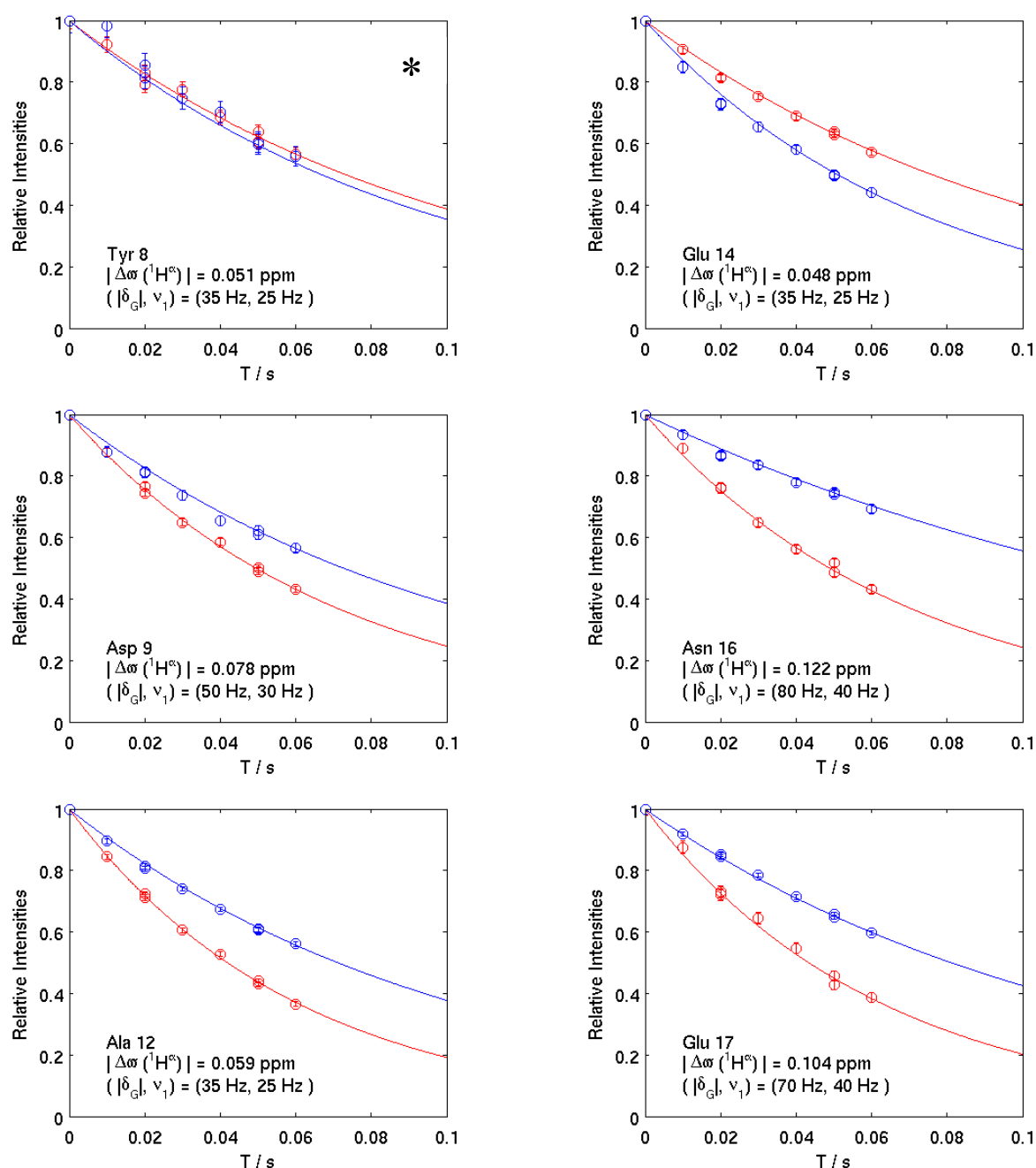
Renate Auer^{1,2}, Philipp Neudecker², D. Ranjith Muhandiram², Patrik Lundström^{2,3}, D.

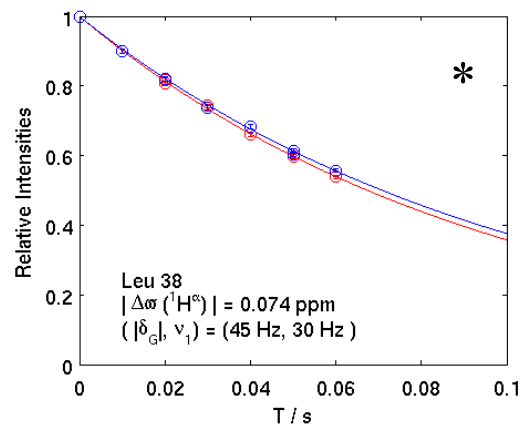
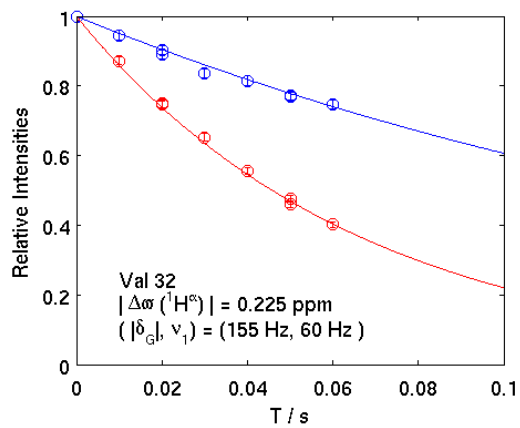
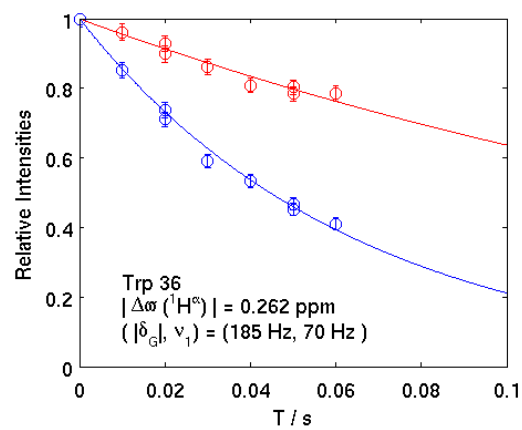
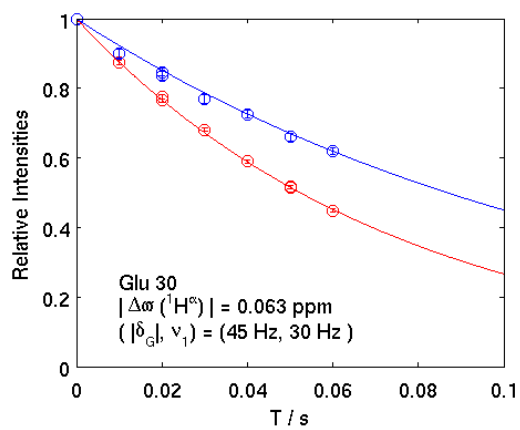
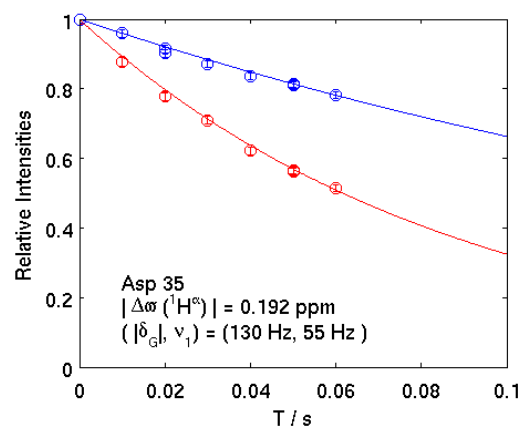
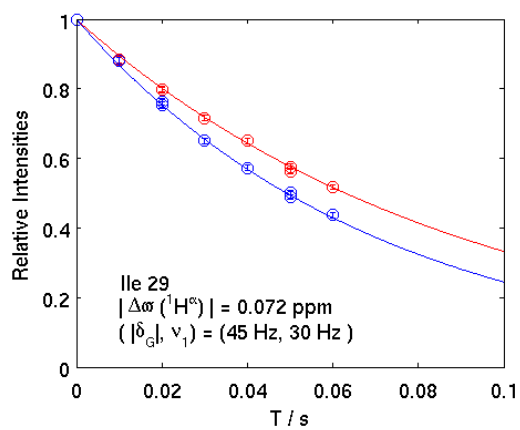
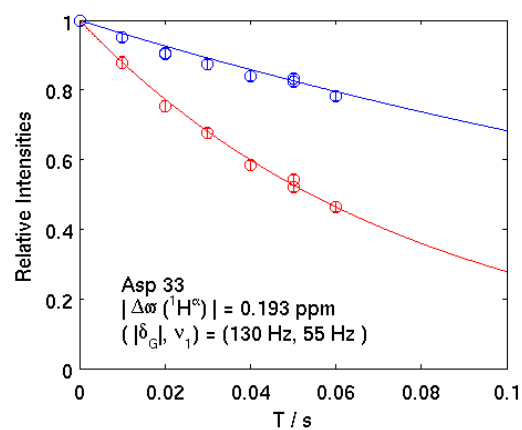
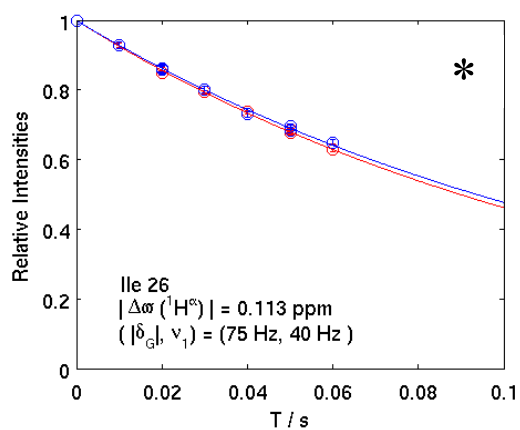
Flemming Hansen², Robert Konrat¹ and Lewis E. Kay²

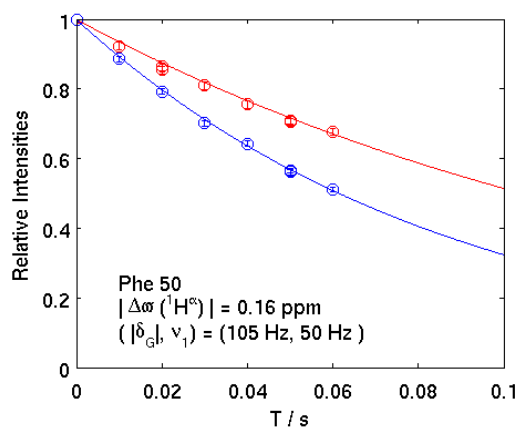
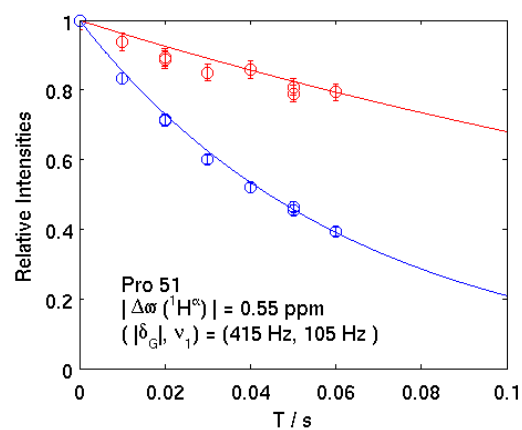
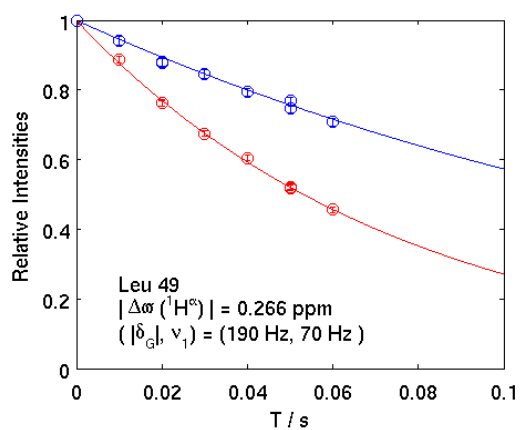
¹*Department of Structural and Computational Biology, Max F. Perutz Laboratories, University of Vienna, Campus-Vienna-Biocenter 5, A-1030 Vienna, Austria,* ²*Departments of Molecular Genetics, Biochemistry and Chemistry, University of Toronto, Toronto, Ontario, Canada, M5S 1A8 and* ³*Molecular Biotechnology/IFM Linköping University, SE-581 83 Linköping, Sweden*

Details of Pulse Scheme (Figure 1): ^1H and ^{13}C carrier frequencies are placed initially on resonance for the peak of interest; subsequently the ^1H carrier is jumped to the position of the spin-lock field immediately prior to the pulse of phase ϕ_4 . All solid pulses have flip angles of 90° and are applied along the x-axis, unless indicated otherwise. Simultaneous $^1\text{H}/^{13}\text{C}$ spin-lock fields (140 Hz) are applied for durations of $1/J_{\text{CH}}$ (between points *a,b* and *c,d*) where J_{CH} is the one-bond $^1\text{H}^\alpha$ - $^{13}\text{C}^\alpha$ scalar coupling constant (≈ 140 Hz). Immediately after gradient 1 ^1H purge pulses are applied (17 kHz) for durations of 2 ms (x-axis) and 1 ms (y-axis) to eliminate residual water signal. ^1H pulses of phase ϕ_4/ϕ_5 are applied with a flip angle θ such that $\tan\theta = \omega_I/|\delta_G|$, using (δ_G, ω_I) optimized as described in the text. During the spin-lock period an on-resonance ^{13}C continuous-wave decoupling field of 2.5 kHz is applied to eliminate scalar coupling modulations and cross-correlation effects between ^1H - ^{13}C dipolar and ^1H CSA interactions. The delay τ_{eq} is set to 5 ms to ensure that the magnetization from each of the exchanging states corresponds faithfully to the equilibrium distribution¹. ^{13}C decoupling during acquisition is achieved with a WALTZ-16 field². The phase cycle is: $\phi_1=(y,-y)$, $\phi_2=2(x),2(-x)$, $\phi_3=4(x),4(-x)$, $\phi_6 = x,2(-x),x-x,2(x),-x$. For the spin-lock carrier upfield(downfield) of the ground state resonance (on Varian spectrometers) $\phi_4=y(-y)$ and $\phi_5=-y(y)$. Gradient strengths and durations are (ms,G/cm): 0=(1,7.5), 1=(0.5,10), 2=(0.8,15), 3=(0.6,-4), 4=(0.2,-4), 5=(0.5,8).

Figure S1. $R_{1\rho}$ values measured using the pulse scheme of Figure 1 (800 MHz) for offsets downfield (red) and upfield (blue) of the major peak. The exchanging system is the Abp1p SH3 domain + 6% Ark1p peptide³. $^1\text{H}^\alpha$ $|\Delta\omega|$ values obtained from analysis of CPMG relaxation dispersion experiments⁴ are indicated in each panel, along with optimal ($|\delta_G|, \nu_1 = \omega_1/2\pi$) values, calculated as described in the text (for a spectrometer field of 800 MHz). The solid lines were obtained from a fit of the data to an exponential decay function, error bars were extracted from duplicate data points. Those panels indicated by * show results from residues whose $\Delta\omega$ values are overestimated from CPMG relaxation dispersion measurements (see Table T1). For these residues it is not possible to confidently predict the sign of $\Delta\omega$ since $R_{1\rho}^\pm$ are not sufficiently different.







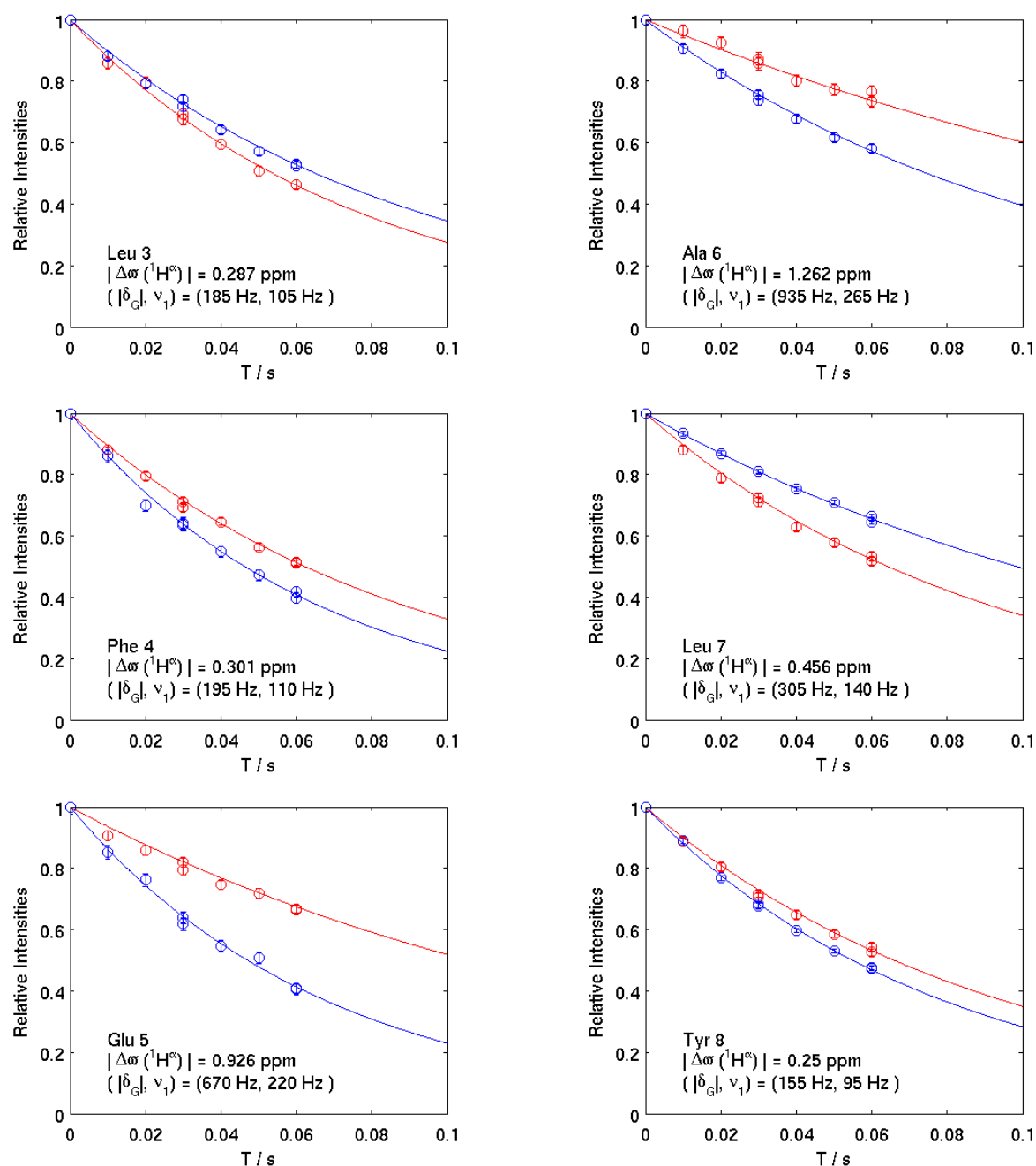
Each data point was obtained in approximately 6 minutes (room temperature probe-head), providing excellent signal-to-noise ($\approx 1 \text{ mM}$ sample).

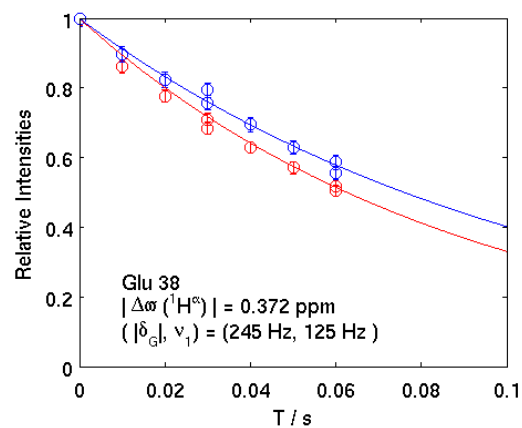
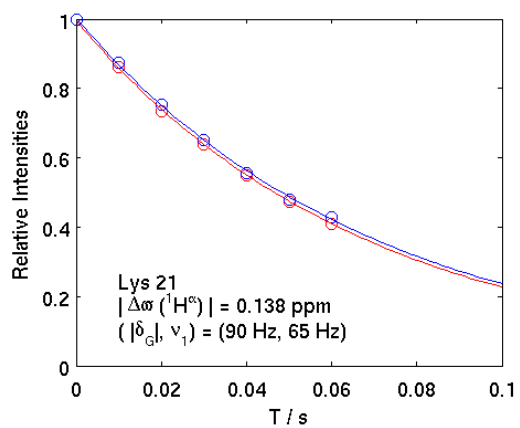
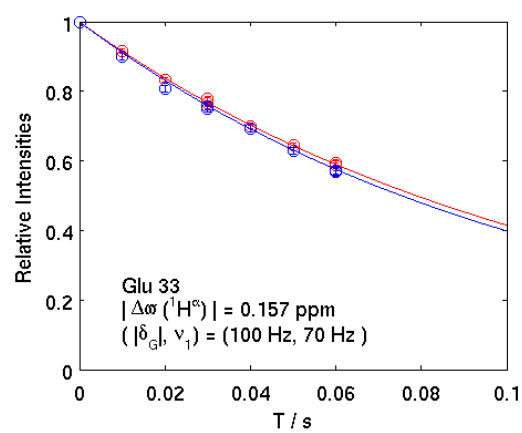
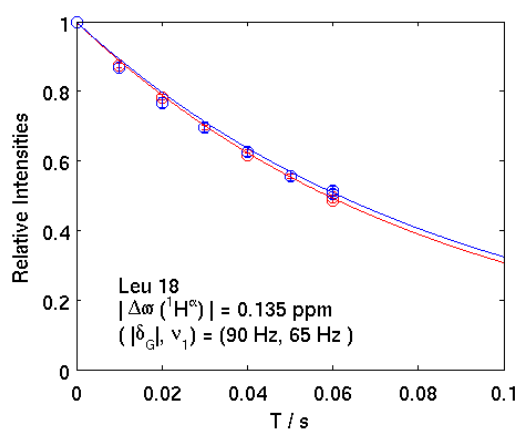
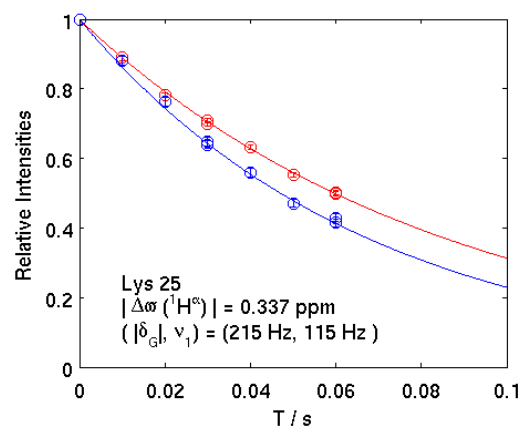
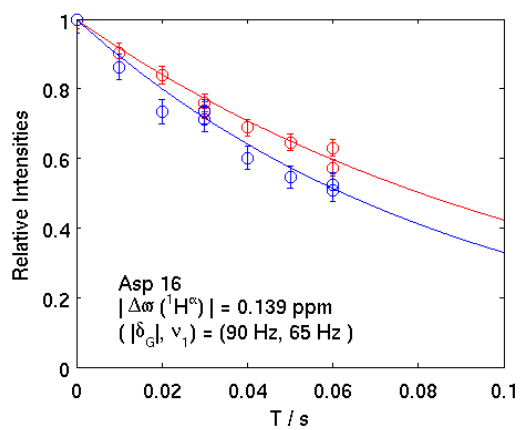
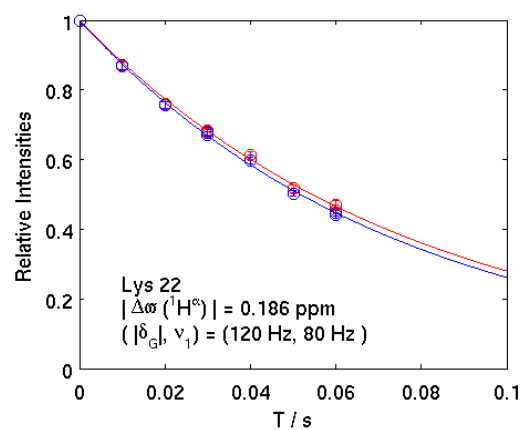
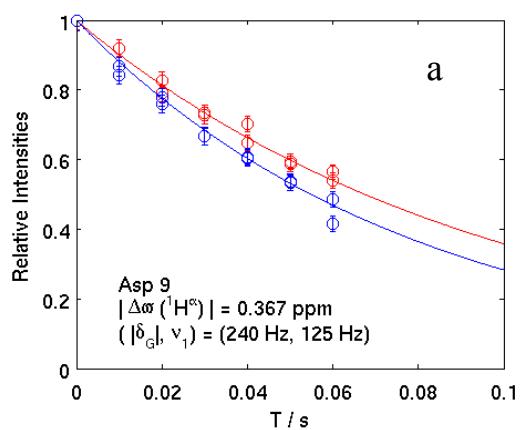
Table T1: 17 residues in the Abp1p SH3 domain, 6% Ark1p sample for which $^1\text{H}^\alpha \Delta\omega$ values were measured via CPMG relaxation dispersion experiments⁴. First column shows signed $\Delta\omega$ values (ppm) obtained directly from spectra of the ligand-free and bound Abp1p SH3 domains. Second column indicates $|\Delta\omega|$ values from the $^1\text{H}^\alpha$ CPMG experiment⁴ along with signs obtained from off-resonance $R_{1\rho}$ measurements using the pulse sequence of Figure 1. Sign information ('no sign') could not be obtained for residues 8, 26 and 38 ('no sign'); these residues have the smallest $|\Delta\omega|$ values of the residues considered (see first column, $\Delta\omega$ (Direct)) and the lowest t-test values (last column).

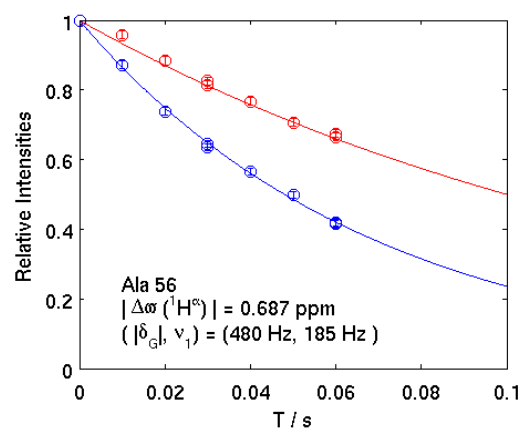
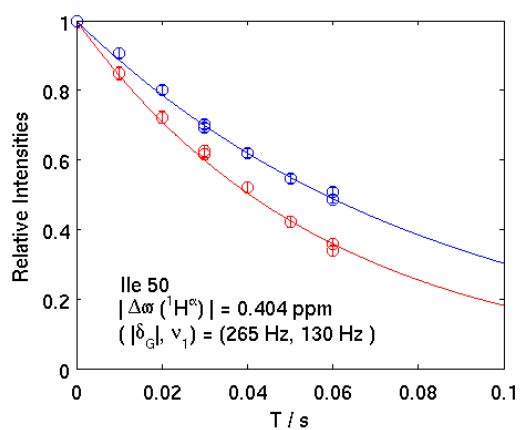
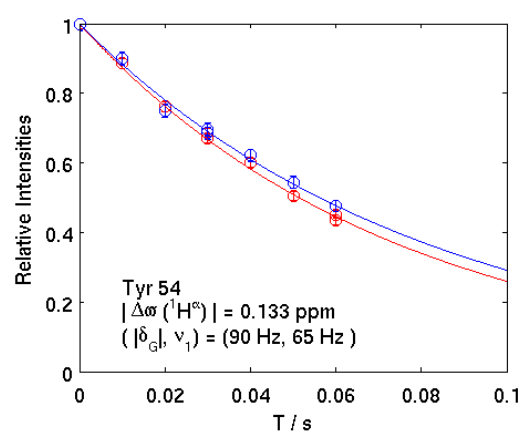
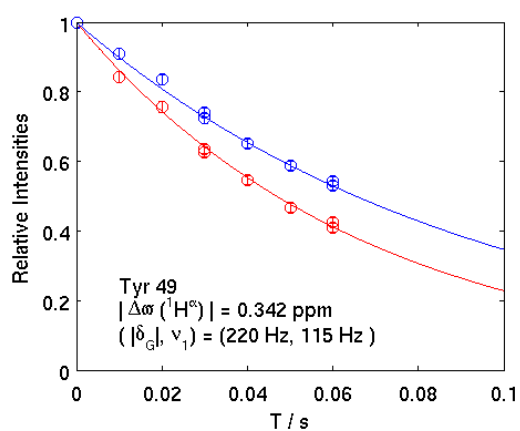
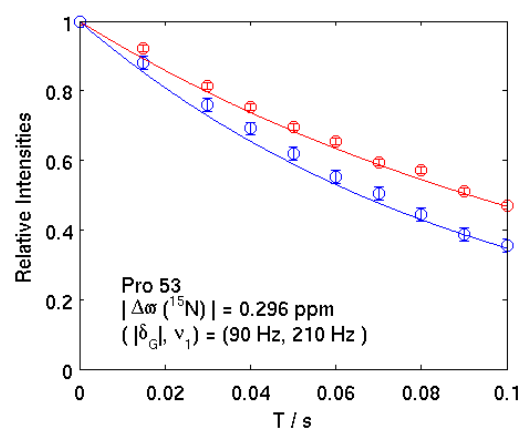
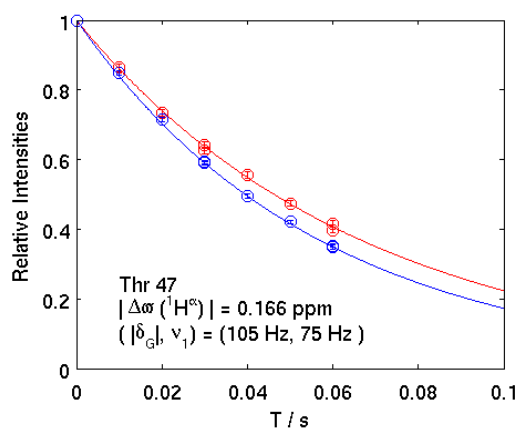
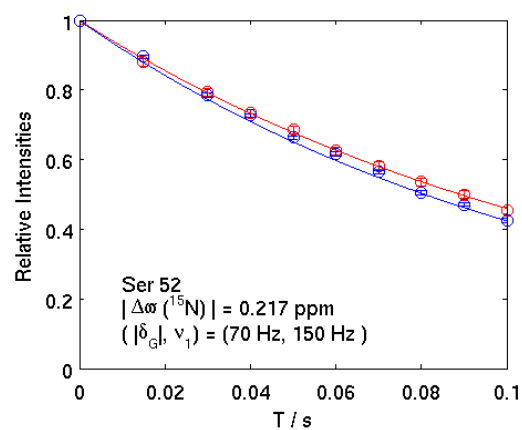
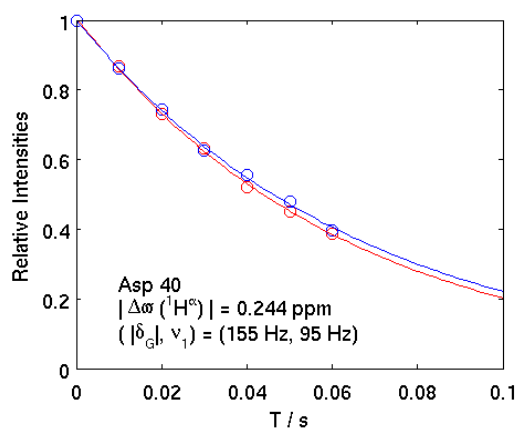
Residue	$\Delta\omega$ (Direct) / ppm	$\Delta\omega$ (Extracted) / ppm	t value ^a
Val 32	+ 0.218	+ 0.225 \pm 0.005	32
Leu 49	+ 0.211	+ 0.266 \pm 0.006	29
Asp 35	+ 0.199	+ 0.192 \pm 0.005	26
Ala 12	+ 0.059	+ 0.059 \pm 0.005	26
Glu 30	+ 0.055	+ 0.063 \pm 0.005	24
Pro 51	- 0.541	- 0.55 \pm 0.01	23
Asp 33	+ 0.188	+ 0.193 \pm 0.005	22
Asn 16	+ 0.116	+ 0.122 \pm 0.004	21
Phe 50	- 0.132	- 0.160 \pm 0.006	20
Trp 36	- 0.293	- 0.262 \pm 0.006	17
Glu 17	+ 0.083	+ 0.104 \pm 0.004	15
Glu 14	- 0.063	- 0.048 \pm 0.007	12
Asp 9	+ 0.061	+ 0.078 \pm 0.007	12
Ile 29	- 0.050	- 0.072 \pm 0.004	12
Leu 38	- 0.012	0.074 \pm 0.004 (no sign)	3
Ile 26	- 0.028	0.113 \pm 0.004 (no sign)	2
Tyr 8	- 0.031	0.051 \pm 0.005 (no sign)	1

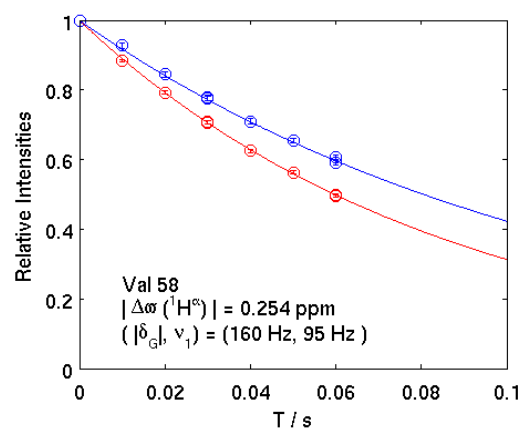
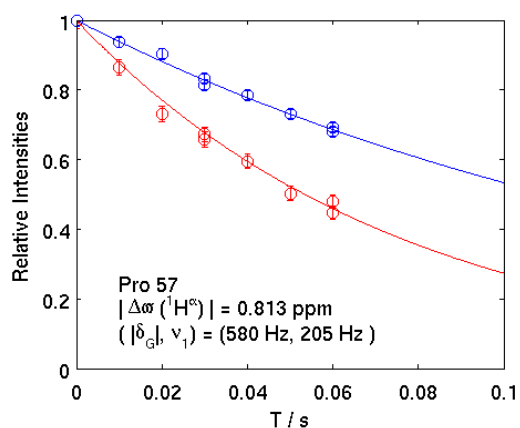
^a Student's t-test value to evaluate whether $R_{1\rho}^\pm$ differ based on equations (18.1) and (18.2) of reference 5. Values $t > t_{\alpha(2),n}$ indicate a statistically significant difference at a confidence limit of $> (1-\alpha)$ with n the number of degrees of freedom $n=2N-4$ (N is the number of points measured per decay curve). For $t \approx t_{\alpha(2),n}$ (shaded) it is important to inspect the decay profiles closely prior to choosing the sign. For $t < t_{\alpha(2),n}$ decay curves for $R_{1\rho}^\pm$ are essentially superimposed and no sign information is available. We chose $\alpha=0.05$ corresponding to a confidence level of 95% which gives $t_{0.05(2),14} = 2.15$.

Figure S2. $R_{1\rho}$ values measured using the pulse scheme of Figure 1 for offsets downfield (red) and upfield (blue) of the major peak. The exchanging system is the A39V/N53P/V55L Fyn SH3 domain⁵. $^1\text{H}^\alpha$ $|\Delta\omega|$ values obtained from analysis of CPMG relaxation dispersion experiments are indicated in each panel, along with optimal ($|\delta_G|, \nu_1 = \omega_1/2\pi$) values, calculated as described in the text (for a spectrometer field of 800 MHz). The solid lines were obtained from a fit of the data to an exponential decay function, error bars were extracted from duplicate data points.









^a Difference in $R_{1\rho}^{\pm}$ decay profiles could not be observed using optimized $(|\delta_G|, \nu_1)$ values. Complete $R_{1\rho}$ vs δ_G profiles were recorded at several ω_1 values to determine the optimal $(|\delta_G|, \nu_1)$ values experimentally. Values of $(|\delta_G|, \nu_1) = (200 \text{ Hz}, 100 \text{ Hz})$ were chosen to produce the $R_{1\rho}^{\pm}$ decay curves in the figure.

Each data point was obtained in approximately 6 minutes (room temperature probe-head), providing excellent signal-to-noise ($\approx 1 \text{ mM}$ sample).

Table T2. 24 residues in the A39V/N53P/V55L Fyn SH3 domain for which $^1\text{H}^\alpha \Delta\varpi$ ($\varpi_E - \varpi_G$) values were measured using the CPMG relaxation dispersion experiment as described in ref 4. $|\Delta\varpi|$ values from CPMG experiments along with signs obtained from off-resonance $R_{1\rho}$ measurements using the pulse sequence of Figure 1 are indicated. Sign information could not be obtained in many cases where $|\Delta\varpi| < 0.25$ ppm (indicated by ‘no sign’). In the case considered here the excited state corresponds to a folding intermediate⁶.

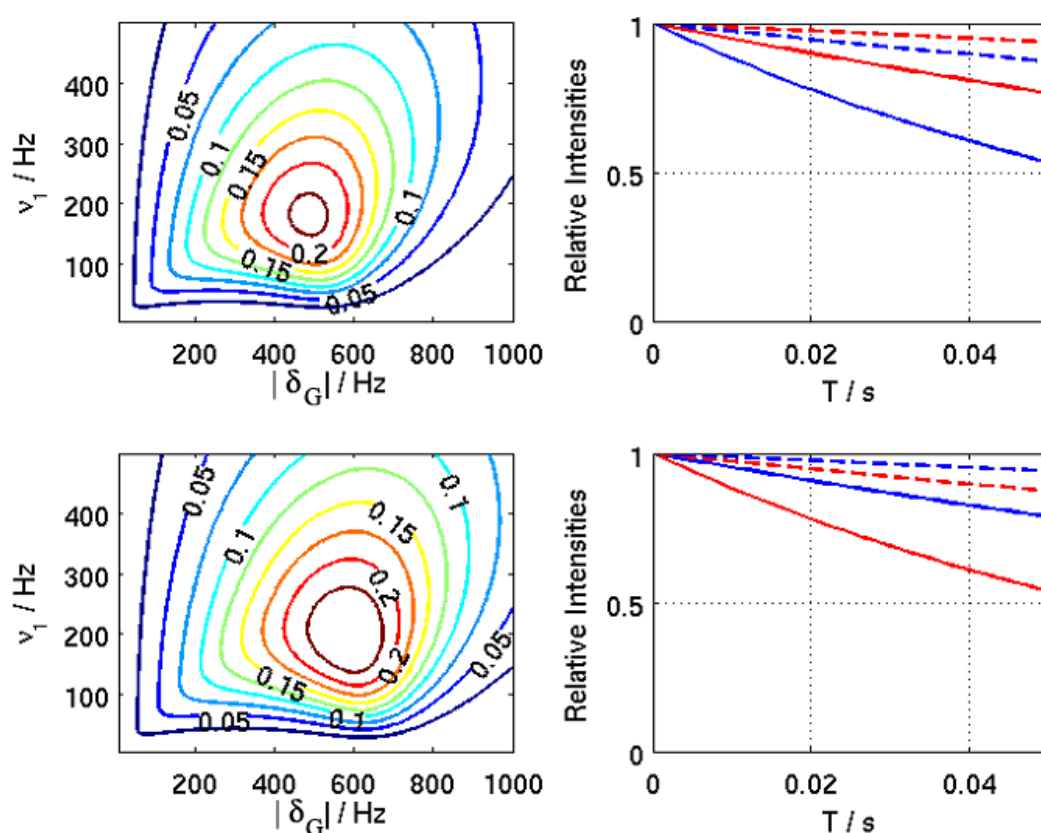
Residue	$\Delta\varpi$ (Extracted) / ppm	t value ^a
Ala 56	- 0.69 ± 0.04	24
Val 58	+ 0.25 ± 0.02	18
Glu 5	- 0.93 ± 0.05	15
Pro 57	+ 0.81 ± 0.05	12
Leu 7	+ 0.46 ± 0.03	12
Pro 53	- 0.30 ± 0.03	11
Ala 6	- 1.26 ± 0.08	10
Ile 50	+ 0.40 ± 0.03	10
Lys 25	- 0.34 ± 0.02	10
Tyr 49	+ 0.34 ± 0.02	10
Thr 47 ^b	- 0.17 ± 0.02	9
Phe 4	- 0.30 ± 0.02	8
Tyr 8	- 0.25 ± 0.02	7
Leu 3	+ 0.29 ± 0.02	6
Ser 52 ^b	- 0.22 ± 0.02	6
Asp 9	+ 0.37 ± 0.03	4
Glu 38	+ 0.37 ± 0.02	3
Asp 16	- 0.14 ± 0.03	3
Tyr 54	+ 0.13 ± 0.02	3
Arg 40	0.24 ± 0.02 (no sign)	3
Lys 22	0.19 ± 0.02 (no sign)	2
Glu 33	0.16 ± 0.01 (no sign)	2
Leu 18	0.14 ± 0.02 (no sign)	2
His 21	0.14 ± 0.02 (no sign)	2

^a See legend ‘a’ for table T1.

^b Note, while the errors of $\Delta\varpi$ values for serine and threonine residues are higher as discussed in detail previously⁴, the signs can still be extracted accurately using the present off-resonance $^1\text{H}^\alpha R_{1\rho}$ experiment.

It is of interest to note that signs were obtained for smaller $|\Delta\varpi|$ values in the case of the Abp1p system than for the A39V/N53P/V55L Fyn SH3 domain, reflecting the different exchange parameters that are operative in each case; $(p_E, k_{ex}) = (6\%, 300\text{s}^{-1})$ and $(1.4\%, 780\text{s}^{-1})$ for Abp1p and A39V/N53P/V55L Fyn SH3, respectively.

Figure S3. The importance of optimizing values of $\Delta(\delta_G, \omega_I)$ used in $R_{1\rho}$ experiments. Values of $\Delta(\delta_G, \omega_I)$ have been optimized (see eqs 3 and 4) for Ala56 (top) and Pro57 (bottom) of the A39V/N53P/V55L Fyn SH3 domain (left panels) using exchange parameters, $k_{ex} = 780 \text{ s}^{-1}$ and $p_E = 1.4\%$ (20°C), along with values of $^1\text{H}^\alpha$ $|\Delta\varpi| = 0.687 \text{ ppm}$ (550 Hz at 800 MHz) and $|\Delta\varpi| = 0.813 \text{ ppm}$ (650 Hz at 800 MHz) for residues 56 and 57, respectively (values obtained from analysis of CPMG data sets). Optimized $(|\delta_G|, \nu_I)$ values are (485 Hz, 180 Hz) for Ala56 and (585 Hz, 195 Hz) for Pro57. $R_{1\rho}$ decay curves calculated using the optimized values are shown in solid lines (right panels) for Ala56 (top) and Pro57 (bottom), with corresponding values calculated using $|\delta_G| = |\delta\varpi|$ and $\nu_I = 50 \text{ Hz}$, dashed lines. Red (blue) decay curves are calculated for the spin-lock field positioned downfield (upfield) of the resonance position of the probe in the ground state. It is clear that larger differences in $R_{1\rho}$ decay curves are obtained with optimized values, leading to more accurate determinations of signs.



- (1) Korzhnev, D. M.; Orekhov, V. Y.; Kay, L. E. *J Am Chem Soc* **2005**, *127*, 713-721.
- (2) Shaka, A. J.; Keeler, J.; Frenkiel, T.; Freeman, R. *J. Magn. Reson.* **1983**, *52*, 335-338.
- (3) Vallurupalli, P.; Hansen, D. F.; Kay, L. E. *Proc Natl Acad Sci U S A* **2008**, *105*, 11766-11771.
- (4) Lundstrom, P.; Hansen, D. F.; Vallurupalli, P.; Kay, L. E. *J Am Chem Soc* **2009**, *131*, 1915-1926.
- (5) Zar, J. H. *Biostatistical Analysis*, 2nd edition, **1984**, Prentice-Hall, New Jersey
- (6) Neudecker, P.; Zarrine-Afsar, A.; Choy, W. Y.; Muhandiram, D. R.; Davidson, A. R.; Kay, L. E. *J Mol Biol* **2006**, *363*, 958-976.

III

Measurement of signs of chemical shift differences between ground and excited protein states: a comparison between H(S/M)QC and $R_{1\rho}$ methods

Renate Auer · D. Flemming Hansen · Philipp Neudecker ·
Dmitry M. Korzhnev · D. Ranjith Muhandiram ·
Robert Konrat · Lewis E. Kay

Received: 20 October 2009 / Accepted: 1 December 2009 / Published online: 22 December 2009
© Springer Science+Business Media B.V. 2009

Abstract Carr-Purcell-Meiboom-Gill (CPMG) relaxation dispersion NMR spectroscopy has emerged as a powerful tool for quantifying the kinetics and thermodynamics of millisecond exchange processes between a major, populated ground state and one or more minor, low populated and often invisible ‘excited’ conformers. Analysis of CPMG data-sets also provides the magnitudes of the chemical shift difference(s) between exchanging states ($|\Delta\omega|$), that inform on the structural properties of the excited state(s). The sign of $\Delta\omega$ is, however, not available from CPMG data. Here we present one-dimensional NMR experiments for measuring the signs of $^1\text{H}^{\text{N}}$ and $^{13}\text{C}^{\alpha}$ $\Delta\omega$ values using weak off-resonance $R_{1\rho}$ relaxation measurements, extending the spin-lock approach beyond previous applications focusing on the signs of ^{15}N and $^1\text{H}^{\alpha}$ shift differences. The accuracy of the method is established by using an exchanging system where the invisible, excited state can be converted to the visible, ground state by altering conditions so that the signs of $\Delta\omega$ values obtained from the spin-lock approach can be validated with those measured directly. Further, the spin-lock experiments are

compared with the established H(S/M)QC approach for measuring the signs of chemical shift differences. For the Abp1p and Fyn SH3 domains considered here it is found that while H(S/M)QC measurements provide signs for more residues than the spin-lock data, the two different methodologies are complementary, so that combining both approaches frequently produces signs for more residues than when the H(S/M)QC method is used alone.

Keywords H(S/M)QC · Off-resonance spin-lock · Relaxation dispersion · Chemical exchange · CPMG · Chemical shift

Introduction

NMR spectroscopy has emerged as a powerful tool for investigating the role of protein dynamics in a variety of biologically important processes that include allostery, ligand binding, catalysis, and molecular recognition (Boehr et al. 2006; Frederick et al. 2007; Henzler-Wildman and Kern 2007; Kay et al. 1998; Popovych et al. 2006; Sugase et al. 2007). Particularly significant in this regard is the fact that motion can be probed over a broad spectrum of time-scales and in a site-specific manner (Ishima and Torchia 2000; Mittermaier and Kay 2006; Palmer et al. 1996) so that a very detailed description of dynamics is, in principle, possible. Over the course of the past several decades a large number of different experiments (Igumenova et al. 2006; Mittermaier and Kay 2006; Palmer et al. 2005) and labeling schemes (Goto and Kay 2000; Kainosho et al. 2006; LeMaster 1999; Tugarinov and Kay 2004; Zhang et al. 2006) have been developed, optimized for different classes of biomolecules and for the investigation of dynamics in different time-regimes. One particular area that has

Electronic supplementary material The online version of this article (doi:10.1007/s10858-009-9394-z) contains supplementary material, which is available to authorized users.

R. Auer · R. Konrat
Department of Structural and Computational Biology,
Max F. Perutz Laboratories, University of Vienna,
Campus-Vienna-Biocenter 5, 1030 Vienna, Austria

R. Auer · D. F. Hansen · P. Neudecker ·
D. M. Korzhnev · D. R. Muhandiram · L. E. Kay (✉)
Departments of Molecular Genetics, Biochemistry
and Chemistry, University of Toronto, Toronto,
ON M5S 1A8, Canada
e-mail: kay@pound.med.utoronto.ca

generated significant recent interest is the study of millisecond (ms) time-scale dynamics, which can be quantified using CPMG relaxation dispersion experiments (Palmer et al. 2001). Although the basic ideas behind this approach date back over 50 years (Carr and Purcell 1954; Meiboom and Gill 1958), the successful application of the CPMG method to complex systems such as biomolecules had to await developments in both pulse sequence methodology and labeling technology (Loria et al. 1999). In the case of protein applications it is now possible to measure backbone $^1\text{H}^{\text{N}}$ (Ishima and Torchia 2003), ^{15}N (Loria et al. 1999; Tollinger et al. 2001), $^{13}\text{C}^{\alpha}$ (Hansen et al. 2008b), $^1\text{H}^{\alpha}$ (Lundstrom et al. 2009a) and ^{13}CO (Ishima et al. 2004; Lundstrom et al. 2008) as well as side-chain $^{13}\text{C}^{\beta}$ (Lundstrom et al. 2009b) and methyl ^{13}C (Lundstrom et al. 2007b; Skrynnikov et al. 2001) CPMG dispersion profiles for systems in exchange between states that include a major conformation and one or more minor conformers so long as their populations are greater than $\approx 0.5\%$ with lifetimes between ≈ 0.5 and 10 ms (Palmer et al. 2001).

The utility of the CPMG relaxation dispersion experiment is several-fold. First, populations of exchanging conformers can be obtained along with rates of exchange (Palmer et al. 2001), so that in cases where experiments are performed as a function of temperature and/or pressure it is possible to generate a detailed one-dimensional energy landscape for the system under study (Korzhnev et al. 2004, 2006). Second, absolute values of chemical shift differences between exchanging states, $|\Delta\sigma|$, are extracted from fits of dispersion profiles. In cases where the signs of $\Delta\sigma$ are available, the chemical shifts of the excited states can be obtained and exploited for structural studies of these conformers (Vallurupalli et al. 2008). This is particularly significant when one considers that these excited states are generally populated at low levels and only very transiently so that they are invisible both to most other NMR methods and to other biophysical techniques in general.

A number of approaches for obtaining the signs of the chemical shift differences that are conspicuously missing from CPMG dispersion experiments have been developed. In one type of experiment, suggested by Skrynnikov et al. (2002), peak positions in the indirect dimensions of HSQC and HMQC data-sets recorded at several static magnetic fields are compared to isolate the sign information for ^{15}N and ^{13}C $\Delta\sigma$ values (referred to in what follows as the H(S/M)QC method). A second approach, termed CEESY, is based on very similar principles except that the sign information is encoded in the relative peak intensities of a pair of data-sets (van Ingen et al. 2006). This approach has been applied to obtain the sign of ^{15}N and $^1\text{H}^{\text{N}}$ $\Delta\sigma$ values. Finally, a third method measures selective $R_{1\rho}$ relaxation rates as a function of spin-lock offset (Auer et al. 2009; Hansen et al. 2009; Korzhnev et al. 2003, 2005; Massi et al.

2004; Trott and Palmer 2002), which can be a sensitive reporter of sign information as well. To date, applications of $R_{1\rho}$ methods have focused on both ^{15}N (Korzhnev et al. 2005) and $^1\text{H}^{\alpha}$ (Auer et al. 2009) spins. Recognizing the importance of chemical shifts in structural studies of excited states, the goal of the present work is to extend the methodology further to include both $^{13}\text{C}^{\alpha}$ and $^1\text{H}^{\text{N}}$ nuclei as well. With the development of several different experimental schemes for measuring such values it is important to establish the limitations and strengths of each approach. With this in mind results from $R_{1\rho}$ and H(S/M)QC approaches are compared and an evaluation of the relative merits of each set of experiments is presented.

Materials and methods

Sample preparation

An NMR sample of U- ^{15}N , ^2H Abp1p SH3 domain was prepared as described in detail previously (Vallurupalli et al. 2007). The final protein concentration was ≈ 1.5 mM, in a buffer consisting of 50 mM sodium phosphate, 100 mM NaCl, 1 mM EDTA, 1 mM NaN_3 , 90% $\text{H}_2\text{O}/10\%$ D_2O , pH = 7.0. Ark1p peptide, which binds the SH3 domain (Haynes et al. 2007), was expressed and purified as described previously (Vallurupalli et al. 2007) and added to the Abp1p SH3 domain sample to produce a complex with $2.5 \pm 0.1\%$ mole fraction bound, as established by ^{15}N CPMG relaxation dispersion experiments (Hansen et al. 2008a). ^{15}N (Korzhnev et al. 2005) and $^1\text{H}^{\text{N}}$ $R_{1\rho}$ experiments, along with ^{15}N – $^1\text{H}^{\text{N}}$ H(S/M)QC data-sets (Skrynnikov et al. 2002) were measured on this sample. A sample of the A39V/N53P/V55L Fyn SH3 domain was prepared as U- ^{13}C , $\approx 50\%$ ^2H , by protein over-expression in M9 minimal media with 50% D_2O and 3 g/l [$^{13}\text{C}_6$, $^2\text{H}_7$]-glucose, as described in detail previously (Neudecker et al. 2006). The sample was 1.0 mM in protein, 0.2 mM EDTA, 0.05% NaN_3 , 50 mM sodium phosphate, pH 7.0, 100% D_2O and was used to record $^1\text{H}^{\alpha}$ $R_{1\rho}$ rates. $^{13}\text{C}^{\alpha}$ $R_{1\rho}$ and H(S/M)QC spectra were recorded on a second A39V/N53P/V55L Fyn SH3 domain sample (1.0 mM) which was generated using [^{13}C]-glucose as the sole carbon source to produce isolated $^{13}\text{C}^{\alpha}$ nuclei, as described previously (Lundstrom et al. 2007a).

NMR spectroscopy

All measurements were carried out at 25°C (Abp1p SH3/Ark1p peptide) or 20°C (A39V/N53P/V55L Fyn SH3) using Varian Inova spectrometers operating at ^1H resonance frequencies of 500 and 800 MHz and equipped with triple-resonance room-temperature probes. Residue selective 1D $R_{1\rho}$ experiments were recorded at 800 MHz. For each

residue known to be affected by exchange two decay curves were recorded, corresponding to $R_{1\rho}^{\pm}$ (see below), with relaxation delays T up to 60 ms ($^1\text{H}^{\alpha}$, $^{13}\text{C}^{\alpha}$) or 100 ms ($^1\text{H}^{\text{N}}$, ^{15}N). For $^{15}\text{N}/^1\text{H}^{\text{N}}$ $R_{1\rho}$ measurements each of the 9 points comprising a single decay curve ($R_{1\rho}^+$ or $R_{1\rho}^-$) was recorded in 1.8/2.35 min, resulting in a total measurement time of 1.1/1.4 h per residue (duplicates for each of the 9 points were obtained). $R_{1\rho}$ values for $^{13}\text{C}^{\alpha}/^1\text{H}^{\alpha}$ were based on 7 time points (duplicates for only 2 of the time points) each requiring 11.3/4.7 min of acquisition time for a net time of 3.4/1.4 h for the complete set of $R_{1\rho}^{\pm}$ decays curves.

Signs of ^{15}N and $^{13}\text{C}^{\alpha}$ shift differences were also obtained from $^{15}\text{N}-^1\text{H}^{\text{N}}$ and $^{13}\text{C}^{\alpha}-^1\text{H}^{\alpha}$ HSQC and HMQC data-sets which were recorded at 500 and 800 MHz in 3 and 2.5 h, respectively. Each data-set was measured in duplicate. Data were processed and analyzed with the nmrPipe/nmrDraw suite of programs (Delaglio et al. 1995) and NMRViewJ (Johnson and Blevins 1994). Simulation and numerical data interpretation were carried out using in-house programs written in Matlab (MathWorks, Inc.).

Statistical analysis

A number of statistical tests have been used to evaluate whether differences in measured $R_{1\rho}^{\pm}$ rates are statistically significant, and hence whether the sign of the chemical shift difference between exchanging states can be extracted from the data (see below). The first approach uses a Student t -test analysis (Zar 1984) in which $R_{1\rho}$ rates are extracted from fits of experimental data to a straight line

$$\ln \frac{I(T)}{I(0)} = y = -R_{1\rho}T \quad (1)$$

and $R_{1\rho}^{\pm}$ values compared according to

$$t = \frac{|R_{1\rho}^+ - R_{1\rho}^-|}{s_{R_{1\rho}^+ - R_{1\rho}^-}} \quad (2)$$

where

$$s_{R_{1\rho}^+ - R_{1\rho}^-}^2 = \frac{s_{yx}^2}{\sum_{i=1}^{n_+} x_{i,+}^2} + \frac{s_{yx}^2}{\sum_{i=1}^{n_-} x_{i,-}^2} \quad (3.1)$$

is the variance of the difference in the slopes $R_{1\rho}^{\pm}$. The value s_{yx}^2 is, in turn, given by

$$s_{yx}^2 = \frac{\sum_{i=1}^{n_+} y_{i,+}^2 - (\sum_{i=1}^{n_+} (x_{i,+})(y_{i,+}))^2 / \sum_{i=1}^{n_+} x_{i,+}^2 + \sum_{i=1}^{n_-} y_{i,-}^2 - (\sum_{i=1}^{n_-} (x_{i,-})(y_{i,-}))^2 / \sum_{i=1}^{n_-} x_{i,-}^2}{n_+ + n_- - 4} \quad (3.2)$$

where $x_{i,\pm}$ are the relaxation time delays (T values in the pulse schemes of Figs. 1 and 6) used to record the decay

curves for measuring $R_{1\rho}^{\pm}$ comprised of n_+ and n_- points, $y_{i,\pm}$ are the corresponding $\ln \left[\frac{I^{\pm}(T)}{I^{\pm}(0)} \right]$ values and $n_+ + n_- - 4 = v$ is the number of degrees of freedom. Calculated Student t -values were compared with two-sided t -test statistics at the 95% confidence level (for example, $t_{0.05(2),14} = 2.15$ for $v = 14$ degrees of freedom, which is germane for the measurements here). For t -values such that $t > t_{\alpha(2),v}$ the $R_{1\rho}^{\pm}$ rates are significantly different with confidence level $>(1 - \alpha)$.

A second method has also been used to evaluate whether $R_{1\rho}^{\pm}$ rates are distinct, based on the F -test statistic (Zar 1984). Here the intensities of the decay curves $I^+(T)$ and $I^-(T)$, from which $R_{1\rho}^+$ and $R_{1\rho}^-$ are obtained, respectively, are used to generate $y'_e(T) = I^+(T)/I^-(T)$. The function $y'_e(T)$ is subsequently fit to (1) a horizontal line $y'_e = k$ and (2) an exponential $y'_e = a \exp(bT)$ and χ^2 values calculated for each fit according to

$$\chi^2 = \sum_i^n \left(\frac{y'_{e,i} - y'_{c,i}}{\sigma_i} \right)^2 \quad (4)$$

where σ_i is the error of each data point, computed as the root mean squared deviations of peak volumes from duplicate measurements. Values of χ^2 obtained from the two models ('linear' vs. 'exponential') are compared using F -test statistics. A cut-off of $p < 2.5\%$ ($1 - p > 97.5\%$) was used to establish whether $R_{1\rho}^{\pm}$ differ. Both the t -test and F -test give consistent results for the protein systems studied here.

Results and discussion

Measuring signs of $\Delta\varpi$ by low power off-resonance $R_{1\rho}$ measurements

For a two-site exchange process involving the interconversion of ground (G) and excited (E) states, $G \xrightleftharpoons[k_{EG}]{k_{GE}} E$, with the population of the ground state, p_G , greatly exceeding that of the excited state, p_E , the rotating frame relaxation rate of a nucleus attached to state G is given by (Trott and Palmer 2002)

$$R_{1\rho} = R_1 \cos^2 \theta + (R_2^o + R_{ex}) \sin^2 \theta \quad (5.1)$$

$$R_{ex} = \frac{p_E \Delta\omega^2 k_{ex}}{\omega_{E,eff}^2 + k_{ex}^2} = \frac{p_E \Delta\omega^2 k_{ex}}{(\delta_G + \Delta\omega)^2 + \omega_1^2 + k_{ex}^2} \quad (5.2)$$

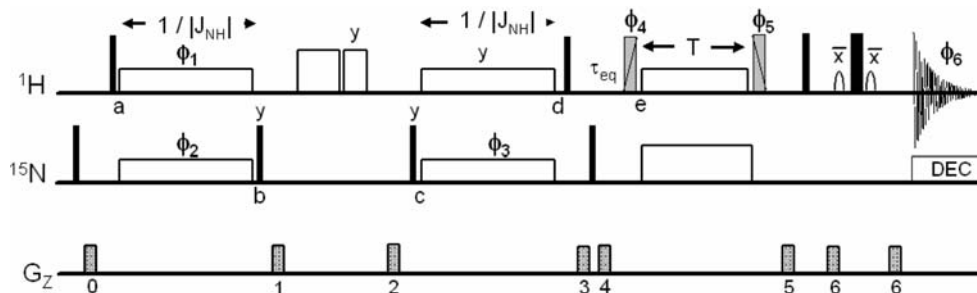


Fig. 1 Pulse scheme for measuring $^1\text{H}^{\text{N}}$ off-resonance $R_{1\rho}$ relaxation rates in $\text{U-}^{15}\text{N}$ labeled proteins. ^1H and ^{15}N carrier frequencies are placed initially on resonance for the peak of interest; subsequently the ^1H carrier is jumped to the position of the spin-lock field immediately prior to the pulse of phase ϕ_4 and then to the water line prior to application of gradient 5. All solid pulses have flip angles of 90° and are applied along the x -axis, unless indicated otherwise. The shaped ^1H pulses are water selective (Piotto et al. 1992). Simultaneous $^1\text{H}/^{15}\text{N}$ spin-lock fields (90 Hz) are applied for durations of $1/|J_{\text{NH}}|$ (between points a , b and c , d) where J_{NH} is the one-bond $^1\text{H}^{\text{N}}$ - ^{15}N scalar coupling constant (≈ -90 Hz). Immediately after gradient 1 ^1H purge pulses are applied (17 kHz) for durations of 4 ms (x -axis) and 2 ms (y -axis) to eliminate residual water signal. ^1H pulses of phases ϕ_4/ϕ_5 are applied with a flip angle θ such that $\tan\theta = \omega_1/\delta_G$, using (δ_G, ω_1) optimized as described in the text. During the spin-lock

period an on-resonance ^{15}N continuous-wave decoupling field of 1.1 kHz is applied to eliminate scalar coupling modulations as well as cross-correlation effects between ^1H - ^{15}N dipolar and ^1H CSA interactions (Peng and Wagner 1992). The delay τ_{eq} is set to 5 ms to ensure that the magnetization from each of the exchanging states corresponds faithfully to the equilibrium distribution (Korzhnev et al. 2005). ^{15}N decoupling during acquisition is achieved with a WALTZ-16 field (Shaka et al. 1983). The phase cycle is: $\phi_1 = (y, -y)$, $\phi_2 = 2(x), 2(-x)$, $\phi_3 = 4(x), 4(-x)$, $\phi_6 = x, -x, 2(x), -x$. For the spin-lock carrier upfield(downfield) of the ground state resonance $\phi_4 = y(-y)$ and $\phi_5 = -y(y)$ (on Varian spectrometers). Gradient strengths and durations are (ms, G/cm): $G_0 = (1, 7.5)$, $G_1 = (0.5, 10)$, $G_2 = (0.8, 15)$, $G_3 = (0.6, -4)$, $G_4 = (0.3, -4)$, $G_5 = (0.5, 8)$, $G_6 = (0.4, -20)$

where R_1 and R_2^0 are longitudinal and intrinsic transverse relaxation rates, respectively, and $R_{\text{ex}}\sin^2\theta$ is the contribution to $R_{1\rho}$ from chemical exchange. In (5.2) $\Delta\omega = \Omega_E - \Omega_G$ (rad/sec), where Ω_i is the chemical shift of the nucleus in state i , $k_{\text{ex}} = k_{\text{GE}} + k_{\text{EG}}$, $\theta = \arctan(\omega_1/\delta_G)$, ω_1 is the strength of the applied field, $\omega_{E,\text{eff}}^2 = \omega_1^2 + \delta_E^2$ and $\delta_E = \Omega_E - \Omega_{\text{SL}}$, $\delta_G = \Omega_G - \Omega_{\text{SL}}$ are the resonance offsets from the spin-lock carrier for states E and G , respectively. Note that the maximum in R_{ex} occurs when the spin-lock field is resonant with the frequency of the minor state (5.2) and that R_{ex} measured for $\delta_G \approx -\Delta\omega$ (i.e., $\Omega_{\text{SL}} \approx \Omega_E$) is larger than the corresponding value obtained for $\delta_G \approx \Delta\omega$. Thus, by recording a pair of $R_{1\rho}$ values, corresponding to $\delta_G \approx \pm \Delta\omega$ it is possible to establish the sign of $\Delta\omega$ since the rate measured for $\delta_G \approx -\Delta\omega$ will be larger than for $\delta_G \approx \Delta\omega$ (Korzhnev et al. 2003, 2005; Massi et al. 2004; Trott and Palmer 2002).

Experiments for measurement of the signs of $\Delta\omega$ using the $R_{1\rho}$ approach have been developed previously for both ^{15}N (Korzhnev et al. 2005) and $^1\text{H}^{\text{z}}$ (Auer et al. 2009) nuclei and are similar to schemes described by Boulat and Bodenhausen for the measurement of ^1H relaxation rates in proteins (Boulat and Bodenhausen 1993) and Hansen and Al-Hashimi for quantifying ^{13}C $R_{1\rho}$ values in nucleic acids (Hansen et al. 2009). The experiments make use of very weak spin-lock fields that are optimized for each spin examined (see below) and are thus best implemented in one-dimensional mode, resolution permitting. Analogous experiments,

exploiting the improved resolution of two-dimensional spectroscopy, and using larger spin-lock fields have also been described (Korzhnev et al. 2003; Massi et al. 2004).

Figure 1 shows the pulse sequence that has been designed for the measurement of $^1\text{H}^{\text{N}}$ $R_{1\rho}$ values (and hence for determination of the sign of $^1\text{H}^{\text{N}}$ $\Delta\omega$; in what follows ω is in units of ppm) using very weak spin-lock fields, following very closely on approaches published for ^{15}N and $^1\text{H}^{\text{z}}$ nuclei (Auer et al. 2009; Korzhnev et al. 2005). Briefly, isolation of the resonance in question is achieved by selective Hartmann-Hahn magnetization transfers from $^1\text{H}^{\text{N}}$ to ^{15}N (a to b) and back (c to d) using matched spin-lock fields of strength 90 Hz (Chiarparin et al. 1998; Pelupessy and Chiarparin 2000); for spin-locks of this magnitude correlations outside $\approx 1.5|J_{\text{NH}}|$ from the positions of the $^1\text{H}/^{15}\text{N}$ radio-frequency carriers are suppressed. The resonance of interest is subsequently aligned along the effective magnetic field by a θ -pulse just prior to point e , followed by a relaxation delay of duration T , during which time the $R_{1\rho}$ decay rate is measured. A pair of relaxation curves are obtained, corresponding to $\delta_G \approx \pm \Delta\omega$, from which the sign of $\Delta\omega$ is established (see below). In order to maximize the difference between $R_{1\rho}$ values recorded for $\delta_G \approx +\Delta\omega$ and $\delta_G \approx -\Delta\omega$, (referred to in what follows as $R_{1\rho}^+$ and $R_{1\rho}^-$, respectively) and hence increase the sensitivity of the experiment, optimal spin-lock offset (δ_G) and field strength (ω_1) values are calculated for each residue by maximizing

$$\Delta = \left| \exp(-R_{1\rho}^+ T) - \exp(-R_{1\rho}^- T) \right| \quad (6)$$

as described previously (Auer et al. 2009). In (6) Δ is the difference in decay curves measured for $\delta_G \approx \pm\Delta\omega$ at time T , normalized to $T = 0$ and T corresponds to the maximum time value used in experiments (either 50 or 100 ms in the applications considered here) with

$$R_{1\rho}^\pm = R_1 \cos^2 \theta + \left(R_2^\circ + \frac{p_E \Delta\omega^2 k_{ex}}{(\pm\delta_G + |\Delta\omega|)^2 + \omega_1^2 + k_{ex}^2} \right) \sin^2 \theta, \quad (7)$$

as given by (5.1) and (5.2).

We have chosen to validate the methodology using an Abp1p SH3 domain–ligand exchanging system described in detail in previous publications (Hansen et al. 2008b;

Vallurupalli et al. 2007, 2008), with only a small mole-fraction of ligand added, $p_E = 2.5\%$, $k_{ex} = 300 \text{ s}^{-1}$, 25°C (as established by CPMG relaxation dispersion). The addition of small amounts of ligand renders the bound conformer the invisible, ‘excited’ state whose chemical shifts can be quantified by CPMG (magnitude) and $R_{1\rho}$ (sign) relaxation experiments. The signs of $\Delta\omega$ obtained using the $R_{1\rho}$ approach can then be directly compared with those measured from spectra of apo and fully ligand-bound conformers as a rigorous test of the method. Figure 2 illustrates a number of examples, focusing on both selective $^1\text{H}^\text{N}$ and ^{15}N $R_{1\rho}$ experiments. Optimized values of (δ_G, ω_1) were calculated using the exchange parameters from CPMG measurements listed above and maximizing Δ of (6). The first column in Fig. 2 shows selected regions of 2D ^{15}N – $^1\text{H}^\text{N}$ correlation maps centered on A12 (a), N28 (b)

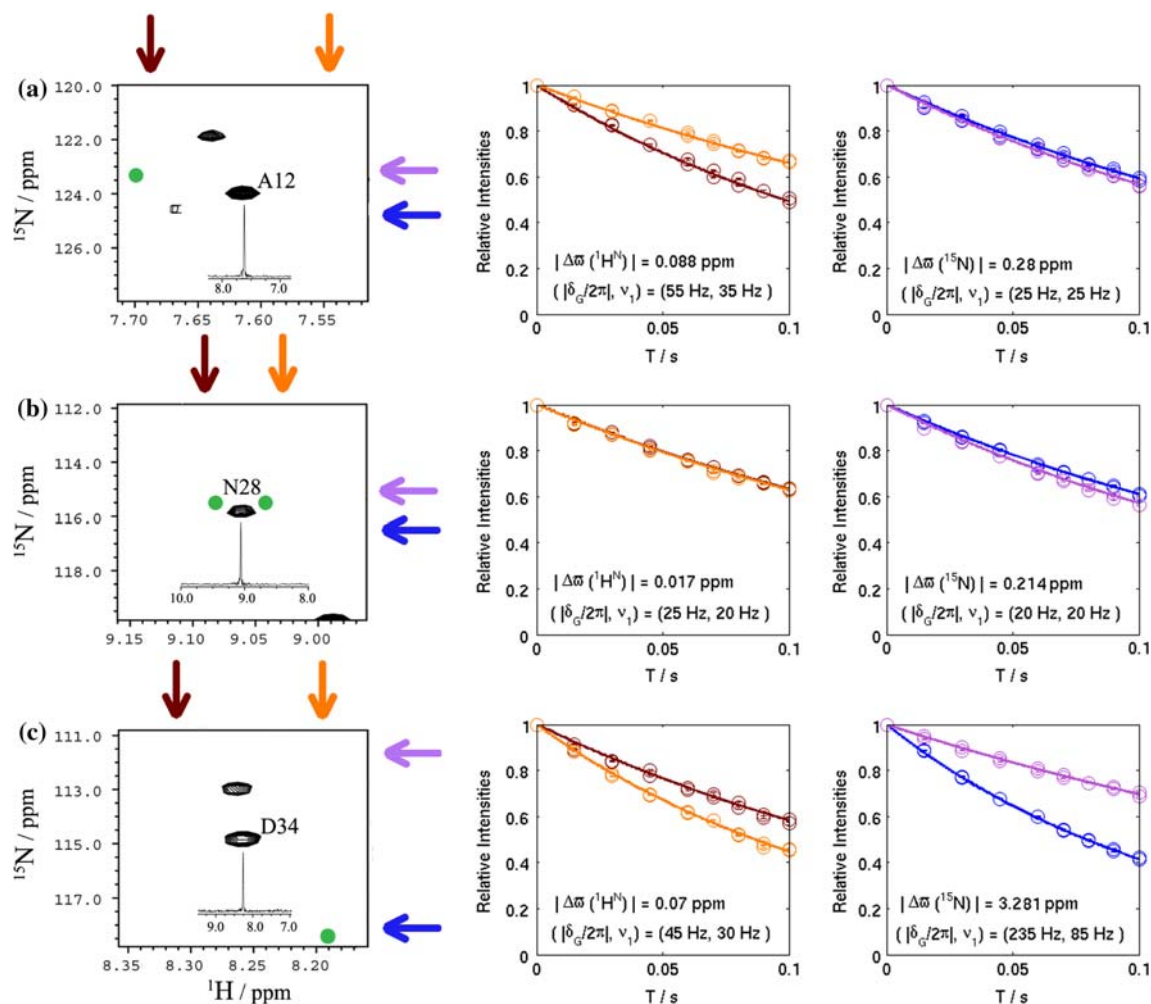


Fig. 2 Selected regions of ^{15}N – $^1\text{H}^\text{N}$ HSQC spectra centered on A12 (a), N28 (b) and D34 (c) of the Abp1p SH3 domain, 2.5% Ark1p peptide, 25°C , 800 MHz. The green dots correspond to positions of the excited state correlations (two dots if the $^1\text{H}^\text{N}$ sign could not be extracted from $R_{1\rho}$ measurements). 1D spectra obtained from the pulse scheme of Fig. 1 are shown as insets. Arrows indicate the

positions of the spin-lock fields that are used to generate the $R_{1\rho}^\pm$ decay curves for $^1\text{H}^\text{N}$ (orange, red; 2nd column) and ^{15}N (purple, blue; 3rd column) nuclei of A12, N28 and D34. Optimized $(|\delta_G/2\pi|, \nu_1)$ values for measurements at 800 MHz calculated from (6, 7) along with $k_{ex} = 300 \text{ s}^{-1}$, $p_E = 2.5\%$ and the value of $|\Delta\omega|$ from CPMG experiments are listed

and D34 (c) with the position of the excited state correlation indicated by the green dot. The 1D spectra obtained from the ^{15}N and $^1\text{H}^{\text{N}}$ selective $R_{1\rho}$ experiments recorded on these particular residues are shown as insets in the figures and the positions of the spin-lock fields are denoted by arrows (orange-upfield and red-downfield for $^1\text{H}^{\text{N}}$ and purple-upfield, blue-downfield for ^{15}N). The $^1\text{H}^{\text{N}}$ and ^{15}N decay curves in columns 2 and 3, respectively, establish that for the most part distinct $R_{1\rho}^{\pm}$ values are measured from which the signs of $\Delta\omega$ are readily obtained. For example, for A12 the red curve decays more rapidly than the orange, establishing that the sign of $\Delta\omega = \Omega_E - \Omega_G$ is positive, consistent with expectations from the direct measurements of chemical shifts of apo- and ligand-saturated SH3 domain (green peak). For N28 $R_{1\rho}^+(^1\text{H}^{\text{N}}) \approx R_{1\rho}^-(^1\text{H}^{\text{N}})$ and it is not possible to obtain the sign of $^1\text{H}^{\text{N}}$ $\Delta\omega$ (ambiguity indicated by the pair of green peaks in the spectrum).

For many residues with $^1\text{H}^{\text{N}}$, ^{15}N chemical shifts such that $|\Delta\omega_{\text{H}^{\text{N}}}| > 0.035$ ppm, $|\Delta\omega_{\text{N}}| > 0.3$ ppm, substantial differences in $R_{1\rho}^{\pm}$ rates are measured (see Fig. 2) and it is straightforward to obtain the desired sign. In cases where values of $\Delta\omega$ are small, leading to similar $R_{1\rho}^{\pm}$ rates we have employed a number of statistical tests, including a Student t -test analysis and an F -test (Zar 1984), to help with the selection of the correct sign, as outlined in “Materials and Methods”. Shown in Fig. 3 are plots of $I^{\pm}(T)$ (a–c), along with $y'_e(T) = I^+(T)/I^-(T)$ and the best fit horizontal line (d–f) for a number of residues. Note that

panels (d–f) provide a complementary visual approach for assessing the data; only in cases where $y'_e(T)$ is ‘distinct’ from the horizontal line does it follow that $R_{1\rho}^+ \neq R_{1\rho}^-$. In order to provide a ‘frame of reference’ for what constitutes ‘distinct’ we have chosen residues where $R_{1\rho}^{\pm}(^1\text{H}^{\text{N}})$ values are different with essentially $1 - p = 100\%$ certainty (N16; a,d), $\approx 97\%$ certainty (E30; b,e) and $<85\%$ certainty (F20; c,f), based on an F -test analysis, with t -values of 50.2, 2.4 and 1.0, respectively. Note that a t -value of 2.15 corresponds to a confidence level of 95% for the 14 degrees of freedom in each fit.

Because the Abp1p SH3 domain–peptide exchanging system has been chosen, for which the signs of $\Delta\omega$ are known a priori, it is possible to establish some general guidelines that are helpful for selecting correct signs from the $R_{1\rho}$ methodology discussed above. (1) For values of $t < 2.15$ (t -test) or $1 - p < 97.5\%$ (F -test) the data must be disregarded even in the few cases where on the basis of inspection of decay curves one might be tempted to choose a sign. Our experience for the several cases in the Abp1p SH3 domain that are in this category is that erroneous signs can be obtained if the data is analyzed by inspection. (2) For borderline cases where $(1 - p)$ -values are on the order of 97.5% (or t values on the order of 2.15 for the decay curves here), each data-set must be inspected carefully and only in cases where all of the data points from one curve are either above or below those of the second decay profile should signs be extracted and they must be treated with skepticism.

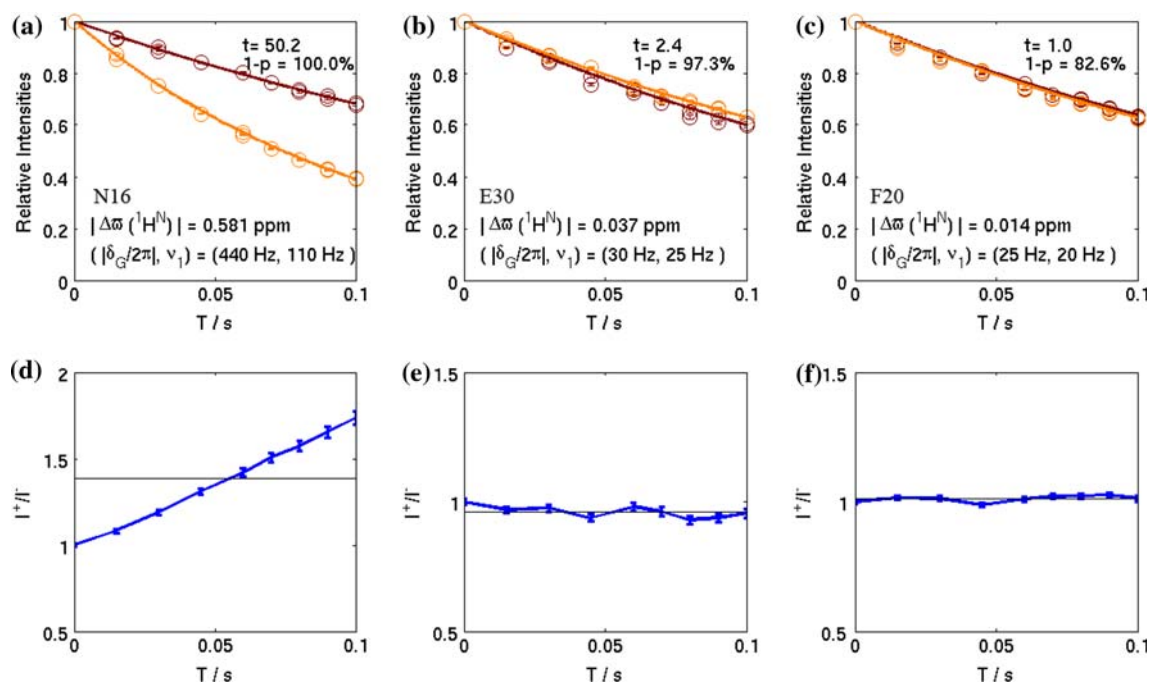


Fig. 3 $^1\text{H}^{\text{N}}$ $R_{1\rho}^{\pm}$ decay curves ($I^+(T)$, $I^-(T)$) for residues N16 (a), E30 (b) and F20 (c) of the Abp1p SH3 domain (Abp1p SH3 domain/Ark1p peptide exchanging system), 25°C, 800 MHz, listing

calculated Student t -values along with $1 - p$ values calculated from an F -test analysis. Also shown are $y'_e(T) = I^+(T)/I^-(T)$ and the best fit horizontal line for N16 (d), E30 (e) and F20 (f)

(3) For values of $t > 3.5$ (t -test) or $1 - p > 99.5\%$ (F -test) accurate values of the sign are obtained.

Comparison of the signs isolated from the $R_{1\rho}$ method, following the criteria listed above, with the ‘correct’ values measured directly from spectra showed that all of the signs for the 29 $^1\text{H}^{\text{N}}$ values that were obtained in confidence were correct, with $\Delta\varpi$ values ≥ 0.03 ppm quantified. In the case of ^{15}N , signs could be obtained for 26 residues using the statistical test criteria described in “Materials and Methods” and for all but one residue $|\Delta\varpi|$ values were larger than 0.15 ppm. Interestingly, for L57, for which $|\Delta\varpi| = 0.1$ ppm, a wrong sign was obtained. We are uncertain as to why this is the case, however, it is worth noting that simulations establish that a statistically significant difference between $R_{1\rho}^{\pm}$ values should not have been obtained for this residue with the exchange parameters of the Abp1p SH3 domain–peptide system used here.

In addition to cross-validating the $R_{1\rho}$ experiments by establishing how many of the determined signs are correct, as discussed above, it is also possible to compare experimental and calculated $|R_{1\rho}|$ rates. Figure 4 shows the correlation between calculated and measured $|\Delta R_{1\rho}|$ values (a, $^1\text{H}^{\text{N}}$; b, ^{15}N), with the former given by

$$\begin{aligned} |\Delta R_{1\rho}| &= |R_{1\rho}^+ - R_{1\rho}^-| = |R_{\text{ex}}^+ - R_{\text{ex}}^-| \sin^2 \theta \\ &= \left| \frac{p_E \Delta\omega^2 k_{\text{ex}}}{(+\delta_G - \Delta\omega)^2 + \omega_1^2 + k_{\text{ex}}^2} - \frac{p_E \Delta\omega^2 k_{\text{ex}}}{(-\delta_G - \Delta\omega)^2 + \omega_1^2 + k_{\text{ex}}^2} \right| \sin^2 \theta \end{aligned} \quad (8)$$

In (8) values of (p_E, k_{ex}) from CPMG measurements were used, with values of $\Delta\omega$ obtained from direct measurement of shift differences. Notably, $\Delta R_{1\rho}$ is independent of R_1 and R_2^0 . As can be seen in Fig. 4, the correlation is

high, providing further confidence in the methodology. It is worth emphasizing that cross-validation is possible even in cases where the signs of $\Delta\omega$ are not known a priori, since the calculated values of $|\Delta R_{1\rho}|$ are derived solely from parameters that are available from CPMG relaxation dispersion experiments.

The experimental results obtained on the SH3 domain–ligand exchanging system presented here establish the robustness of the methodology, at least in this case. It is of interest, however, to explore the sensitivity of the approach to the full range of exchange parameters that might in general be encountered in studies of excited protein states. Figure 5 plots Δ values of (6) ($T = 100$ ms) as a function of $(p_E, k_{\text{ex}}, |\Delta\varpi|)$. For reference, a plot of Δ vs. $|\Delta\varpi|$ is presented in Fig. 5a using values of $(p_E, k_{\text{ex}}) = (2.5\%, 300 \text{ s}^{-1})$ that are germane for the Abp1p SH3 system, with a horizontal line at $\Delta = 4\%$, corresponding to a threshold above which differences in $R_{1\rho}^{\pm}$ values have been found to be reliable in this case. As p_E increases values of Δ become larger so that it is easier to measure signs of shift differences, as expected (Fig. 5b). Further, as k_{ex} increases, it becomes increasingly difficult to obtain the signs of small shift differences, but easier for large $\Delta\varpi$ values, Fig. 5c. Thus, the $R_{1\rho}$ methodology is optimal for systems with large p_E and relatively small k_{ex} values. In cases where temperature dependent CPMG data is available it is worthwhile simulating similar curves to those in Fig. 5a to establish the best set of conditions to record experiments. It should be noted that values of Δ do depend on R_1 and R_2^0 , with transverse relaxation rates available from CPMG dispersion profiles recorded at high ν_{CPMG} . Here we have used values of $R_1 = 1 \text{ s}^{-1}$, $R_2^0(^1\text{H}^{\text{N}}) = 10 \text{ s}^{-1}$, $R_2^0(^{15}\text{N}) = 10 \text{ s}^{-1}$, $R_2^0(^1\text{H}^{\alpha}) = 35 \text{ s}^{-1}$ and $R_2^0(^{13}\text{C}^{\alpha}) = 35 \text{ s}^{-1}$ (approximate values obtained for the A39V/N53P/V55L Fyn SH3 domain, 20°C, see below).

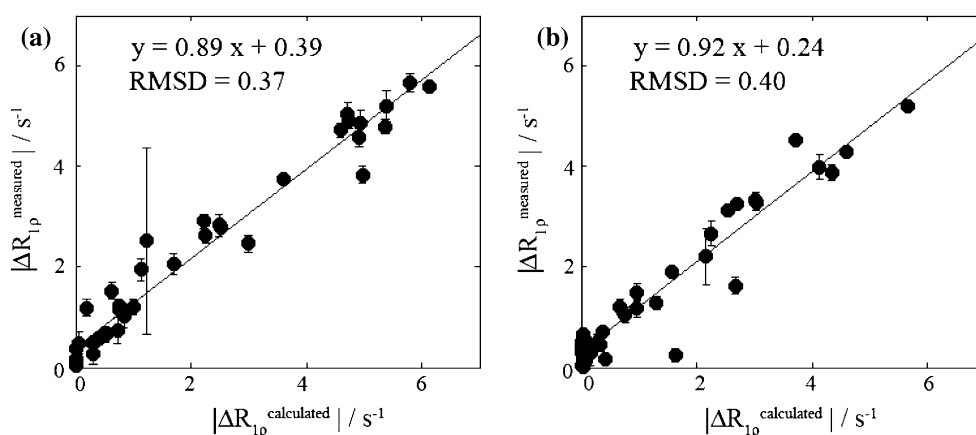


Fig. 4 Correlation between measured $|\Delta R_{1\rho}|$ values (Y-axis) and $|\Delta R_{1\rho}|$ calculated according to (8) (X-axis) for $^1\text{H}^{\text{N}}$ (a) and ^{15}N (b) nuclei of the Abp1p SH3 domain. Calculated values use $\Delta\varpi_{\text{HN}}$ and $\Delta\varpi_{\text{N}}$ shift differences based on direct measurements of apo- and fully

ligated protein and values of k_{ex} and p_E extracted from CPMG measurements. A large error is noted for N53 that arises from the weak peak intensity for this residue. The lines indicated are the best fits from linear regression

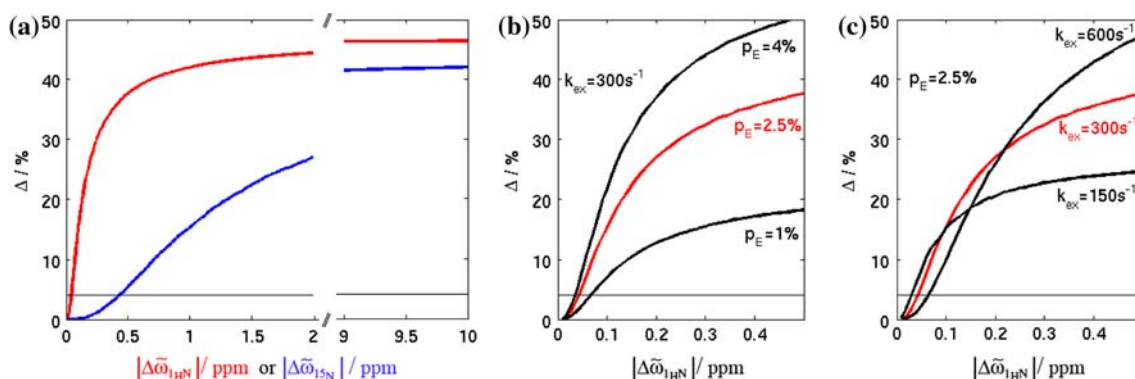


Fig. 5 **a** Values of Δ (6, $T = 100$ ms) vs. $|\Delta\omega|$ calculated for exchange parameters of the Abp1p-Ark1p system ($k_{\text{ex}} = 300 \text{ s}^{-1}$, $p_E = 2.5\%$) for $^1\text{H}^{\text{N}}$ (red) and ^{15}N (blue) nuclei. **b** Δ vs. $|\Delta\omega|$ for $k_{\text{ex}} = 300 \text{ s}^{-1}$ as a function of p_E . **c** Δ vs. $|\Delta\omega|$ for $p_E = 2.5\%$ as a

function of k_{ex} . The horizontal line at $\Delta = 4\%$ is the threshold below which it is not possible to obtain signs of chemical shift differences on the protein systems examined here

In addition to the $^1\text{H}^{\text{N}}$ $R_{1\rho}$ scheme presented here and the corresponding ^{15}N and $^1\text{H}^{\text{z}}$ experiments published previously (Auer et al. 2009; Korzhnev et al. 2005), we have also developed an analogous sequence for obtaining the signs of $^{13}\text{C}^{\text{z}}$ $\Delta\omega$ values, Fig. 6. This scheme, along with the $^1\text{H}^{\text{z}}$ version, is applied to a protein folding ‘reaction’ involving an on-pathway folding intermediate of the A39V/N53P/V55L Fyn SH3 domain (Neudecker et al. 2006), where the intermediate state ($p_E = 1.4\%$) exchanges with the folded (ground) conformer with a rate of $k_{\text{ex}} = 780 \text{ s}^{-1}$ at 20°C . $^1\text{H}^{\text{z}}$ and $^{13}\text{C}^{\text{z}}$ $R_{1\rho}$ decay curves for E33 and T47 are shown in Fig. 7, illustrating the quality of data that can be obtained on this system. Of the 45 residues for which $^{13}\text{C}^{\text{z}}$ dispersion profiles could be quantified,

signs were obtained for 19 with values of $\Delta\omega_{\text{C}^{\text{z}}}$ down to 0.5 ppm. All the signs obtained are in agreement with those measured using the H(S/M)QC approach of Skrynnikov et al. (Skrynnikov et al. 2002). Finally, signs for $\Delta\omega_{\text{H}^{\text{z}}}$ were obtained for 19 residues with shift differences as low as 0.17 ppm (Auer et al. 2009).

Comparison of low power off-resonance $R_{1\rho}$ and H(S/M)QC measurements for the determination of the sign of $\Delta\omega$

To date the most common approach for measuring the signs of ^{15}N or ^{13}C shift differences between exchanging states involves comparison of HSQC and HMQC data-sets

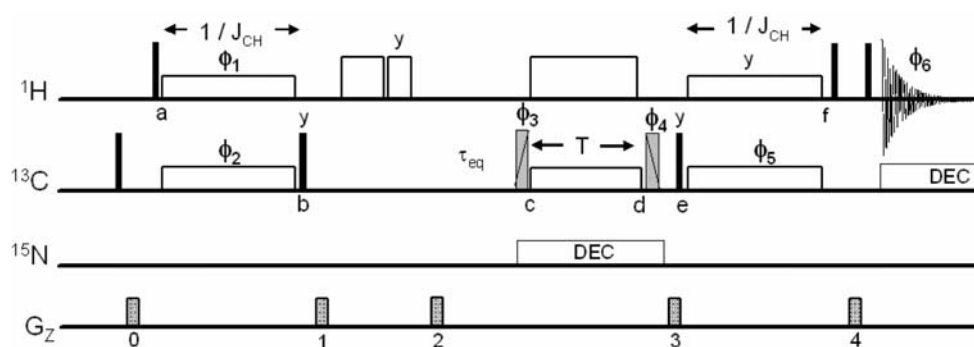


Fig. 6 Pulse sequence for measuring $^{13}\text{C}^{\text{z}}$ off-resonance $R_{1\rho}$ relaxation rates in proteins labeled with ^{13}C at the C^{z} position. ^1H and ^{13}C carrier frequencies are placed initially on resonance ($^1\text{H}^{\text{z}}$ and $^{13}\text{C}^{\text{z}}$ positions) for the cross-peak of interest; subsequently the ^{13}C carrier is jumped to the position of the spin-lock field immediately prior to the pulse of phase ϕ_3 and then back on-resonance prior to point e. All solid pulses have flip angles of 90° and are applied along the x-axis, unless indicated otherwise. Simultaneous $^1\text{H}/^{13}\text{C}$ spin-lock fields (140 Hz) are applied for durations of $1/J_{\text{CH}}$ (between points a, b and again between points e, f) where J_{CH} is the one-bond $^1\text{H}^{\text{z}}\text{--}^{13}\text{C}^{\text{z}}$ scalar coupling constant ($\approx 140 \text{ Hz}$). Immediately after gradient 1 ^1H purge pulses are applied (17 kHz) for durations of 2 ms (x-axis) and 1 ms (y-axis) to eliminate the residual water signal. The delay τ_{eq} is set to 5 ms. ^1H pulses of

phases ϕ_3/ϕ_4 are applied with a flip angle θ such that $\tan\theta = \omega_1/\delta\omega_1$, using $(\delta\omega_1, \omega_1)$ optimized as described in the text. During the spin-lock period an on-resonance ^1H continuous-wave decoupling field of 13.8 kHz is applied to eliminate scalar coupling modulations and cross-correlation effects between $^1\text{H}\text{--}^{13}\text{C}$ dipolar and ^{13}C CSA interactions (Peng and Wagner 1992). ^{15}N decoupling during the spin-lock and ^{13}C decoupling during acquisition are achieved with WALTZ-16 fields (Shaka et al. 1983). The phase cycle is: $\phi_1 = (y, -y)$, $\phi_2 = 2(x), 2(-x)$, $\phi_3 = 4(x), 4(-x)$, $\phi_4 = x, 2(-x), x-x, 2(x), -x$. For the spin-lock carrier upfield(downfield) of the ground state resonance $\phi_3 = y(-y)$ and $\phi_4 = -y(y)$ (on Varian spectrometers). Gradient strengths and durations are (ms, G/cm): G0 = (1.7, 5), G1 = (0.5, 10), G2 = (0.8, 15), G3 = (0.6, -4), G4 = (0.2, -4)

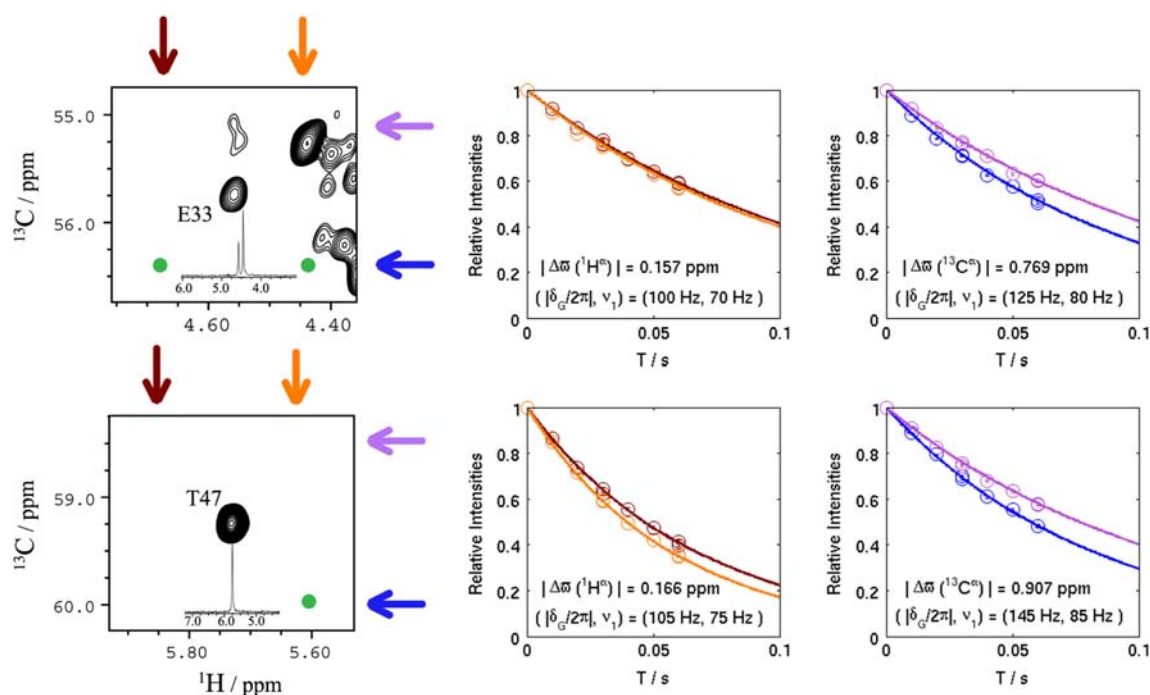


Fig. 7 Selected regions of $^{13}\text{C}^\alpha\text{--}^1\text{H}^\alpha$ HSQC spectra centered on residues E33 and T47 of the A39V/N53P/V55L Fyn SH3 domain, 20°C, 800 MHz along with $R_{1\rho}^\pm$ measured for $^1\text{H}^\alpha$ (orange, red) and $^{13}\text{C}^\alpha$ (purple, blue) nuclei. Optimized $(|\delta_G/2\pi|, \nu_1)$ values for measurements at 800 MHz calculated from (6, 7) along with

$k_{ex} = 780 \text{ s}^{-1}$, $p_E = 1.4\%$ and the value of $|\Delta\omega|$ from CPMG experiments are listed. The peak flanking the E33 line in the 1D spectrum is due to M-1 and D35; the separation is sufficiently large such that there is not a problem with quantification of the E33 peak. Other details are as in Fig. 2

recorded at a number of static magnetic fields (Skrynnikov et al. 2002). More specifically, Skrynnikov et al. (2002) have shown that the difference in peak positions (ppm) in HSQC spectra recorded at a pair of fields, $B_0^{(i)}$ and $B_0^{(ii)}$ ($B_0^{(i)} < B_0^{(ii)}$), is given by

$$\tilde{\sigma}_X = \frac{k_{GE}\tilde{\xi}_X}{1 + (\gamma_X B_0^{(i)} \tilde{\xi}_X)^2} - \frac{k_{GE}\tilde{\xi}_X}{1 + (\gamma_X B_0^{(ii)} \tilde{\xi}_X)^2} \quad (9)$$

with a shift (ppm) also noted between peaks in HSQC and HMQC data-sets recorded at a single magnetic field,

$$\tilde{\Omega}_X = k_{GE} \left\{ \frac{\tilde{\xi}_X}{1 + \tilde{\xi}_X^2} - \frac{1}{2} \left[\frac{\tilde{\xi}_X + \tilde{\xi}_H}{1 + (\tilde{\xi}_X + \tilde{\xi}_H)^2} + \frac{\tilde{\xi}_X - \tilde{\xi}_H}{1 + (\tilde{\xi}_X - \tilde{\xi}_H)^2} \right] \right\} \quad (10)$$

where $\tilde{\xi}_X = \Delta\omega_X/k_{EG}$ and it is assumed that nuclei in states G and E have the same intrinsic transverse relaxation rates. It can be shown that $\tilde{\sigma}_X$ and $\Delta\omega_X$ have the same sign, as do $\tilde{\Omega}_X$ and $\Delta\omega_X$ for the most part (but see below), facilitating extraction of the sign of $\Delta\omega_X$ (Skrynnikov et al. 2002). It is of considerable interest to compare the $R_{1\rho}$ method with the more established methodology in cases where both are applicable. Figure 8a shows values of Δ (6) as a function of $\Delta\omega_{C^\alpha}$ for a number of (p_E, k_{ex}) values, including those measured for the A39V/N53P/V55L Fyn SH3 domain. The

4% threshold (horizontal line) above which meaningful differences in $R_{1\rho}^\pm$ can be measured is shown. It is worth noting that for exchange parameters of $(p_E, k_{ex}) = (1.4\%, 780 \text{ s}^{-1})$, signs are predicted to be measurable in cases where $\Delta\omega_{C^\alpha} > 0.5 \text{ ppm}$, as observed experimentally. By means of comparison, plots of differences in peak positions in HSQC spectra recorded at 500 and 800 MHz, $\tilde{\sigma}_{C^\alpha}$, for a number of (p_E, k_{ex}) values are shown in Fig. 8b, where $\tilde{\sigma}_{C^\alpha} = \omega_{C^\alpha}(500 \text{ MHz}) - \omega_{C^\alpha}(800 \text{ MHz})$, while in Fig. 8c a contour plot of $\tilde{\Omega}_{C^\alpha}$ as a function of $(\Delta\omega_{C^\alpha}, \Delta\omega_{H^\alpha})$ is presented for $(p_E, k_{ex}) = (1.4\%, 780 \text{ s}^{-1})$, 500 MHz. Shown also in Fig. 8b are horizontal lines at $\pm 2 \text{ ppb}$, the experimentally determined lower limit for measuring accurate $\tilde{\sigma}_{C^\alpha}$ values for the Fyn SH3 domain based on the reproducibility of ‘exchange-free’ peak positions in HSQC spectra. It is clear from a comparison of the plots, focusing on $(p_E, k_{ex}) = (1.4\%, 780 \text{ s}^{-1})$, that measurements of $R_{1\rho}$ and $\tilde{\sigma}$ methods are sensitive to the sign of $\Delta\omega$ only for relatively large chemical shift differences, on the order of greater than 0.5 ppm in this case. By contrast, the measurement of $\tilde{\Omega}_{C^\alpha}$ provides accurate sign information for much smaller $\Delta\omega_{C^\alpha}$ values ($\approx 0.14 \text{ ppm}$), although only if $\Delta\omega_{H^\alpha} \neq 0$. An additional advantage with the $\tilde{\Omega}_X$ measurements is that because spectra recorded at a single magnetic field are compared the reproducibility of peak

positions is very high; for the Fyn SH3 domain ‘exchange free peaks’ were within 0.5 ppb in HSQC/HMQC spectra recorded at the same field so that $\tilde{\Omega}_X$ values as low as 1 ppb are significant. A (small) disadvantage with the approach, however, is that there is a region in $(\Delta\varpi_{C^\alpha}, \Delta\varpi_{H^\alpha})$ space where negative values of $\tilde{\Omega}_{C^\alpha}$ correspond to positive $\Delta\varpi_{C^\alpha}$ and vice versa, indicated in Fig. 8c by shading. It should be noted that in this region values of $\tilde{\Omega}_{C^\alpha}$ are typically very small (<0.5 ppb in the example considered here), making it hard to extract reliable shift differences in any event. Often an indication that values of $(\Delta\varpi_{C^\alpha}, \Delta\varpi_{H^\alpha})$ lie in a ‘problem’ region is that opposite signs are obtained from measurement of $\tilde{\sigma}_{C^\alpha}$ and $\tilde{\Omega}_{C^\alpha}$. However, so long as the magnitudes of $\Delta\varpi_{C^\alpha}$ and $\Delta\varpi_{H^\alpha}$ are known, along with the exchange parameters, it is possible to establish the reliability of the method through simulation (10).

Of the 46 $|\Delta\varpi_N|$ values that were quantified from fits of CPMG dispersion profiles recorded on the Abp1p-ligand exchanging system, signs have been obtained for 28 residues from measurement of $\tilde{\sigma}_N$ and $\tilde{\Omega}_N$. The signs of chemical shift differences, $|\Delta\varpi_N|$, as low as 0.06 ppm could be determined. By comparison, 25 signs ($|\Delta\varpi_N| > 0.15$ ppm) were obtained from the $R_{1\rho}$ method. Notably, 4 signs could be obtained only using the $R_{1\rho}$ approach since for these residues $\Delta\varpi_{H^N} \approx 0$, preventing quantitation from a comparison of HSQC and HMQC data-sets, while 7 signs were only available from the H(S/M)QC methodology (see supporting information). Similar trends are noted from $^{13}\text{C}^\alpha$ measurements on the A39V/N53P/V55L Fyn SH3 domain. Out of a

total of 45 $|\Delta\varpi_{C^\alpha}|$ values quantified by CPMG relaxation dispersion experiments, signs were obtained for 34 $\Delta\varpi_{C^\alpha}$ values larger than 0.3 ppm from a combined $\tilde{\sigma}_{C^\alpha}$, $\tilde{\Omega}_{C^\alpha}$ analysis, while signs were available for 19 residues with $\Delta\varpi_{C^\alpha} > 0.5$ ppm based on the $R_{1\rho}$ method (see supporting information).

The experimental results establish that in general the H(S/M)QC method is preferred over the $R_{1\rho}$ approach, at least for obtaining signs of chemical shift differences of heteronuclei. However, the methods are complementary. For example, simulations establish that over a reasonable range of k_{ex} values that are normally relevant for systems studied by CPMG dispersion experiments $\tilde{\Omega}_X$ values increase with exchange rate (see supporting information), while the sensitivity of the off-resonance spin-lock method decreases, at least for relatively small chemical shift differences (Fig. 8a). By contrast, a strength of the $R_{1\rho}$ approach is that the differences in $R_{1\rho}^\pm$ values increase with $\Delta\varpi$, while both $\tilde{\sigma}$ and $\tilde{\Omega}$ values have definite maxima, depending on the exchange parameters (Fig. 8a–c). Figure 8d–f presents an example of an exchanging system where the sign information is forthcoming from $R_{1\rho}$ measurements but potentially not from H(S/M)QC spectra. Here $(p_E, k_{ex}) = (1.4\%, 200 \text{ s}^{-1})$ and so long as $|\Delta\varpi_{C^\alpha}| > 0.3$ ppm, the sign of $\Delta\varpi_{C^\alpha}$ can be obtained from a comparison of $R_{1\rho}^\pm$ rates, Fig. 8d. The very small $\tilde{\sigma}_{C^\alpha}$ values obtained in this case (<1 ppb), Fig. 8e, preclude sign extraction from HSQC spectra and likewise the small values of $\tilde{\Omega}_{C^\alpha} < 2$ ppb could very well complicate the

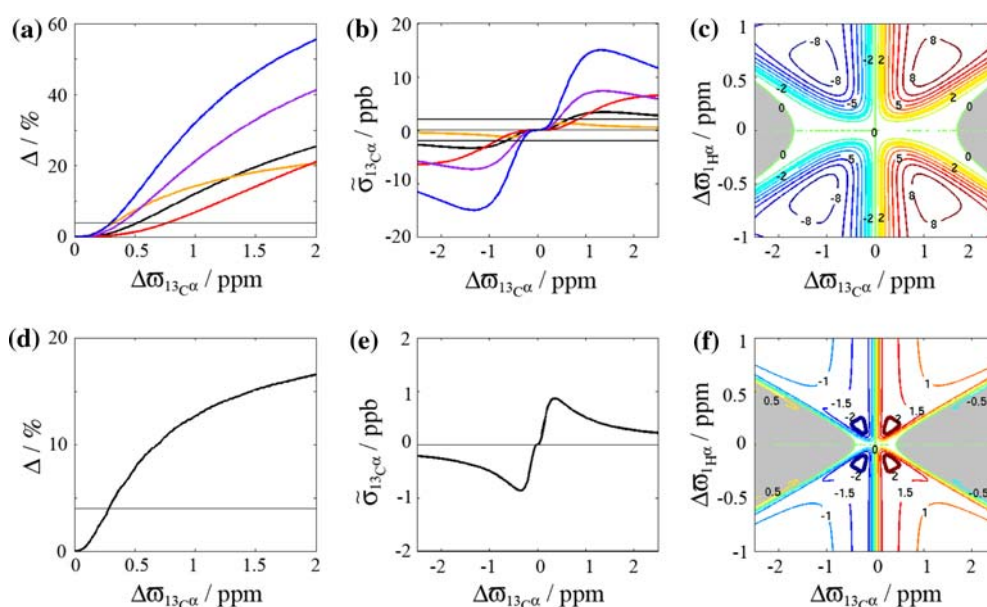


Fig. 8 Simulations of Δ (a, 6) and $\tilde{\sigma}_{C^\alpha}$ (b, 9) as a function of $\Delta\varpi_{C^\alpha}$ for a number of $(k_{ex}[\text{s}^{-1}]/p_E[\%])$ values: black (780/1.4), orange (300/1.4), red (1,500/1.4), purple (780/3), blue (780/6). c Contour plot of $\tilde{\Omega}_{C^\alpha}$ as a function of $(\Delta\varpi_{C^\alpha}, \Delta\varpi_{H^\alpha})$ (contours are in ppb) for $(p_E, k_{ex}) = (1.4\%, 780 \text{ s}^{-1})$, 500 MHz. The gray shaded areas denote

regions where negative values of $\tilde{\Omega}_{C^\alpha}$ correspond to positive $\Delta\varpi_{C^\alpha}$ and vice versa. d–f Corresponding simulations for $k_{ex} = 200 \text{ s}^{-1}$ and $p_E = 1.4\%$. For $|\Delta\varpi_{H^\alpha}| > 0.3$ ppm, the sign of $\Delta\varpi_{C^\alpha}$ can be obtained from a comparison of $R_{1\rho}^\pm$ rates (d), while the sign is likely to be difficult to obtain from the H(S/M)QC approach (e, f)

determination of sign from this method as well, Fig. 8f. Certainly for $|\Delta\varpi_{C^{\alpha}}| > 1$ ppm the sign information is not available from any combination of HMQC and HSQC data-sets. It is also noteworthy that while the H(S/M)QC approach is the first choice for ^{15}N and ^{13}C nuclei, the $R_{1\rho}$ method is now commonly used in our laboratory for extracting signs of $^1\text{H}^{\text{N}}$ and $^1\text{H}^{\text{Z}}$ shift differences. Previously, we have compared double- and zero-quantum ^{15}N – $^1\text{H}^{\text{N}}$ relaxation dispersion profiles to obtain the relative signs of $\Delta\varpi_{H^{\text{N}}}$ and $\Delta\varpi_{\text{N}}$ from which the sign of $\Delta\varpi_{H^{\text{N}}}$ can be obtained so long as (1) the sign of $\Delta\varpi_{\text{N}}$ is known and (2) that $\Delta\varpi_{\text{N}}$ is sufficiently large that differences in the profiles are present in the first place (Orekhov et al. 2004). Extraction of robust sign information for $\Delta\varpi_{H^{\text{N}}}$ from $R_{1\rho}^{\pm}$ measurements is not dependent on the value of $\Delta\varpi_{\text{N}}$. Finally, the spin-lock approach remains the most convenient method for measuring signs of $\Delta\varpi_{H^{\text{Z}}}$, especially since the same sample used to record $^1\text{H}^{\text{Z}}$ CPMG dispersion profiles can be used in this case as well (Auer et al. 2009).

In summary, we have presented pulse schemes for the measurement of $^1\text{H}^{\text{N}}$ and $^{13}\text{C}^{\alpha}$ $R_{1\rho}^{\pm}$ relaxation rates, complementing schemes previously published for ^{15}N and $^1\text{H}^{\text{Z}}$ (Auer et al. 2009; Korzhnev et al. 2005). The methodology is shown to be robust, although for ^{15}N and $^{13}\text{C}^{\alpha}$ at least, fewer signs are available than from the H(S/M)QC approach (Skrynnikov et al. 2002). In addition, the H(S/M)QC method is less time consuming and the information is available in the form of 2D data-sets, as opposed to the 1D spectra recorded here, that leads to increased numbers of residues that can be quantified. We therefore suggest that sign determination for ^{15}N and $^{13}\text{C}^{\alpha}$ be carried out using $\tilde{\sigma}_X$ and $\tilde{\Omega}_X$ values from HSQC and HMQC data-sets recorded at no fewer than a pair of static magnetic fields. In some cases where data might be ambiguous or for exchanging systems for which the sign information is difficult to extract from the H(S/M)QC method (low k_{ex} and p_E), $R_{1\rho}^{\pm}$ measurements can readily be performed. For measurement of signs of $^1\text{H}^{\text{N}}$ and $^1\text{H}^{\text{Z}}$ shift differences the $R_{1\rho}$ approach has been very useful for the small protein systems that we are currently studying. It is clear that chemical shifts will play a critical role in structural studies of invisible, excited states. The development of a number of robust approaches to extract such information is thus an important goal as a prerequisite for the in-depth characterization of these biologically important conformers.

Supporting material

Tables of signed $\Delta\varpi$ values for the Abp1p-Ark1p exchanging system (^{15}N , $^1\text{H}^{\text{N}}$) and the A39V/N53P/V55L Fyn SH3 domain ($^{13}\text{C}^{\alpha}$, $^1\text{H}^{\text{Z}}$). Figures of contour plots of $\tilde{\Omega}_X$ for different values of exchange parameters and static

magnetic fields. Pulse sequence code for measurement of $^1\text{H}^{\text{N}}$ and $^{13}\text{C}^{\alpha}$ $R_{1\rho}$ rates.

Acknowledgments R.A. is a recipient of a DOC-fORTE-fellowship of the Austrian Academy of Sciences. P.N. and D.F.H. are recipients of postdoctoral fellowships from the Canadian Institutes of Health Research (CIHR). This work was supported by a grant from the CIHR. L.E.K. holds a Canada Research Chair in Biochemistry.

References

- Auer R, Neudecker P, Muhandiram DR, Lundstrom P, Hansen DF, Konrat R, Kay LE (2009) Measuring the signs of $^1\text{H}(\alpha)$ chemical shift differences between ground and excited protein states by off-resonance spin-lock R(1rho) NMR spectroscopy. *J Am Chem Soc* 131:10832–10833
- Boehr DD, McElheny D, Dyson HJ, Wright PE (2006) The dynamic energy landscape of dihydrofolate reductase catalysis. *Science* 313:1638–1642
- Boulat B, Bodenhausen G (1993) Measurement of proton relaxation rates in proteins. *J Biomol NMR* 3:335–348
- Carr HY, Purcell EM (1954) Effects of diffusion on free precession in nuclear magnetic resonance experiments. *Phys Rev* 54:630–638
- Chiarparin E, Pelupessy P, Bodenhausen G (1998) Selective cross-polarization in solution state NMR. *Mol Phys* 95:767–769
- Delaglio F, Grzesiek S, Vuister GW, Zhu G, Pfeifer J, Bax A (1995) NMRPipe: a multidimensional spectral processing system based on UNIX pipes. *J Biomol NMR* 6:277–293
- Frederick KK, Marlow MS, Valentine KG, Wand AJ (2007) Conformational entropy in molecular recognition by proteins. *Nature* 448:325–329
- Goto NK, Kay LE (2000) New developments in isotope labeling strategies for protein solution NMR spectroscopy. *Curr Opin Struct Biol* 10:585–592
- Hansen DF, Vallurupalli P, Kay LE (2008a) An improved ^{15}N relaxation dispersion experiment for the measurement of millisecond time-scale dynamics in proteins. *J Phys Chem B* 112:5898–5904
- Hansen DF, Vallurupalli P, Lundstrom P, Neudecker P, Kay LE (2008b) Probing chemical shifts of invisible states of proteins with relaxation dispersion NMR spectroscopy: how well can we do? *J Am Chem Soc* 130:2667–2675
- Hansen AL, Nikolova EN, Casiano-Negroni A, Al-Hashimi HM (2009) Extending the range of microsecond-to-millisecond chemical exchange detected in labeled and unlabeled nucleic acids by selective carbon R(1rho) NMR spectroscopy. *J Am Chem Soc* 131:3818–3819
- Haynes J, Garcia B, Stollar EJ, Rath A, Andrews BJ, Davidson AR (2007) The biologically relevant targets and binding affinity requirements for the function of the yeast actin-binding protein 1 SRC-homology 3 domain vary with genetic context. *Genetics* 176:193–208
- Henzler-Wildman K, Kern D (2007) Dynamic personalities of proteins. *Nature* 450:964–972
- Igumenova TI, Frederick KK, Wand AJ (2006) Characterization of the fast dynamics of protein amino acid side chains using NMR relaxation in solution. *Chem Rev* 106:1672–1699
- Ishima R, Torchia DA (2000) Protein dynamics from NMR. *Nat Struct Biol* 7:740–743
- Ishima R, Torchia D (2003) Extending the range of amide proton relaxation dispersion experiments in proteins using a constant-time relaxation-compensated CPMG approach. *J Biomol NMR* 25:243–248

- Ishima R, Baber J, Louis JM, Torchia DA (2004) Carbonyl carbon transverse relaxation dispersion measurements and ms-micros timescale motion in a protein hydrogen bond network. *J Biomol NMR* 29:187–198
- Johnson BA, Blevins RA (1994) NMRView: a computer program for the visualization and analysis of NMR data. *J Biomol NMR* 4:603–614
- Kainosho M, Torizawa T, Iwashita Y, Terauchi T, Mei Ono A, Guntert P (2006) Optimal isotope labelling for NMR protein structure determinations. *Nature* 440:52–57
- Kay LE, Muhandiram DR, Wolf G, Shoelson SE, Forman-Kay JD (1998) Correlation between binding and dynamics at SH2 domain interfaces. *Nat Struct Biol* 5:156–163
- Korzhnev DM, Orekhov VY, Dahlquist FW, Kay LE (2003) Off-resonance R1rho relaxation outside of the fast exchange limit: an experimental study of a cavity mutant of T4 lysozyme. *J Biomol NMR* 26:39–48
- Korzhnev DM, Salvatella X, Vendruscolo M, Di Nardo AA, Davidson AR, Dobson CM, Kay LE (2004) Low-populated folding intermediates of Fyn SH3 characterized by relaxation dispersion NMR. *Nature* 430:586–590
- Korzhnev DM, Orekhov VY, Kay LE (2005) Off-resonance R1rho NMR studies of exchange dynamics in proteins with low spin-lock fields: an application to a Fyn SH3 domain. *J Am Chem Soc* 127:713–721
- Korzhnev DM, Bezsonova I, Evanics F, Taulier N, Zhou Z, Bai Y, Chalikian TV, Prosser RS, Kay LE (2006) Probing the transition state ensemble of a protein folding reaction by pressure-dependent NMR relaxation dispersion. *J Am Chem Soc* 128:5262–5269
- LeMaster DM (1999) NMR relaxation order parameter analysis of the dynamics of protein side chains. *J Am Chem Soc* 121:1726–1742
- Loria JP, Rance M, Palmer AG (1999) A relaxation compensated CPMG sequence for characterizing chemical exchange. *J Am Chem Soc* 121:2331–2332
- Lundstrom P, Teilum K, Carstensen T, Bezsonova I, Wiesner S, Hansen DF, Religa TL, Akke M, Kay LE (2007a) Fractional ¹³C enrichment of isolated carbons using [1-¹³C]- or [2-¹³C]-glucose facilitates the accurate measurement of dynamics at backbone C α and side-chain methyl positions in proteins. *J Biomol NMR* 38:199–212
- Lundstrom P, Vallurupalli P, Religa TL, Dahlquist FW, Kay LE (2007b) A single-quantum methyl ¹³C-relaxation dispersion experiment with improved sensitivity. *J Biomol NMR* 38:79–88
- Lundstrom P, Hansen DF, Kay LE (2008) Measurement of carbonyl chemical shifts of excited protein states by relaxation dispersion NMR spectroscopy: comparison between uniformly and selectively (¹³C) labeled samples. *J Biomol NMR* 42:35–47
- Lundstrom P, Hansen DF, Vallurupalli P, Kay LE (2009a) Accurate measurement of alpha proton chemical shifts of excited protein states by relaxation dispersion NMR spectroscopy. *J Am Chem Soc* 131:1915–1926
- Lundstrom P, Lin H, Kay LE (2009b) Measuring ¹³C β chemical shifts of invisible excited states in proteins by relaxation dispersion NMR spectroscopy. *J Biomol NMR* 44:139–145
- Massi F, Johnson E, Wang C, Rance M, Palmer AG 3rd (2004) NMR R1 rho rotating-frame relaxation with weak radio frequency fields. *J Am Chem Soc* 126:2247–2256
- Meiboom S, Gill D (1958) Modified spin-echo method for measuring nuclear magnetic relaxation times. *Rev Sci Instrum* 29:688–691
- Mittermaier A, Kay LE (2006) New tools provide new insights in NMR studies of protein dynamics. *Science* 312:224–228
- Neudecker P, Zarrine-Afsar A, Choy WY, Muhandiram DR, Davidson AR, Kay LE (2006) Identification of a collapsed intermediate with non-native long-range interactions on the folding pathway of a pair of Fyn SH3 domain mutants by NMR relaxation dispersion spectroscopy. *J Mol Biol* 363:958–976
- Orekhov VY, Korzhnev DM, Kay LE (2004) Double- and zero-quantum NMR relaxation dispersion experiments sampling millisecond time scale dynamics in proteins. *J Am Chem Soc* 126:1886–1891
- Palmer AG, Williams J, McDermott A (1996) Nuclear magnetic resonance studies of biopolymer dynamics. *J Phys Chem* 100:13293–13310
- Palmer AG, Kroenke CD, Loria JP (2001) NMR methods for quantifying microsecond-to-millisecond motions in biological macromolecules. *Methods Enzymol* 339:204–238
- Palmer AG, Grey MJ, Wang C (2005) Solution NMR spin relaxation methods for characterizing chemical exchange in high-molecular-weight systems. *Methods Enzymol* 394:430–465
- Peluessy P, Chiapparini E (2000) Hartmann-Hahn polarization transfer in liquids: an ideal tool for selective experiments. *Concepts Magn Reson* 12:103–124
- Peng JW, Wagner G (1992) Mapping of spectral density functions using heteronuclear NMR relaxation measurements. *J Magn Reson* 98:308–332
- Piotto M, Saudek V, Sklenar V (1992) Gradient-tailored excitation for single-quantum NMR spectroscopy of aqueous solutions. *J Biomol NMR* 2:661–665
- Popovych N, Sun S, Ebricht RH, Kalodimos CG (2006) Dynamically driven protein allostery. *Nat Struct Mol Biol* 13:831–838
- Shaka AJ, Keeler J, Frenkiel T, Freeman R (1983) An improved sequence for broadband decoupling: WALTZ-16. *J Magn Reson* 52:335–338
- Skrynnikov NR, Mulder FAA, Hon B, Dahlquist FW, Kay LE (2001) Probing slow time scale dynamics at methyl-containing side chains in proteins by relaxation dispersion NMR measurements: application to methionine residues in a cavity mutant of T4 lysozyme. *J Am Chem Soc* 123:4556–4566
- Skrynnikov NR, Dahlquist FW, Kay LE (2002) Reconstructing NMR spectra of “invisible” excited protein states using HSQC and HMQC experiments. *J Am Chem Soc* 124:12352–12360
- Sugase K, Dyson HJ, Wright PE (2007) Mechanism of coupled folding and binding of an intrinsically disordered protein. *Nature* 447:1021–1024
- Tollinger M, Skrynnikov NR, Mulder FAA, Forman-Kay JD, Kay LE (2001) Slow dynamics in folded and unfolded states of an SH3 domain. *J Am Chem Soc* 123:11341–11352
- Trott O, Palmer AG 3rd (2002) R1rho relaxation outside of the fast-exchange limit. *J Magn Reson* 154:157–160
- Tugarinov V, Kay LE (2004) An isotope labeling strategy for methyl TROSY spectroscopy. *J Biomol NMR* 28:165–172
- Vallurupalli P, Hansen DF, Stollar EJ, Meirovitch E, Kay LE (2007) Measurement of bond vector orientations in invisible excited states of proteins. *Proc Natl Acad Sci USA* 104:18473–18477
- Vallurupalli P, Hansen DF, Kay LE (2008) Structures of invisible, excited protein states by relaxation dispersion NMR spectroscopy. *Proc Natl Acad Sci U S A* 105:11766–11771
- van Ingen H, Vuister GW, Wijmenga S, Tessari M (2006) CEESY: characterizing the conformation of unobservable protein states. *J Am Chem Soc* 128:3856–3857
- Zar ZH (1984) Biostatistical analysis. Prentice-Hall, Englewood Cliffs
- Zhang Q, Sun X, Watt ED, Al-Hashimi HM (2006) Resolving the motional modes that code for RNA adaptation. *Science* 311:653–656

Supporting material

Table S1. $\Delta\varpi_N$ values measured on the Apb1p SH3 domain – 2.5% Ark1p peptide exchanging system, 25°C, from CPMG relaxation dispersion and direct measurements along with signs of $\Delta\varpi_N$ from H(S/M)QC and $R_{1\rho}$ approaches

res ^a	$\Delta\varpi^{\text{CPMG}}$	$\Delta\varpi^{\text{direct}}$	H(S/M)QC	$R_{1\rho}$	t	1-p / % ^b
D34	3.281	+3.545	+	+	86.8	100.0
F31	1.873	+1.919	+	+	56.0	100.0
D15	1.753	-1.523	-	-	45.0	100.0
D35	0.763	-0.881	-	-	30.8	100.0
E17	0.913	-0.993	-	-	26.1	100.0
D33	1.636	+1.709	+	+	20.6	100.0
E14	0.960	-1.054	-	-	20.4	100.0
N16	0.494	-0.645	-	-	17.9	100.0
S52	0.910	-1.158	-	-	15.7	100.0
W37	1.520	-1.650	-	-	14.3	100.0
Y8	0.638	-0.833	-	-	10.2	100.0
W36	0.374	-0.474	-	-	9.5	100.0
Y10	0.431	+0.575	+	+	7.9	100.0
T5	0.381	+0.401	+	+	7.7	100.0
E30	0.330	-0.425	-	-	6.7	100.0
L49	0.821	-0.947		-	6.7	100.0
N28	0.214	-0.137		-	6.1	100.0
L18	0.325	-0.475	-	-	5.4	100.0
T19	0.240	-0.318	-	-	4.7	100.0
A12	0.280	-0.250	-	-	4.5	100.0
D11	0.291	-0.299	-	-	3.5	99.5
N53 ^c	0.834	+0.808	-	+	3.5	99.5
L57 ^d	0.312	+0.100		-	3.5	99.8
A4	0.158	-0.152		-	3.3	99.0
K25 ^e	0.150	+0.162	+	+	2.8	100.0
A13	0.173	-0.280	-	-	2.7	95.4
S56	0.079	+0.065		0 ^f	2.4	98.0
A6	0.109	+0.095		0	2.0	92.8
G58	0.227	+0.115		0	1.9	98.3
V21	0.154	+0.106		0	1.8	90.8
G39	0.411	+0.666		0	1.5	88.6
G48	0.300	-0.177		0	1.5	74.9
D9	0.451	+0.345	+	0	1.4	79.0
W3	0.241	+0.136		0	1.2	97.7
V55	0.260	+0.228		0	0.9	78.1
I29	0.105	-0.124		0	0.5	48.7
F50	0.075	-0.122	-	0	0.5	0.0
N59	0.154	+0.017		0	0.3	31.9
A1	0.313	+0.117		0	0.1	22.8
D24	0.230	+0.074		0	0.1	0.0
V32	7.152	-7.150	-			
K47	0.402	-0.190				

L38	0.204	-0.188	-
N23	0.018	-0.151	
E40	0.133	+0.136	
L41	0.021	-0.070	-
E42	0.059	-0.066	
F20	0.114	-0.064	
D44	0.025	+0.057	+
G45	0.046	+0.035	
E7	0.011	-0.032	-
Y54		-0.011	
K43		-0.003	
I27		-0.001	

^aResidues are sorted by t-value where $R_{I\rho}$ measurements are made and then by magnitude of $\Delta\varpi_N$ (direct).

^bProbability that $R_{I\rho}^{\pm}$ values are not equivalent as established by F-test analysis (described in text).

^cVery weak signal.

^dAccording to simulation should not be able to measure by $R_{I\rho}$.

^eShaded regions denote residues with boarderline t values where inspection of decay curves is necessary.

^f'0' indicates that sign could not be obtained from $R_{I\rho}$ measurements.

Total CPMG $|\Delta\varpi_N|$ values: 46

Total signs from H(S/M)QC: 28 right, 1 wrong

Total signs from $R_{I\rho}$: 25 right, 1 wrong

Table S2. $\Delta\varpi_{H^N}$ values measured on the Apb1p SH3 domain – Ark1p peptide exchanging system, 25°C, from CPMG relaxation dispersion and direct measurements along with signs of $\Delta\varpi_{H^N}$ from the $R_{1\rho}$ approach

res ^a	$\Delta\varpi^{\text{CPMG}}$	$\Delta\varpi^{\text{direct}}$	$R_{1\rho}$	t	1-p / % ^b
N16	0.581	-0.562	-	50.2	100.0
W36	0.270	-0.317	-	30.8	100.0
D9	0.153	+0.145	+	30.2	100.0
F31	0.225	+0.221	+	32.7	100.0
D33	0.307	-0.311	-	29.4	100.0
A13	0.211	-0.213	-	29.2	100.0
W37	0.418	-0.412	-	27.7	100.0
D11	0.091	-0.099	-	27.1	100.0
A12	0.088	+0.087	+	23.2	100.0
D15	0.311	-0.291	-	19.8	100.0
S52	0.231	+0.225	+	18.5	100.0
L49	0.324	+0.299	+	18.3	100.0
G39	0.117	+0.118	+	15.2	100.0
L38	0.290	-0.303	-	14.0	100.0
D34	0.070	-0.088	-	14.0	100.0
L18	0.083	-0.094	-	11.6	100.0
F50	0.042	-0.054	-	10.8	100.0
T19	0.054	+0.047	+	8.8	100.0
T5	0.043	+0.041	+	7.6	100.0
D35	0.063	-0.069	-	7.5	100.0
G48	0.040	+0.026	+	7.5	100.0
K25	0.043	+0.038	+	6.5	100.0
Y54	0.046	-0.053	-	6.1	100.0
E14	0.053	+0.047	+	5.9	99.7
Y10	0.028	-0.035	-	5.2	99.8
A6	0.044	+0.038	+	5.2	99.9
V21	0.030	+0.029	+	3.6	99.0
V32	0.060	+0.049	+	3.1	98.8

res	$\Delta\varpi^{\text{CPMG}}$	$\Delta\varpi^{\text{direct}}$	$R_{1\rho}$	t	1-p / %
E30 ^c	0.037	+0.031	+	2.4	97.4
Y8	0.050	+0.046	0 ^d	1.9	86.3
V55	0.029	+0.017	0	1.9	90.8
K43	0.013	+0.008	0	1.5	97.4
N53	0.075	-0.061	0	1.2	0.0
L57	0.033	+0.031	0	1.1	53.8
S56	0.017	+0.011	0	1.1	87.3
F20	0.014	+0.011	0	1.0	83.6
N28	0.017	+0.009	0	0.5	68.6
E40	0.112	-0.016	0	0.3	0.0
I29	0.012	+0.005	0	0.3	0.0
K47		-0.085			
L41		-0.018			
N59		-0.015			
G58		+0.012			
A1		+0.011			
G45		-0.011			
I27		-0.006			
E7		-0.004			
N23		-0.004			
D24		+0.004			
E17		-0.003			
W3		+0.002			
E42		+0.001			
D44		-0.001			
A4		-0.000			

^aResidues are sorted by t-value where $R_{1\rho}$ measurements are made and then by magnitude of $\Delta\varpi_{H^N}$.

^bProbability that $R_{1\rho}^{\pm}$ values are not equivalent as established by F-test analysis (described in text).

^cShaded regions denote residues with borderline t values where inspection of decay curves is necessary.

^d'0' indicates that sign could not be obtained from $R_{1\rho}$ measurements.

Total CPMG $|\Delta\varpi_{H^N}|$ values: 39

Total signs from $R_{1\rho}$: 29 (all correct)

Table S3. $\Delta\varpi_{c^\alpha}$ values measured on the A39V/N53P/V55L Fyn SH3 domain, 20°C, from CPMG relaxation dispersion experiments along with signs of $\Delta\varpi_{c^\alpha}$ from both H(S/M)QC and $R_{1\rho}$ approaches

res ^a	$\Delta\varpi^{\text{CPMG}}$	H(S/M)QC	$R_{1\rho}$	t	1-p / % ^b
F26	0.963	-	-	34.3	100.0
Y54	2.517	-	-	21.8	100.0
W36	1.182	-	-	20.7	100.0
A6	0.883	+	+	18.7	100.0
A56	0.795	+	+	14.9	100.0
S32	0.860	-	-	13.1	100.0
T47	0.907	+	+	13.0	100.0
P53	1.775	-	-	11.5	100.0
E33	0.769	+	+	9.1	100.0
Y10	0.628	-	-	7.8	100.0
D9	0.683	-	-	5.8	100.0
Y49	0.681	-	-	8.7	100.0
P51	1.335	+	+	7.7	100.0
E38	0.588	+	+	6.0	99.9
T43	0.560	-	-	5.4	100.0
E5	0.865	+	+	4.4	100.0
S41	0.520	+	+	4.2	99.7
Q27 ^c	0.815	+	+	2.5	98.4
H21	0.494		0 ^d	2.3	98.6
E24	0.735	-	-	2.1	100.0
R40	0.462	-	0	1.6	94.0
Y8	0.775	+	0	1.4	0.0

res	$\Delta\varpi^{\text{CPMG}}$	H(S/M)QC	$R_{1\rho}$	t	1-p / %
P57	0.519	+	0	0.8	65.1
D17	0.581	-	0	0.5	0.0
G34	0.447				
S31	0.450	-			
R13	0.424	-			
E11	0.421	+			
E15	0.399	-			
F20	0.362	+			
S52	0.357	-			
G23	0.345				
K22	0.341				
E46	0.341	-			
K25	0.326	+			
S19	0.295	-			
N30	0.286				
F4	0.275	+			
D59	0.275				
T14	0.257				
T2	0.255				
A12	0.245	-			
D16	0.223				
T44	0.242				
G48	0.034				

^aResidues are sorted by t-value where $R_{1\rho}$ measurements are made and then by magnitude of $\Delta\varpi_{c^\alpha}$.

^bProbability that $R_{1\rho}^\pm$ values are not equivalent as established by F-test analysis (described in text).

^cShaded regions denote residues with borderline t values where inspection of decay curves is necessary.

^d0' indicates that sign could not be obtained from $R_{1\rho}$ measurements.

Total CPMG $|\Delta\varpi_{c^\alpha}|$ values: 45

Total signs from H(S/M)QC: 34

Total signs from $R_{1\rho}$: 19 (all consistent with H(S/M)QC)

Table S4. $\Delta\varpi_{H^\alpha}$ values measured on A39V/N53P/V55L Fyn SH3 domain, 20°C, from CPMG relaxation dispersion along with signs of $\Delta\varpi_{H^\alpha}$ from the $R_{1\rho}$ approach.

res ^a	$\Delta\varpi^{\text{CPMG}}$	$R_{1\rho}$	t	1-p / % ^b
A56	0.687	-	24.3	100.0
L7	0.456	+	19.4	100.0
V58	0.254	+	18.0	100.0
E5	0.926	-	14.9	100.0
P57	0.813	+	12.1	100.0
I50	0.404	+	10.4	100.0
A6	1.262	-	10.0	100.0
Y49	0.342	+	9.8	100.0
K25	0.337	-	9.6	100.0
T47	0.166	-	9.4	100.0
L3	0.287	+	6.0	100.0
Y8	0.250	-	7.2	100.0
F4	0.301	-	8.0	100.0
S52	0.217	-	5.1	100.0
P53	0.461	-	4.2	98.9
D9	0.367	+	3.6	98.9
E38	0.372	+	3.3	99.9
G54	0.133	+	3.2	99.4
D16 ^c	0.139	-	2.8	99.2
R40	0.244	0 ^d	2.6	99.2
L18	0.135	0	2.4	95.9
K22	0.186	0	2.1	100.0
E33	0.157	0	1.8	95.6

res	$\Delta\varpi^{\text{CPMG}}$	$R_{1\rho}$	t	1-p / %
H21	0.138	0	1.5	95.6
R13	0.121			
F20	0.120			
L29	0.113			
W36	0.113			
I28	0.111			
N30	0.101			
L42	0.092			
Q27	0.091			
D59	0.089			
E11	0.084			
E24	0.083			
E46	0.082			
F26	0.081			
A12	0.074			
V39	0.074			
D17	0.073			
T14	0.065			
T43	0.039			
S19	0.035			
S32	0.009			
T2	0.003			
T44	0.002			
S41	0.001			

Total CPMG $|\Delta\varpi_{H^\alpha}|$ values: 47

Total signs from $R_{1\rho}$: 19

^aResidues are sorted by t-value where $R_{1\rho}$ measurements are made and then by magnitude of $\Delta\varpi_{H^\alpha}$.

^bProbability that $R_{1\rho}^\pm$ values are not equivalent as established by F-test analysis (described in text).

^cShaded regions denote residues with borderline t values where inspection of decay curves is necessary.

^d'0' indicates that sign could not be obtained from $R_{1\rho}$ measurements.

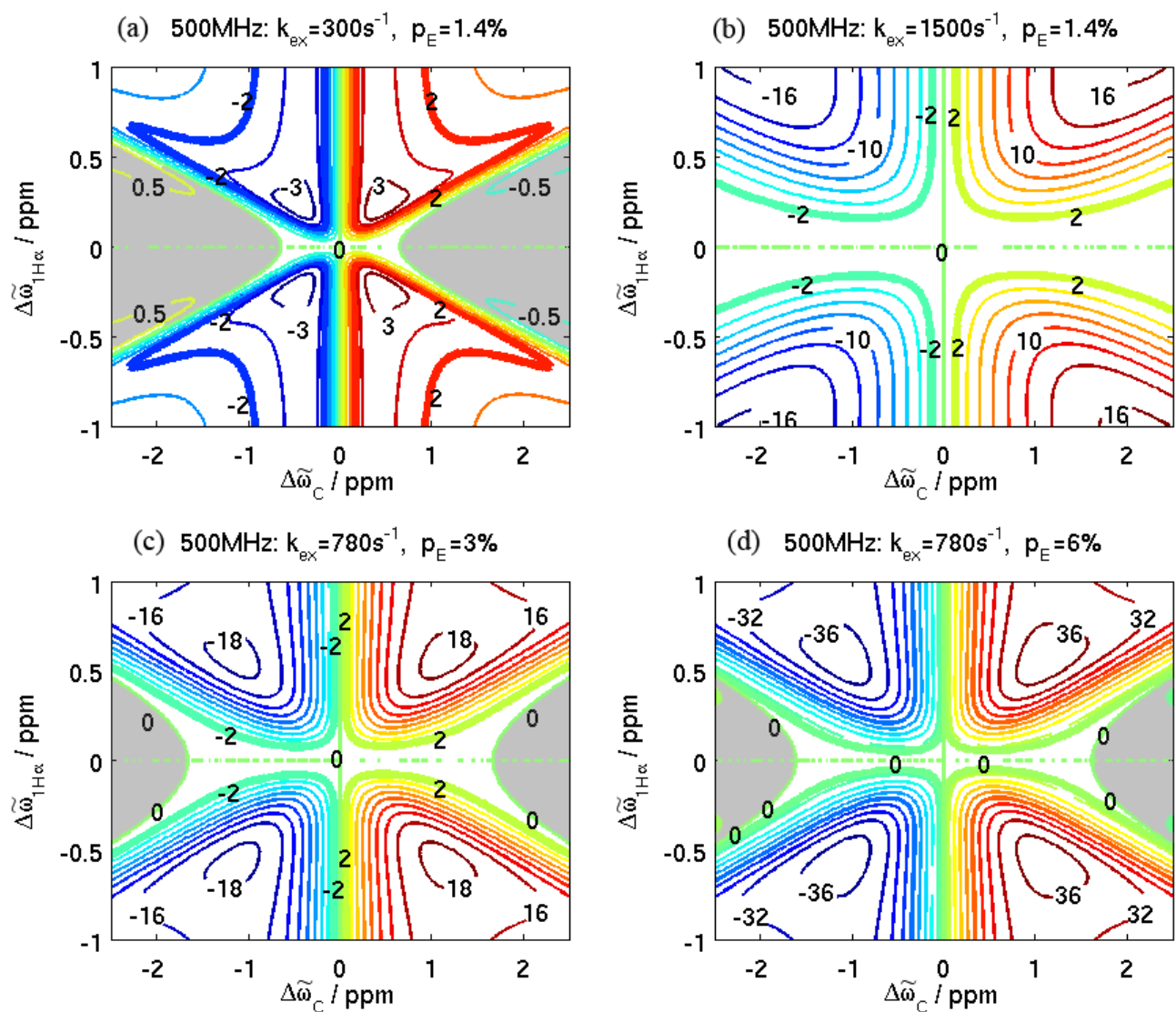


Fig S1 Contour plots of $\tilde{\Omega}_x$ (Eq 10) as a function of $(\Delta\varpi_{C^a}, \Delta\varpi_{H^a})$ at 500 MHz. The gray shaded areas denote regions where negative values of $\tilde{\Omega}_x$ correspond to positive $\Delta\varpi_x$ values and vice versa.

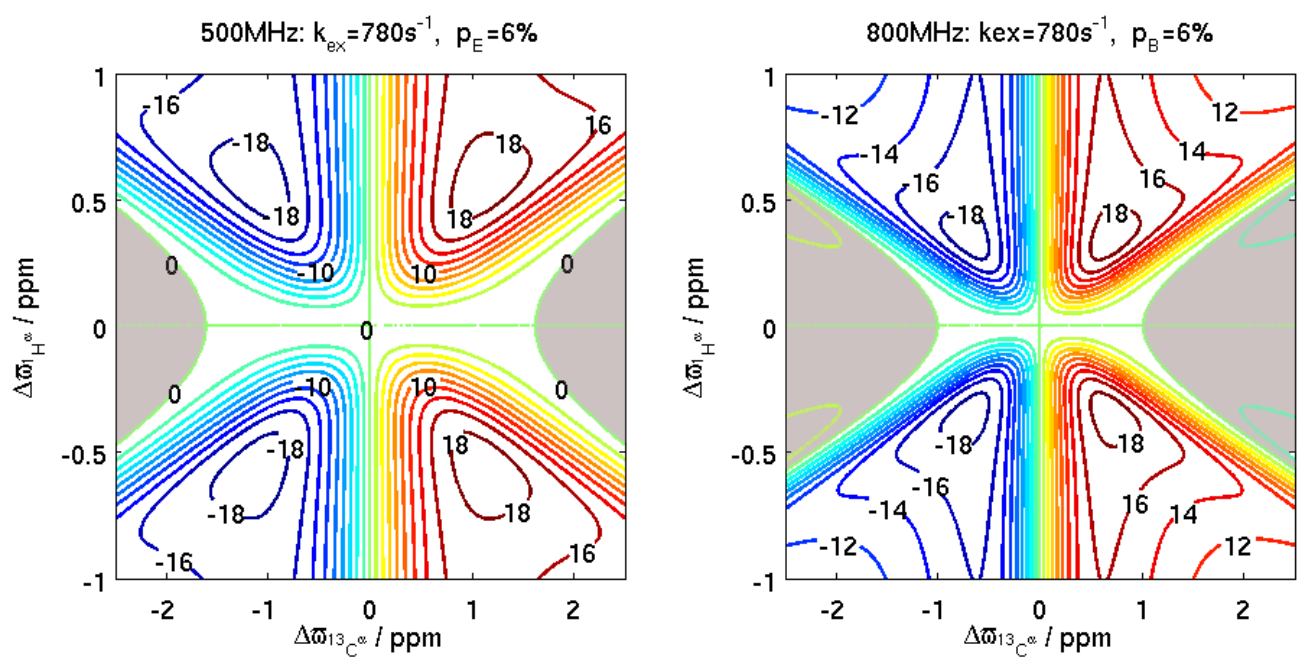


Fig S2 Contour plots of Ω_χ (Eq 10, but in Hz) as a function of $(\Delta\sigma_{C^\alpha}, \Delta\sigma_{H^\alpha})$ for (p_E, k_{ex})